Call: H2020-ICT-2020-2

Project reference: 101015956

Project Name:

A flagship for B5G/6G vision and intelligent fabric of technology enablers connecting human, physical, and digital worlds

Hexa-X

Deliverable D3.3
Final models and measurements for localisation and sensing

Date of delivery:	01/05/2023	Version:	1.4
Start date of project:	01/01/2021	Duration:	30 months

Document properties:

Document Number:	D3.3
Document Title:	Final models and measurements for localisation and sensing
Editor(s):	Henk Wymeersch
Authors:	Henk Wymeersch (CHA), Athanasios Stavridis (EAB), Kim Schindhelm (SAG), Hui Chen (CHA), Hao Guo (CHA), Musa Furkan Keskin (CHA), Simon Lindberg (QRT), José Miguel Mateos-Ramos (CHA), Mohammad Hossein Moghaddam (QRT), Mohammad Ali Nazari (CHA), Indika Perera (OUL), Alejandro Ramirez (SAG), Rafaela Schroeder (OUL), Tommy Svensson (CHA), Andreas Wolfgang (QRT), Vijaya Yajnanarayana (EAB).
Contractual Date of Delivery:	01/05/2023
Dissemination level:	PU[1]/
Status:	Final
Version:	1.4
File Name:	Hexa-X D3.3_v1.4

Revision History

Revision	Date	Issued by	Description
0.1	12.02.2023	Hexa-X WP3	Initial draft
1.0	12.03.2023	Hexa-X WP3	First complete draft
1.2	19.03.2023	Hexa-X WP3	Draft for external review
1.3	02.04.2023	Hexa-X WP3	Draft for GA review
1.4	28.04.2023	Hexa-X WP3	Final version for EC and Hexa-X site

[1] CO = Confidential, only members of the consortium (including the Commission Services)

PU = Public

Abstract

This report provides the final models and measurements, performance evaluation of new signal designs, and algorithms and evaluation of location-based services from Hexa-X work package 3, “6D high resolution localisation and sensing”. The report also provides final recommendations from Hexa-X regarding the interaction of communication, localisation, and sensing.

Keywords

6G localisation and sensing, methods, signals, services, demonstrations.

This project has received funding from the European Union’s Horizon 2020 research and innovation programme under grant agreement No 101015956.

Executive Summary

This report is the third and final deliverable of the Hexa-X project Work Package 3 (WP3): "6D High-Resolution Localisation and Sensing". This deliverable focuses on the final (in terms of the Hexa-X project) models and measurements, performance evaluation of new signal designs, including results from measurements from the over-the-air (OTA) demonstration, and algorithms and evaluation of location-based services.

This report starts by relating the activities of WP3 with respect to the rest of the Hexa-X project. Then, terminologies introduced in previous deliverables are recapped and refined to specify the terms: localisation, positioning, and sensing, as well as joint vs. integrated sensing and communication. To aid the reader in navigating the deliverable, a brief recap of the previous deliverables (D3.1 "Localisation and sensing use cases and gap analysis" and D3.2 "Initial models and measurements for localisation and sensing") is provided.

This deliverable covers the role of localisation and sensing in the 6G ecosystem considering three complementary aspects: the emerging services layer (including the processes and needed exposure), the implications regarding the key performance indicators (KPIs), and the implications regarding the key value indicators (KVIs). The basic sensing processes and functional view are presented within the 6G future ecosystem, comprising the sensing function layer, the sensing data processing layer, and the emerging application and service layer, as well as aspects related to management and orchestration, and sensor fusion. In terms of meeting the KPIs, this report considers the underlying requirements in terms of radio hardware and synchronization, as well as spectrum, resource optimization and infrastructure optimization. Finally, the relation of accurate localisation and sensing with the main KVIs is revealed, including inclusiveness and sustainability, but with a strong focus on trustworthiness, where aspects related to security, dependability, safety, and privacy are discussed.

The deliverable then addresses the final models and algorithms from WP3 in Hexa-X. Both channel models and hardware models are detailed for use in the algorithm development. Localisation and sensing algorithms have been developed for various scenarios, including 6D localisation (estimating both the 3D position and 3D orientation of a user, and optimising deployment and array sizes), as well as monostatic and bistatic sensing, integrated sensing and communication, and, finally, location-aided communications. Both model-based and AI-based methods have been developed and evaluated. While centimetre-level accuracies can be attained in these simulation-based studies, it was found that hardware impairments and calibration issues can limit the performance.

To better understand the impact of hardware impairments, dedicated studies on the quantitative performance degradation of each impairment are reported. These studies consider both the channel parameter estimation problem (i.e., detecting paths and the corresponding angles, delays, Dopplers), as well as the localisation and radar sensing problems. The studies show that array calibration errors (e.g., coupling, radiation pattern, displacement) have a larger effect on localisation and sensing than communications, and careful calibration and compensation of hardware impairments are necessary to attain very high accuracies. OTA results of waveforms developed in Hexa-X (in the form of spatial precoders) show that standard communication waveforms may be sub-optimal when used for sensing or localisation reference/probing signals. OTA experiments at 69 GHz and 400 MHz bandwidth in a controlled indoor line-of-sight environment demonstrate angle-of-departure (AoD) estimation accuracies on the order of 0.01-0.2 degrees. With a bi-static sensing setup operating at 60 GHz and bandwidth of 800 MHz, a moving person could be tracked with a precision of 0.1-0.3 m depending on the position relative to the radios. Several improvements of the measurements are proposed, which are expected to increase the precision further.

The report ends with the main conclusions from Hexa-X WP3. It was found that 6G radio design should be holistic, in the sense that communication, localisation, and sensing must be integrated from the onset, to optimize overall performance. Sharing of resources between the three functions as well as the security

and privacy implications deserve further study. In terms of performance, this deliverable confirmed that the envisioned technical enablers towards 6G hold great promise for accurate localisation and sensing, though calibration and hardware aspects may limit the final performance.

Table of Contents

List of Figures

List of Tables

List of Acronyms and Abbreviations

Term	Description
3D	Three dimensional
3GPP	3rd generation partnership project
ACF	Auto-correlation function
ADC	Analog-to-digital converter
ADE	Antenna displacement error
AI	Artificial intelligence
AGE	Array gain error
AGV	Autonomous guided vehicle
AoA	Angle-of-arrival
AoD	Angle-of-departure
AP	Access point
API	Application programming interface
AR	Augmented reality
AWGN	Additive white Gaussian noise
B5G	Beyond 5G
BLE	Bluetooth Low Energy
BS	Base station
CCPA	California Consumer Privacy Act
CCDF	Complementary cumulative distribution function
CFAR	Constant false alarm rate
CFO	Carrier frequency offset
CNN	Convolution neural network
CRB	Cramér-Rao bound
CSI	Channel state information
CSIT	Channel state information at the transmitter side
DFTS-OFDM	Discrete Fourier Transform Spread-OFDM
DAC	Digital-to-analogue converter
DD	Doppler-delay
ED/LC	Early detect late commit
ESPRIT	estimation of signal parameters via rotational invariance techniques
FIM	Fisher information matrix
FFT	Fast Fourier transform
FMCW	Frequency-modulated continuous wave

FRO	Free-running oscillator
GDOP	Geometric dilution of precision
GDPR	General Data Protection Regulation
GNSS	Global navigation satellite systems
HOM	High order modulation
HWI	Hardware impairment
IAB	Integrated access and backhaul
IBO	Input back-off
ICI	Intercarrier interference
ISAA	Iterated small angle approximation
IOO	Indoor open office
IoV	Internet-of-vehicles
IQI	In-phase and quadrature imbalance
ISAC	Integrated sensing and communication
JCAS	Joint communication and sensing
KPI	Key performance indicator
KVI	Key value indicator
LB	Lower bound
LEO	Low-earth orbit
LO	Local oscillator
LOS	Line-of-sight
LS	Least square
LSRPA	large-scale based RIS pre-assignment
MAP	Maximum a-posteriori
M&O	Management and orchestration
MC	Mutual coupling
MCRB	Misspecified Cramér-Rao bound
MCS	Modulation and coding scheme
MF	Matched filter
MIMO	Multiple input multiple output
MLE	Maximum likelihood estimation
MMSE	Minimum mean squared error
MR	Mixed reality
NLOS	Non-line-of-sight
NR	New radio
NTN	Non-terrestrial network
OFDM	Orthogonal frequency-division multiplexing

OEB	Orientation error bound
OTA	Over-the-air
PAN	Power amplifier nonlinearity
PAPR	Peak-to-average-power ratio
PEB	Position error bound
PL	Protection level
PLL	Phase-locked loop
PN	Phase noise
PrA	Predictor antenna
PRS	Positioning reference signal
QAM	Quadrature amplitude modulation
QoS	Quality of service
QPSK	Quadrature phase shift keying
RA	Receive antenna
RAIM	Receiver autonomous integrity monitoring
RAN	Radio access network
RCS	Radar Cross Section
RE	Resource element
RFC	Radio frequency chain
RIS	Reconfigurable intelligent surface
RMSE	Root mean-squared-error
RRU	Remote radio unit
RS	Reference signal
RTK	Real-time kinematic
Rx	Receiver
SA	Sub-array
SAA	Small angle approximation
SAR	Synthetic aperture radar
SINR	Signal-to-interference-and-noise-ratio
SNR	signal-to-noise-ratio
SRS	Sounding reference signal
STF	Space-time-frequency
SV	Saleh-Valenzuela
TIR	Target integrity risk
TDoA	Time-difference-of-arrival
TF	Time-frequency
ToA	Time-of-arrival

Tx	Transmitter
UAV	Unmanned aerial vehicle
UE	User equipment
ULA	Uniform linear array
Uma	Urban macro
UMi	Urban micro
UWB	Ultra-wideband
V2X	Vehicle-to-anything
VR	Virtual reality
WP	Work package
XR	Extended reality
ZF	Zero-forcing

1 Introduction

Hexa-X is one of the 5G-PPP projects under the EU Horizon 2020 framework. It is a flagship project that develops a Beyond 5G (B5G)/6G vision and an intelligent fabric of technology enablers connecting human, physical and digital worlds.

This document is the third deliverable of Work Package 3 (WP3) - "6D high-resolution localisation and sensing". The work in WP3 focuses on the exploration of technological advances in communication systems (both within and outside Hexa-X) for the purpose of accurate localisation and sensing, as well as the use of location and sensing information to support existing and new services. The research is broken down into three tasks (T3.1, T3.2, and T3.2) focusing on the following complementary aspects:

- T3.1: Definition of use cases and requirements, complemented with a gap analysis.
- T3.2: Development of methods, signals, and protocols for localisation and mapping.
- T3.3: Establishment of location and mapping-enhanced service operation.

The relation of WP3 within Hexa-X, its tasks, and main interfaces are shown in Figure 1-1.

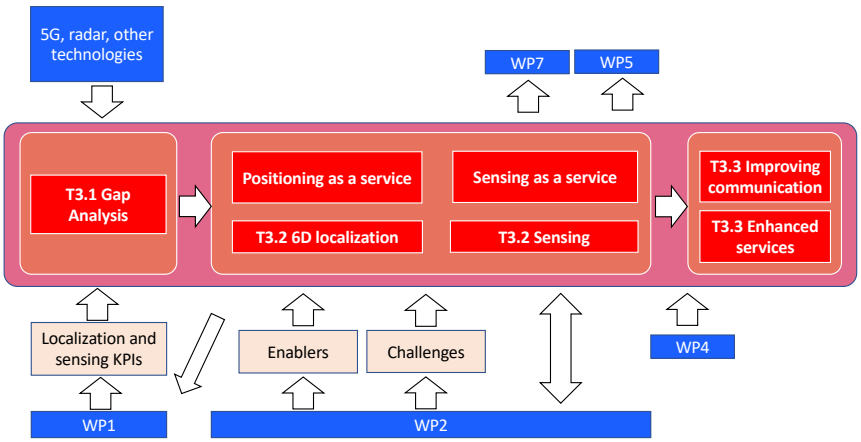

Figure 1-1 WP3 and its tasks in relation to Hexa-X.

This deliverable builds on [HEX22-D32], which provided initial findings regarding methods, models, and measurements for localisation, sensing, and enhanced services that benefit from location and sensing information. The deliverable also capitalises on the work in Hexa-X WP2 "Novel radio access technologies towards 6G", by utilising recent developments in terms of models and technologies for radio communication. More specifically, this deliverable provides the final models and measurements, performance evaluation of new signal designs, and algorithms and evaluation of location-based services from Hexa-X WP3, "6D high resolution localisation and sensing". Finally, the deliverable provides final recommendations from Hexa-X regarding the interaction of communication, localisation, and sensing.

1.1 Hexa-X objectives on radio performance towards 6G

The work in WP3 related to the project-level objective "Radio performance towards 6G", which is shared with WP2. This section given an overview of the work in Hexa-X towards this objective.

1.1.1 Hexa-X outputs towards radio performance towards 6G

The outputs towards the objective are reported in the three WP3 deliverables:

[HEX21-D31] Hexa-X, "Deliverable D3.1: Localisation and sensing use cases and gap analysis," Dec. 2021.

[HEX22-D32] Hexa-X, "Deliverable D3.2: Initial models and measurements for localisation and sensing," Oct. 2022.

[HEX23-D33] Hexa-X, "Deliverable D3.3: Final models and measurements for localisation and sensing," May 2023. (this document).

1.1.2 Hexa-X measurable results towards radio performance towards 6G

The following measurable results for the objective are completed in the WP3 deliverables.

To deliver models and radio-based solutions to support high-precision localisation, high-fidelity digital representations of the physical world, improved communications, and new services.

Different models and algorithms have been developed for accurate localisation and sensing, including both model-driven methods and methods based on artificial intelligence. Based on geometric models of the mmWave (30-100 GHz) and sub-THz (0.1-1 THz) channels, locations of incidence points in the environment as well as large surfaces can be estimated, providing a map of the environment. These methods have been reported in [Section 4, HEX21-D31], [Section 3, HEX22-D32], and this document (Section 4.1 and Section 4.2). Methods to improve the communication quality by harnessing location information have been devised to avoid blockages and to improve energy efficiency. New services have also been developed, based on sensing information, e.g., to determine the propagation environment. These methods and associated models have been reported in [Section 4, HEX22-D32] and in this document (Section 4.2.7).

Novel models and algorithms for localisation and sensing, tailored to B5G signals and use cases.

Several novel methods for localisation and sensing, building on agreed waveforms, have been devised and evaluated in terms of the agreed key performance indicators (KPIs). These methods aim for extremely high accuracy, low latency, and high resolution, tailored to the use cases from [HEX21-D31]. The methods and their evaluation have been reported in [Section 4, HEX21-D31], and [Section 3, HEX22-D32]. The final models and methods can be found in this document, Section 4.1 and Section 4.2.

Demonstration of improved energy efficiency and safety/security by harnessing and predicting precise locations of users and objects.

Improvements in energy efficiency based on channel knowledge maps have been studied in [Section 4.2.2, HEX22-D32]. The results indicate that higher location accuracy of the users leads to increased energy efficiency, due to reduced training overheads. In parallel, [HEX22-D32] also reports gains in achievable rate for a fixed energy when using location knowledge about objects in the environments, in particular blockages, in [Section 4.2.1, HEX22-D32] and Section 4.2.7 in this document. Energy efficiency is also treated in this document in Section 3.3.2, building on resource optimization from Section 3.2.3 and infrastructure optimization from Section 3.2.4. Enhancements of security use cases have been listed in [Section 4.1.1, HEX22-D32]. A more complete view of security and location information is provided in this document in Section 3.3.1.

Enabling convergence of communication and sensing by realising performance similar to that of dedicated radar and LiDaR sensors.

The performance of dedicated radar and LiDaR sensing has been established in [Section 3.2.2, HEX21-D31]. Sensing with OFDM waveforms at mmWave with 800 MHz has been demonstrated in this report (Section 5.2.2), leading to accuracies ranging from 0.1 to 0.3 m, which is similar to the radar resolution reported in [Table 3-28, HEX21-D31]. In terms of positioning, angle estimation accuracy between 0.01 and 0.2 degrees has been reported in Section 5.2.1, which is similar to lidar angle resolution, reported in [Table 3-29, HEX21-D31]. The requirements in terms of bandwidth and array size in order to realise resolution similar to radar and LiDaR are detailed in Section 3.2.1.

1.1.3 Hexa-X quantified results towards radio performance towards 6G

The following quantified results for the objective are completed in the WP3 deliverables.

(<1 cm) positioning precision

The precision of 1 cm has been established in simulation studies, reported in [Section 4, HEX21-D31] and [Section 3, HEX22-D32] and in Section 4.2. More realistic studies that account for hardware impairments and calibration are reported in Section 5.1.2. Finally, demonstration of mmWave positioning and sensing has been reported in Section 5.2. The demonstrated 2D positioning accuracy of a passive object was around 0.1-0.3 meter (see Section 5.2.2), which is similar to the size of the object, so that further improvements are not possible when treating the object as a point. For positioning of a connected device, angle-of-departure (AoD) estimation performance was in the order of 0.01-0.2 degrees, which translates to a 2D positioning error of a device 10 meters away of approximately 0.002 m to 0.03 m. Further improvements are possible using new beams (Section 5.2.1), by using more bandwidth or more antennas, and by applying more sophisticated signal processing methods.

1.2 Structure of the document

This deliverable is structured as follows. In the current section, a brief overview of terminology related to integrated sensing and communication is provided. Section 2 contains a short summary of the previous deliverables in WP3. Section 3 describes how localisation and sensing are envisioned to be integrated into the 6G ecosystem, and considers aspects related to architecture and resource allocation, as well as KPIs and key value indicators (KVIs). Then, Section 4 details the models and algorithms developed within Hexa-X WP3. The section starts with a review of relevant channel and hardware models, followed by contributions related to localisation, sensing, and the use of location information for improving communication. In Section 5.2, the gap between theory and practice is bridged, first through an analysis of the impact of hardware impairments on localisation and sensing, and then by the reporting of the results of over-the-air (OTA) demonstrations of localisation and sensing. Finally, Section 6 provides the final recommendation from Hexa-X WP3 regarding the integration of localisation and sensing towards 6G.

1.3 Terminology

The purpose of this section is to explicitly state the definitions for positioning, localisation, and sensing, building on the initial descriptions from [HEX21-D31, Section 2.2], as well as to relate these definitions to the various concepts and terminologies in the technical literature.

1.3.1 Definitions of positioning, localisation, and sensing

The following definitions are considered in this deliverable, though it should be noted that other disciplines (e.g., robotics or global navigation satellite systems (GNSS) navigation) use slightly different definitions. All terms are tacitly assumed to be related to radio signals (e.g., “positioning” should be understood as “radio positioning”), with the understanding that the terms may have other meanings in other contexts.

Positioning refers to the estimation of the geometric state of a connected device (a user equipment (UE)) based on radio signals from/to one or more reference points (typically base stations (BSs) or access points (APs)). The geometric state includes the position (either in 3D or in a lower dimension), and possibly the orientation (either in 3D or in a lower dimension). Positioning requires transmission, reception and processing of radio signals and knowledge of the position and orientation of the reference point. In positioning, the clock bias of the UE with respect to the BSs is an unknown that must be estimated.

Example of positioning: by estimating the time-of-arrival (ToA) from at least 4 synchronised BSs, a UE can determine its 3D position (i.e., location), by computing the intersection of 3 hyperbola, induced by differential ToA measurements.

Localisation is in this document considered equivalent to positioning, but in general may also comprise "device-free localisation", i.e., determining the location of passive objects.

Sensing refers to the detection of events or changes in an environment, based on radio signals. Hence, it is much broader than positioning. To provide structure to this broad definition, it is useful to classify sensing based on (i) the architecture; or on (ii) the function. From an architectural perspective, there are four common sensing modes [Han86, KCO19]:

- *Monostatic sensing:* A transmitter and receiver are located on the same device and share a common clock and knowledge about the transmitted signal.
- *Bistatic sensing:* A transmitter and receiver are located on separate devices. They may or may not share a common clock and full knowledge of the transmitted signal. Hence, positioning of a UE relies on bistatic sensing to/from multiple BSs.
- *Multistatic sensing:* A system comprising at least 2 transmitters (and 1 receiver) and/or at least 2 receivers (and 1 transmitter) separated in space, without a common clock.
- *Passive sensing:* The transmitted signal is provided by an external system (e.g., radio broadcast tower), while there is a sensing receiver, which has limited knowledge regarding the transmitted signal (e.g., only carrier frequency and bandwidth).

From a functional perspective, there are two common modes, which may be combined with any of the architectural modes:

- *Radar-like sensing:* the radio signal is processed to extract distances, angles, or Doppler shifts, to detect the presence and state (position, velocity) of objects/targets and track them over time. Radar-like sensing thus starts with detection/channel parameter estimation, followed by data association and by tracking. When objects are static, the process is called mapping, whereas when objects are moving, the process is called tracking.
- *Non-radar-like sensing:* any other type of sensing, including pollution monitoring, weather monitoring, as well detection and tracking based directly on the received waveform or features extracted from the received waveform. These features can be applied to machine learning for classification or regression.

Note that positioning can be based on radar-like sensing (by extracting the line-of-sight (LOS) distances, angles, or Dopplers under bistatic sensing) or on non-radar-like sensing (e.g., fingerprinting).

Example: a vehicular radar emits and receives a wideband waveform, from which it estimates distances and velocities to targets. This is a form of radar-like monostatic sensing, whereby the state of the targets is defined in the coordinate system of the radar.

From these architectures and functions, other types of sensing can be constructed. Among those is synthetic aperture radar (SAR), which has been used in remote sensing applications for several decades [Sou99]. Compared with standard monostatic radar, SAR can offer higher resolution in the angular domain (azimuthal precision), and, in that sense, it is well-suited for high-precision environment mapping. By utilizing the motion path of the host platform, SAR can simulate a large aperture (larger than a classic radar can provide) and provides high cross-range resolution. By exploiting this capability, it is possible to make high-resolution 2D or 3D images of the surrounding. There are also some methods that use SAR for moving targets, but here the focus is more on scanning the environment, which is supposed to be static in one course of measurements by SAR. One application is to equip moving devices like cars and unmanned aerial vehicles (UAVs) with sensors for SAR. Then, the high-resolution environment mapping of SAR can be used for localisation and sensing applications (or in general for collective perception). There are several post-processing algorithms for SAR, including spatial frequency-domain interpolation, range stacking, time-domain correlation, and back projection.

A visual comparison of the different sensing types is provided in Figure 1-2.

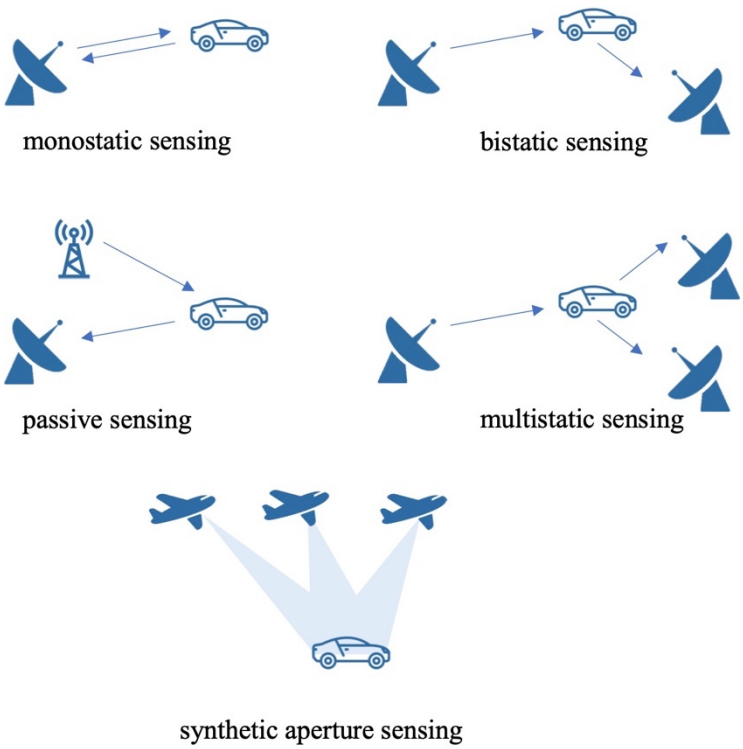

Figure 1-2 Different types of sensing. In the examples, the vehicle is considered as a passive object.

1.3.2 Integrated sensing, localisation, and communication

The tight integration of localisation and sensing within a 6G communication system [LCM+22], [ZLM+21], [ZRW+22], [ONA+22] is natural progression of the much weaker integration of localisation within the current 5G communication system [DSM+21].

In 5G, the integration of localisation with communication relies on (i) a *common set of devices* for localisation and communication (i.e., the BSs and UEs used for communication are reused for localisation); (ii) a *common waveform* for localisation and communication (i.e., a multicarrier orthogonal frequency-division multiplexing (OFDM) waveform); (iii) *separate time-frequency resources* for localisation and communication, by the use of dedicated pilot signals for accurate positioning (i.e., positioning reference signal (PRS) in downlink and sounding reference signal (SRS) in uplink) [DSM+21]. Nevertheless, there have also been studies on re-using unknown data symbols for positioning [AH13], which can be seen as a joint communication and positioning approach.

In 6G, where sensing, in a broader sense (not only limited to localisation), will be integrated with communication, there are more opportunities for using the same time-frequency resources. These opportunities are mainly driven by the potential introduction of monostatic sensing in 6G, where the transmitter co-located receiver share a common clock as well as common knowledge of the transmitted data. This turns the received data-bearing signal into a pilot signal from the receiver's perspective, also called *opportunistic sensing* [GLV+18], [GLV20], so that no dedicated pilot resources are needed for sensing [ZLM+21], [KWK21] (though stringent sensing requirements might necessitate additional dedicated sensing signals in certain scenarios). In this case, the same device, the same waveform and the same resources are used for both communicating to a remote (communication) receiver and performing sensing at the co-located sensing receiver. This concept can be applied also to a bistatic case (as shown in [AH13]), provided that the receiver knows the transmitter location, can recover the signal clock (e.g., from the LOS signal path) and the unknown transmitted data, reminiscent of classical decision-directed receivers [VMJ+22].

The terms *joint communication and sensing* (JCAS) and *integrated sensing and communication* (ISAC), which are considered equivalent in this document, cover not only this limited case, but all possibilities

of using the communication system for supporting sensing functionalities. This includes bistatic sensing and, thus, also localisation, and the use of sensing/localisation data for improving communication.

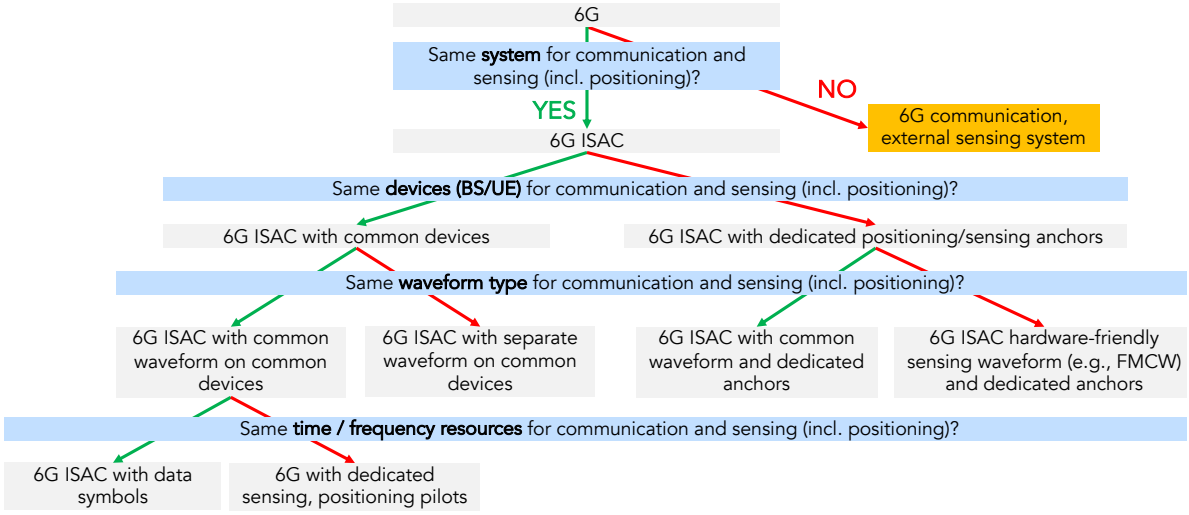

Figure 1-3 Different perspectives on integration of localisation, sensing, and communication.

These different perspectives are visualised in Figure 1-3 and encompass the following combinations:

- *Separate devices, separate waveform:* In this least-integrated variant of ISAC/JCAS, there are dedicated 6G sensing stations emitting pilot waveforms, which may in general be different from the communication waveform, to be more energy efficient and hardware friendly (e.g., less sensitive to hardware impairments, such as frequency-modulated continuous wave (FMCW)). The same spectrum may be used by the sensing devices and the communication devices. However, this leads to potential high interference between communication and sensing waveforms, unless some form of scheduling is applied.
- *Separate devices, same waveform:* In this variant, the waveform is shared and the same spectrum is used, but still dedicated sensing devices are considered [SWS+18]. The use of the same waveform has benefits in terms of cost scaling and possibly also in terms of interference reduction by scheduling transmissions.
- *Same devices, separate waveform, separate resources:* In this case, the devices are shared between communication and sensing functions, but the sensing takes place over dedicated time-frequency resources and uses a dedicated pilot waveform [AKG+21]. This variant has benefits in terms of sensitivity to hardware impairments, e.g., for monostatic sensing where a constant envelope signal can be used during sensing periods.
- *Same devices, separate waveform, same resources:* This variant is unlikely to be considered, as the superimposed communication and sensing waveforms require either sophisticated signal processing or lead to degradation of both communication and sensing quality.
- *Same devices, same waveform, separate resources:* This variant is mostly similar to current 5G positioning, where a dedicated pilot signal is used for positioning, but within the OFDM waveform [WWM+22]. This allows optimization of the sensing pilot in time, frequency, and space, as well as adaptation to different requirements and time-varying conditions [BLH+21], [BK19]. This variant is a probable candidate for 6G ISAC.
- *Same devices, same waveform, same resources:* The same waveform is used at the same time for both communication and sensing [SW11], [ZLM+21], [LCM+22]. Though this variant is attractive because "sensing comes for free", meaning that no radio resources need to be dedicated for sensing, there are several considerations. First, there are opportunities for optimizing the transmitted signal (in time-frequency by power and bit allocation [KKW21] and in space by precoding [LZM+18]), which lead to possibly conflicting designs if communication or sensing performance metrics are optimized. Second, since the transmitted data and user channels are random, so will be the sensing performance, which can be referred to as

deterministic vs. random trade-off in the ISAC/JCAS nomenclature [LZC+22]. This means that for some use cases that require regular and guaranteed sensing quality, this variant is not suitable, without complementing by dedicated sensing pilots.

2 Summary of previous deliverables

In this section, the previous two deliverables are briefly summarized, for the reader to understand their relation to the current deliverable and its background.

2.1 D3.1 — Localisation and sensing use cases and gap analysis

In D3.1, "Localisation and sensing use cases and gap analysis" [HEX21-D31], the focus was on the introduction of performance indicators, the elaboration of use cases (based on [HEX20-D11] and [HEX21-D12]), and a gap analysis with respect to current sensors (e.g., radar and lidar) and 5G positioning (according to the 3rd generation partnership project (3GPP) Release 16). In addition, preliminary findings on localisation and sensing, as well as location- and sensing-enhanced services were reported.

2.1.1 Performance indicators, use cases, and gap analysis

In [HEX21-D31] a list of 19 performance indicators was defined. Among them, several are considered as most relevant for the use-case and gap analysis. For localisation, these are accuracy, latency, availability, and scalability. For sensing, these are accuracy, range/distance resolution, velocity and angle, unambiguous range, latency, and availability.

Four sensing use cases and 17 localisation use cases were defined, based on [HEX20-D11] and [HEX21-D12], and the performance requirements were specified, in terms of the listed performance indicators. A baseline evaluation was conducted, based on 3GPP Release 16 for localisation, and based on radar and lidar for sensing, in terms of the specified performance indicators. Combining the use case requirements and the baseline evaluation, the main result of D3.1 was the gap analysis, which is summarised in Figure 2-1 (localisation) and Figure 2-2 (sensing) [BYK+22]. The gap analysis for localisation indicates that while 5G can support some of the use cases under some conditions, it cannot meet the demanding requirements of most of the considered use cases. In terms of sensing, it was observed that the conventional sensors are not able to meet all the requirements. 6G, as the next generation of mobile communication networks, potentially exploiting a wide bandwidth and large antenna arrays, among other enablers, must be able to support and meet the sensing requirements of the identified use cases.

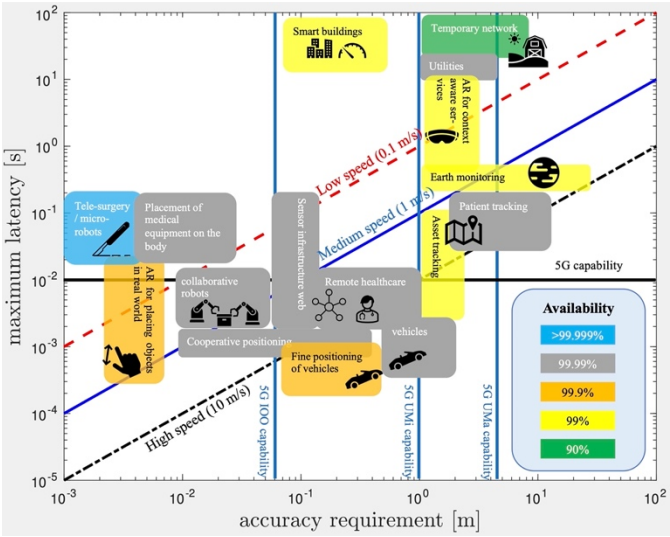

Figure 2-1 Gap analysis for localisation, inspired by [BYK+22]. Accuracy, latency, mobility, and availability are shown. The 5G capabilities are show in terms of latency (horizontal line) and accuracy (vertical lines) for indoor open office (IOO), urban micro (UMi), and urban macro (UMa) deployments.

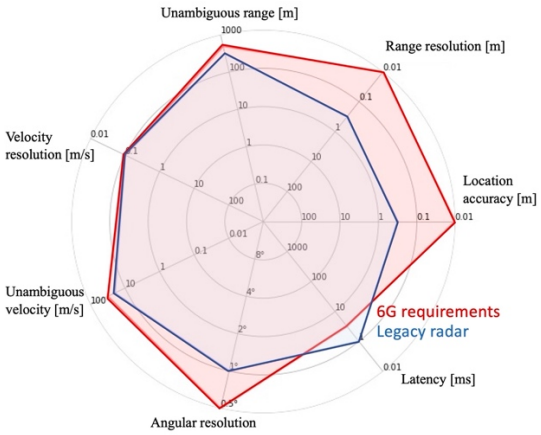

Figure 2-2 Gap analysis for sensing, inspired by [BYK+22]. 6G is envisioned to outperform legacy (standard) radar in all performance indicators.

2.1.2 Preliminary results on models and methods for localisation and sensing

D3.1 presented several initial results on *localisation* (including orientation estimation), comparing 5G with a possible 6G system, as well as radar-type *bistatic sensing*, and *simultaneous localisation and mapping* (including those based on graphical models and on Bayesian filtering). Non-radar type sensing of landscapes and materials was also reported. Combined, these results indicate the potential for 6G and ISAC/JCAS and show that 6G can outperform 5G in several of the performance indicators. The impact of hardware impairments was identified as one of the main unknowns requiring further analysis.

An ISAC/JCAS study in D3.1 showed that radio resource optimization for communication and for sensing are not identical, leading to an inherent trade-off. The importance of sensor fusion was highlighted, where 6G should provide the appropriate exposure framework to allow fusion with other on-board sensors. In addition, several approaches for reducing interference (in case dedicated sensing waveforms were used) were proposed and placed in a 6G context. These are especially important under uncoordinated transmissions, e.g., for side link or in unlicensed spectrum.

2.1.3 Preliminary view on location and sensing-enhanced operation

D3.1 also provided a preliminary view on localisation and sensing, as those can enhance existing services (including communication) and allow for new services and applications in the Hexa-X use-case families. In the former category (enhancing communication), location and mapping information is envisioned to reduce signalling overheads at lower layers, to provide blockage prediction, and to enable formation of local networks, and edge computing. In the latter category (new services), security and safety aspects were highlighted, where location information can help avoid safety risks. The availability of location and sensing information provides both opportunities and challenges in terms of security, which should be designed into the 6G system from the outset. Finally, initial implications on the 6G network were studied in terms of signal numerology and interference coordination.

2.2 D3.2 — Initial models and measurements for localisation and sensing

D3.2 presented preliminary findings on spatial signal design, detection and channel estimation, localisation/sensing methods, and experimental activities. Regarding the experimental setups developed within Hexa-X, a platform has been developed for integrated communication, localisation, and sensing. Moreover, the view of how the localisation and sensing information can be used for enabling applications, supporting communications, and enhancing security was introduced.

2.2.1 Methods, signals, and protocols for localisation and mapping

The first step in a radio-based localisation and sensing system is the design of the transmitted waveform. D3.2 reported findings on spatial signal design for a mmWave multiple-input-multiple-output (MIMO) downlink localisation setup. This study shows that a balanced combination of directional and so-called derivative beams (which have a sharp curvature around the desired angle to improve angle estimation performance; see Figure 2-3-(b)) improves the localisation accuracy. Since channel estimation and detection are essential before localisation and sensing, preliminary studies on this topic were provided in D3.2. Several methods for localisation and sensing in a 6G context were described in D3.2. These methods were categorized into model-based methods and AI-based methods. Regarding the model-based methods, a study on the impact of hardware impairments (HWIs) shows that dedicated pilot signal design, HWIs estimation, and mitigation algorithms are essential for accurate localisation in 6G. Also, D3.2 reported initial findings on AI-based methods for integrated sensing and communication under model mismatch. In addition, the first demonstration of the platform for integrated communication, localisation, and sensing was provided. Selected scenarios and results are visualised in Figure 2-3.

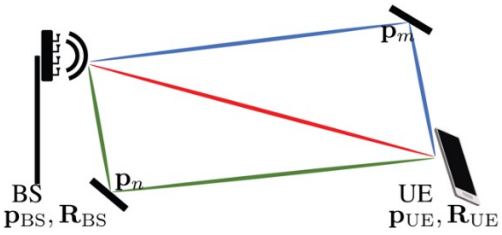

(a) 6D localisation setup [Section 3.3.1.1, HEX22-D32]

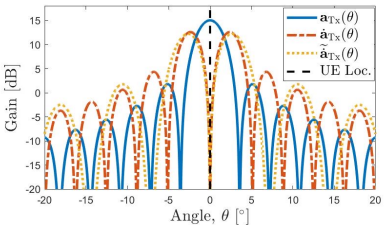

(b) Spatial signal design example [Section 3.1, HEX22-D32]

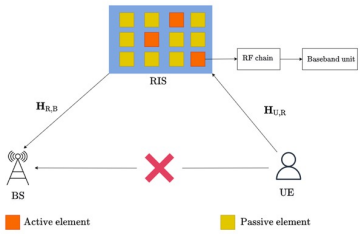

(c) Localisation aided by a reconfigurable intelligent surface [Section 3.2.1, HEX22-D32]

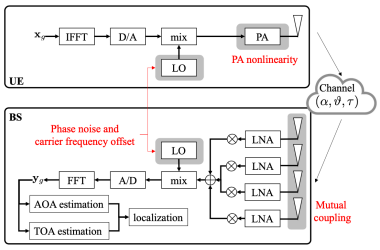

(d) Impact of hardware impairments on localization [Section 3.3.1.3, HEX22-D32]

Figure 2-3 Example scenarios and results on methods, signals, and protocols for localisation and mapping from [HEX22-D32].

2.2.2 Enhanced location and sensing services

D3.2 described an initial view of how localisation and sensing can enhance several use cases, such as security, non-radar-type sensing, weather monitoring, and factory optimization. Example scenarios are shown in Figure 2-4. Concerning communication aspects, D3.2 reported that location information can be exploited to avoid blockages and improve spectral efficiency. The implications and requirements for localisation/sensing in a 6G context were introduced, including hardware requirements, spectrum considerations, and time-sharing resource allocation. Finally, D3.2 provided the requirements for the new context-aware services and the first view on the localisation-and-sensing ecosystem.

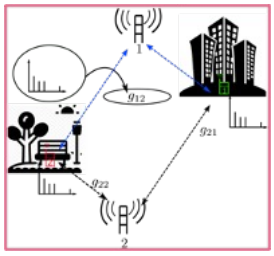

(a) Landscape sensing [Section 4.1.2.1, HEX22-D32]

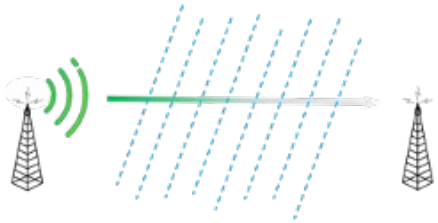

(b) Weather monitoring [Section 4.1.2.3, HEX22-D32]

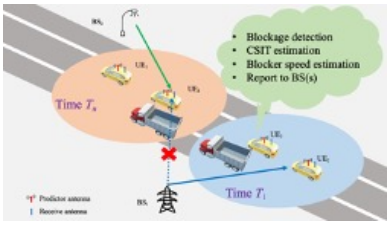

(c) Blockage prediction [Section 4.2.1, HEX22-D32]

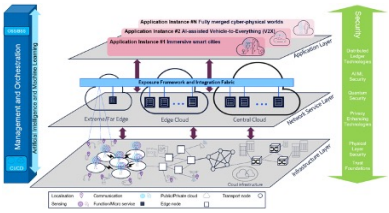

(d) Localisation and sensing as part of the architecture [Section 4.3.3, HEX22-D32]

Figure 2-4 Example scenarios and results on enhanced location and sensing services [HEX22-D32].

3 Localisation and sensing in the 6G ecosystem

This section describes the role of localisation and sensing within the 6G ecosystem and considers three complementary aspects: the emerging services layer (including the processes and needed exposure), the implications regarding the KPIs, and the implications regarding the KVIs. See also [HEX22-D13] for an architectural perspective.

3.1 Emerging service layer and 6G localisation and sensing

The localisation accuracy of UEs is enhanced with each new generation of mobile networks and is becoming an established feature of mobile networks. Moreover, sensing aspects, such as localisation and feature extraction of passive objects (i.e., not equipped with UEs), is gaining a significant momentum as an additional promising feature [DBB+21].

With these enhancements and evolving capabilities, new applications and services are emerging. As described in [HEX22-D32], a new ecosystem of services, applications, and features will arise, making use of artificial-intelligence capabilities and serving various digital twins (e.g., factory digital twin by tracking process flows or network digital twin by offering insights of UE locations). This new ecosystem can only emerge if the interaction between several providers taking care of platforms (e.g., cloud platform, service platform), infrastructures, services, applications, and device vendors is easy and beneficial for each stakeholder. Hexa-X collects findings, implications and requirements and present them in the following sections.

3.1.1 Basic process and functional view

The ecosystem consists of three main functional layers that take care of different tasks. Figure 3-1 depicts the three functional layers: *Sensing Functions and Services* which must run in parts on the network infrastructure, *Sensing Data Processing Functions and Services* and the *Emerging Applications and Service* that consume the processing results. In this context the term function refers to a specific task whereas services may bundle multiple tasks. Usually, it is the services that offer interfaces for access from other layers. One example for a function on the Data Processing Layer is the geometric approximation of an intersection of two hyperbolas, whereas a service could be to offer the final position of a UE (which is calculated using hyperbola intersection function and additional functions such as Kalman filter to perform tracking).

One option to categorise Sensing Data Processing algorithms are *Geometric* and *Data-driven approaches*. For data-driven approaches often artificial intelligence (AI) functionalities are required. Application programming interfaces (APIs) allow for easy and standardized access to services and functions within each layer, from functions and services in the other layers, but also from management-and-orchestration functions and services (which is shown in Section 3.1.2) and from external components. For example, raw sensing data should be accessible, as well as pre-trained neural-network models or sensing results. Control mechanisms ensure secure information exchange for external and internal service usage, based on defined access rights.

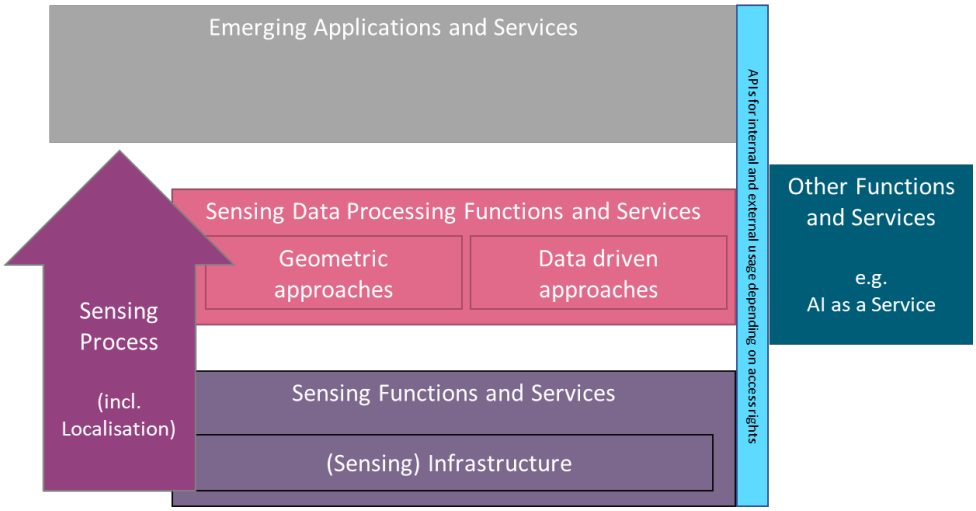

Figure 3-1 Basic overview of the Sensing Process and the Emerging Applications and Services which add value to sensing results. The infrastructure, services, functions, and applications should be accessible via well-defined APIs. (This view is not supposed to specify a hardware/software deployment view.

Sensing Functions and Services Layer

The sensing layer comprises all required infrastructure to perform sensing (this can be dedicated sensing hardware, firmware, software, or the shared network used for communication), and all means to configure the infrastructure in accordance with the requirements. The sensing layer can receive commands to start and stop the sensing process, usually managed, and controlled by management-and-orchestration functions and services. Depending on the underlying infrastructure and requirements, the required sensing data can be generated by reusing signals sent for communication purposes, or a dedicated sensing process can be started. **ISAC/JCAS** is explained in more detail in Section 1.3.2 and has implications on **management and orchestration** (M&O) components (see Section 3.1.2).

Results of the sensing process can be angle information (arrival, departure), channel states, Doppler information, or timestamps of signal arrival or departure etc. The generation of signals is prone to attacks, which may alter information in a way leading to wrong results [SRR+22]. This topic is discussed in more depth in Section 3.3.1.

Sensing is not restricted to only 6G-generated information. Many scenarios arise when considering sensing as an ecosystem. One example is sensing information generated by smartphones that are equipped with other sensors (e.g., Bluetooth Low Energy (BLE) information used for localisation, air pressure sensors to detect floor level). The results may be transferred and used by 6G services and applications. Another example is additional external localisation systems, for example based on GPS, Wi-Fi, or ultra-wideband (UWB). If multiple sources of sensing information are available at the same location, sensor fusion is an interesting task. Sensor fusion can be performed at different stages / layers depending on the availability of data. Further details and implications are presented in Section 3.1.3.

Sensing Data Processing Functions and Services Layer

Once sensing data is available, this data can be processed to calculate the required information. A main goal of services in this layer is to detect objects in the environment and changes of those objects over time either via classic UE localisation or radar-like sensing. Together with added domain knowledge, this information can be interpreted for example as a specific movement pattern of an observed object or conclusions can be drawn which kind of landscape is being sensed or what kind of gestures are being made.

Functions usually take care of tasks which often can be used for multiple services, whereas services bundle various functions to reach a more complex goal. Different concepts for localisation and sensing can be applied [ZDD19]:

- *Geometric/model-based:* This class of approaches makes use of geometric relations and physical models to calculate the desired quantities (e.g., the position of a UE). Standard existing approaches are circular or hyperbolic multi-lateration and angulation [HEX21-D31, Section 2.2]. Based on the classic example of a service for localisation of a UE, functions needed are calculating hyperbolas, approximating the intersection of multiple hyperbolas using filter mechanisms (such as Kalman filter).
- *Data-driven/AI-based:* This class of approaches relies on features (either hand-crafted or learned) to perform regression or classification [LXW+19]. The regression output variable can comprise the position of a UE or a sensed object (see Sections 4.2.3 and 4.2.4), while classification can refer, e.g., to detect and distinguish between certain human activity patterns (e.g., walking slowly, running) or a type of landscape [HEX22-D32, Section 4.1.2]. As before, the classic service example could be localisation of a UE, but the used functions differ from the previous geometric approach, as for AI approaches the position is estimated based on trained models which are used to interfere positions during operations.

Hexa-X studies both classes of approaches, and the results as well as the models are presented in Section 4. Depending on the approaches used, additional data may be required. Especially geometric approaches require, for example, information about the base stations' location and (antenna) orientation. For uplink time-based lateration algorithms, base stations need synchronized clocks in the magnitude of picoseconds to enable cm-level accuracy (recall that 1 ns refers to ~30 cm in deviations according to the speed of light). In addition, also waveform-related parameters must be known or configurable to reach certain KPI levels (see Section 3.2). AI-based approaches, on the other hand, generally require an abundance of labelled training data, which may be obtained from experiments or synthetically generated based on a model. Comparisons of geometric/model-driven and data-driven/AI-based approaches can be found in Section 4.2.3 and Section 4.2.4.

Emerging Applications and Services

A classic example of an application within the *emerging application and services layer* is the optimisation towards a specific goal based on location-based services. *Location-based services* make use of the current absolute or relative location of targets by evaluating geometric conditions. Independently whether this information is received by UE localisation or by radar-like sensing without UEs, some typical services are:

- Searching/finding UEs in real time or historical tracking of certain objects.
- Geo-fencing for determining whether a UE or an object is within a certain (mobile or static) predefined area.
- Collision avoidance between two mobile targets or one mobile target and a static area.
- Routing and navigation of targets through the environment. An important scenario is the optimisation of the network.

Context and Domain Information Services deliver additional (non-sensing-based) information of the surroundings, such as process or domain information, to optimise certain scenarios or processes. Planned routes, schedules, and trajectories of autonomous guided vehicles (AGVs) could be additional information to optimise factory processing [HEX22-D32, HEX22-D72]. Services in this layer can be network-external services or used for internal optimisation. Two examples are shown in the following two figures. An internal location-based service could optimise the resource-allocation service by integrating knowledge such as the current UE position and additional context information such as its planned trajectory (see Figure 3-2).

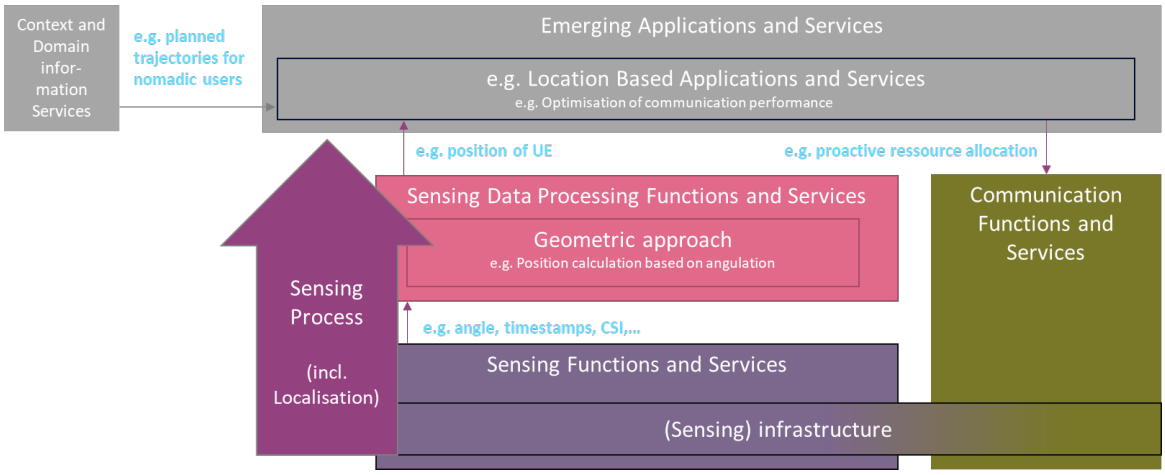

Figure 3-2 Example for optimisation of communication and network functionalities based on localisation of UEs. In this example, the underlying infrastructure is used both for sensing and communication purposes (see ISAC/JCAS). Parameter changing of sensing may have implications on communication and vice versa.

Another example for location-based services is the optimisation of factory processes by taking into account real-time asset tracking and additional asset information, such as process flow and schedules, to monitor throughput and for fast intervention if errors occur (see Figure 3-3).

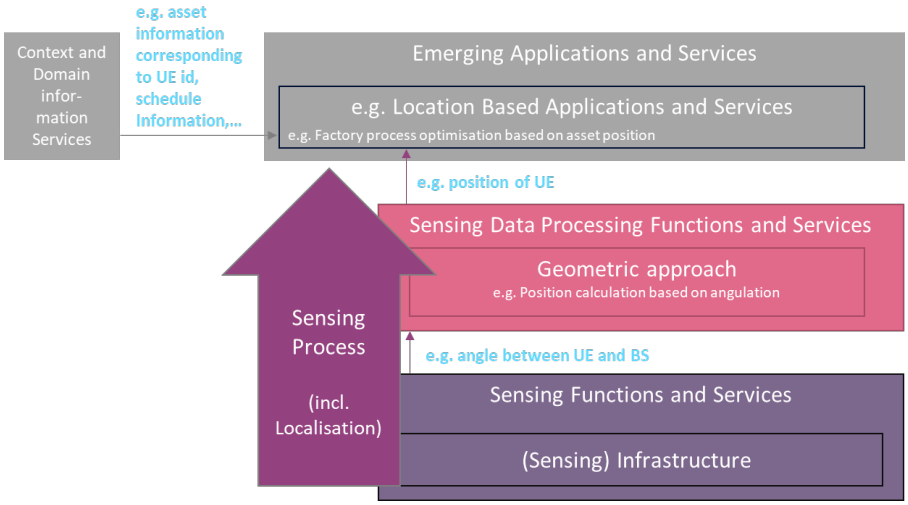

Figure 3-3 Example for optimisation of factory processes based on combination of asset tracking, context, and domain information.

3.1.2 ISAC/JCAS influences on management and orchestration

Sensing and localisation can be integrated into the communication network in various manners, as it is discussed in Section 1.3.2, and, in particular, Figure 1-3. Sensing (and localisation) can be performed stand-alone if applications and users do not need the network for communication purposes. In that case, the infrastructure and all signals could be used for sensing (and localisation) purposes. As this will probably rarely be the case and communication will be required by most applications, the concept of ISAC (or equivalently, JCAS) holds key requirements regarding M&O. M&O distinguish between objects / resources that are being managed / orchestrated and objects that perform management / orchestration [HEX22-D62] on all layers (infrastructure, network, and service layer). Since in many cases communication and sensing are done on the same infrastructure (hardware and network perspective) the M&O plays a very important role. M&O should take care of receiving the requirements coming from services and applications (both from the network external as well as from the network internal functions, services, and applications). M&O needs to determine whether the requirements of the applications and services towards ISAC/JCAS can be fulfilled by the network.

- M&O needs to consider many aspects, like available infrastructure, available methods for sensing and localisation and the application and service requirements (both for communication and sensing).
- M&O may need knowledge of sensing processes (in case multiple localisation mechanisms are available) to decide which one fits best.
- M&O needs then mechanisms for calculating the trade-off between sensing and communication. These mechanisms are described in Section 3.2.3.
- M&O needs standardised ways to communicate towards services and applications whether requirements are achievable or if losses (either on the communication or sensing side) must be accepted (e.g., lower communication bandwidth or lower update rate for localisation results).

Requirements may change over time, and M&O should be able to perform adjustments and recommendations in a very flexible way.

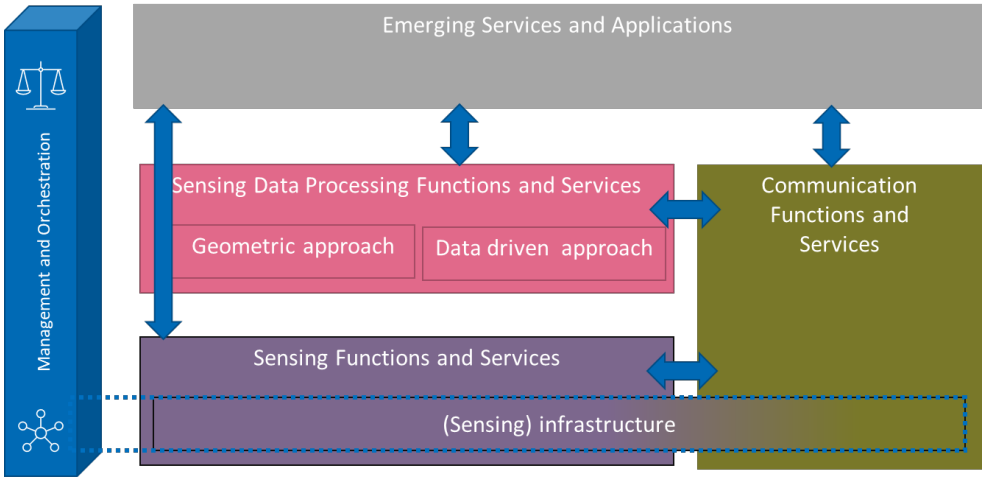

Figure 3-4 M&O in context of ISAC/JCAS. Sensing and communication are built on top of some infrastructure and must be carefully managed (coordinated and configured according to service and applications requirements).

3.1.3 Sensor fusion influences on management and orchestration

The purpose of sensor fusion is to combine data from multiple sources, to produce a more accurate measurement than with a single sensor. There are a few mainstream approaches to sensor fusion [Hol11]:

1. *Loose coupling*, in which two independent systems are combined at a higher layer, like the position coordinates of a device or the orientation direction. As an example, position calculated by GPS and WLAN can be combined for an improved position. The raw GPS signals are not an input to the sensor fusion algorithm, only the calculated 3D position and the estimated horizontal and vertical error. These error indications can be used to weight the position incoming from the WLAN system properly as to create an improvement overall. Loose coupling is often used when access to the lower layer signals/data is not possible, as is the case of a GPS on a smartphone, for which a typical software application only has access to the calculated position.
2. *Tight coupling*, in which sensor data measuring the same or similar aspects of a physical representation are combined to improve the accuracy overall. This will require some synchronisation between low-level data sources to be able to go beyond the inherent limits a single sensor. Typical data sources are time stamps. For instance, distance or time measurements done in the lower layers through 5G and UWB can be combined to estimate a better position, which is closer to the real position than what a single technology could be able to obtain. As a second example, measuring signal strength from WLAN infrastructure and

additional Bluetooth infrastructure can be used as a motion detector for people not carrying a wireless device, which would be more accurate than when using only one technology.

3. *Ultra-tight coupling*, which consists of combining very low-level data, which could be I-Q samples, to achieve the highest accuracy possible. An example is the use if 5G and 6G were deployed in the same area and were used as a radar. The phase data from both source can be fused together to achieve maximum resolution, but that requires very accurate synchronization of both signals. Access to such a low-level source of data can be a challenging task, as typical commercial-off-the-shelf hardware, as a closed chip does not provide an interface for it. Fortunately, this is changing with new 5G and future 6G deployments using open architecture models.

3.2 KPIs and implications

The KPIs for localisation and sensing include location accuracy, orientation accuracy, update rate, availability, but also maximum link range (unambiguous range), angular resolution, and velocity/range resolution [HEX21-D31]. Meeting these KPIs imposes requirements on the used signal (including the bandwidth), as well as on the transmitter and receiver array aperture. These are treated in detail in Section 3.2.1. The bandwidth requirement is closely related to the available spectrum. Requirements on the spectrum are discussed in Section 3.2.2. Optimization of the system for localisation and sensing from a resource and infrastructure perspective is treated in Sections 3.2.3 and 3.2.4, respectively.

3.2.1 Array apertures and bandwidths

In this section, three exemplifying use cases with varying and challenging requirements are considered, based on the related scenarios defined in [HEX23-D23]. These use cases cover both positioning and sensing:

A. *An extended-reality positioning use case*, with very high accuracy requirements (1 cm in position and 1 degree in orientation), low mobility (1 m/s), short range (up to 10 m), and clutter objects within short range (10 cm).
B. *A bistatic digital twin use case*, with high accuracy requirements (10 cm), low mobility (1 m/s), long range (100 m), and clutter objects within short range (10 cm).
C. *A monostatic sensor infrastructure web scenario*, with high accuracy requirements (20 cm), medium mobility (10 m/s), medium range (50 m), and clutter objects within medium range (1 m).

Table 3-1 Order-of-magnitude array and bandwidth requirements. Bandwidth and array sizes are specified in case resolution is only provided in that parameter (e.g., only bandwidth for delay resolution or only array size for angle resolution). Hence, these values can be reduced when resolution is provided by both domains jointly.

Parameter / Use case	**A** Extended reality positioning	**B** Bistatic digital twin use	**C** Monostatic sensor infrastructure web
Bandwidth	3 GHz	3 GHz	300 MHz
Synchronization requirements	3 ps	30 ps	70 ps
Maximum end-to-end-latency	1 ms	10 ms	2 ms
UE antenna array size	2 cm x 2 cm	N/A	N/A
UE beam resolution	1 degree	N/A	N/A
Sensor antenna array size	20 cm x 20 cm	214 cm x 214 cm	10 cm x 10 cm

With this subset of KPIs, an initial set of parameters can be defined. The results are listed in Table 3-1. All systems consider a 140 GHz carrier frequency.

Bandwidth requirement

The bandwidth is determined by the required resolution. When the object/UE of interest is separated a certain distance δ from other objects, the bandwidth needed to separate these objects is proportional to c/δ, where c is the speed of light. For example, use case C in Table 3-1 is the least demanding in terms of bandwidth, as it has the least stringent accuracy requirement.

Synchronization requirement

Whenever time-based measurements are used, there are requirements for the synchronization between devices involved in the measurements. As an approximation for these requirements, consider that a small fraction (e.g., 10%) of the localisation accuracy budget can be devoted to synchronization errors. This means that the synchronization requirements can be approximated by 10% of the localisation accuracy over the speed of light. All use cases require sub-ns synchronization, and the most demanding requirement is in use case A.

Latency requirement

Due to mobility, the UE/object displacement within the end-to-end latency should also be only a fraction of the localisation accuracy (e.g., 10%). Hence, for nearly static UEs/objects, the tolerable end-to-end latency can be large, while still meeting the localisation accuracy. The corresponding end-to-end latency that can be tolerated limits the transmit waveform (and thus the integrated signal-to-noise ratio (SNR)), as well as the processing times. It is important to point out that reducing latency by shorter symbols comes at a risk of reducing the maximum range. Hence, subcarrier spacing, bandwidth, and transmission duration should be carefully designed to meet the localisation and sensing KPIs. Similarly, reducing latency by sending fewer symbols affects the Doppler resolution and integrated SNR.

UE antenna array size

The UE array size is mainly relevant to use case A and is largely determined by the requirements for orientation accuracy, via the angle of arrival (AoA) estimation. When the AoA (and thus also the orientation) is estimated from simple beam direction measurements, the directions of arrival can only be estimated within a fraction, say $0 < \rho < 1$ of the beamwidth (which itself is inversely proportional to the array aperture). Table 3-1 reports the array sizes for $\rho = 0.1$. The corresponding beam resolution is then found from the required array size.

Sensor antenna array size

If bandwidth is scarce, the sensor array (which corresponds to a BS or a UE, depending on the application) can be used to provide the necessary position resolution, which imposes different angle resolutions at different distances. If the position resolution is δ and the maximum range is R, then the angle resolution requirement is $\Theta = \frac{\delta}{R}$. To meet such a requirement, the sensor array size should be $D = \lambda/\Theta = \lambda R/\delta$ [Rao17], where λ is the wavelength.

3.2.2 Spectrum

Among the most important requirements for accurate localisation and sensing is the availability of sufficient spectrum [WPA+22, TSB16] to provide sufficient delay (distance) resolution, and complementation angle resolution using large arrays. Depending on the use case and corresponding accuracy and latency requirements, bandwidth requirements vary from less than 400 MHz to 10 GHz [WPA+22, Table I]. Irrespective of the use case, there are several important considerations related to the spectrum:

- *Spectrum contiguity:* To avoid grating lobes in the delay ambiguity function, the allocated spectrum band is preferably contiguous, without any gaps.

- *Spectrum phase coherence:* If the allocated spectrum comprises several sub-bands (contiguous or not), it is critical that these bands are phase coherent. This, in turn, places demand on the transmitter and receiver hardware and oscillators.
- *Spectrum availability:* Certain applications require certain update periods for the sensing and localisation process. This means that sufficient spectrum should be pre-allocated to these allocations with guaranteed bandwidth and time.
- *Adjacent channel interference:* In lower frequency bands, the spectrum requirements on adjacent channel leakage are very stringent. In the upper mm-wave range and beyond, more channel leakage is expected, which needs to be considered when designing sensing applications.

3.2.2.1 Spectrum contiguity

The need for spectrum contiguity is demonstrated in Figure 3-5, which shows the range (distance) ambiguity function for an OFDM system with 400 MHz bandwidth and 3300 subcarriers. The ambiguity function indicates how well different paths or objects can be separated by the localisation or sensing application. With spectrum contiguity (shown in black) there is a peak at the correct distance, though with sidelobes that can be suppressed by suitable frequency-domain windowing. Without contiguous spectrum (in this example 100 out of 3300 subcarriers are used), additional peaks in the ambiguity function appear. If the used spectrum is periodic, the peaks occur periodically, in this case every 75.8 meters. If the used spectrum is non-periodic (in the example in Figure 3-5, 100 random subcarriers are used, shown in red), there are no periodic peaks, but rather strong sidelobes. These additional peaks do not correspond to any physical path/object and thus lead to severe ambiguities or ghost objects. From the example, some amount of spectrum non-contiguity can be tolerated but requires a careful design or dedicated signal processing.

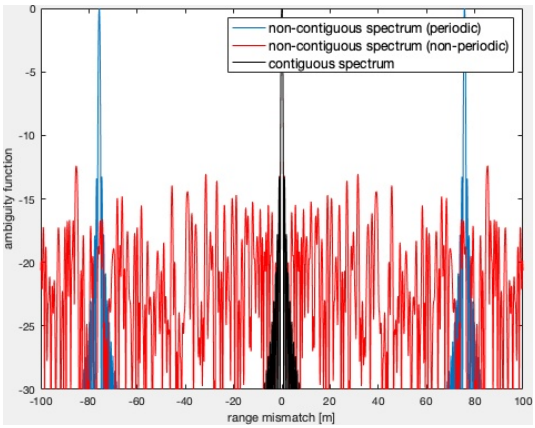

Figure 3-5 Impact of spectrum non-contiguity on the range ambiguity function. The periodic spectrum leads to additional peaks around 76 and -76 m.

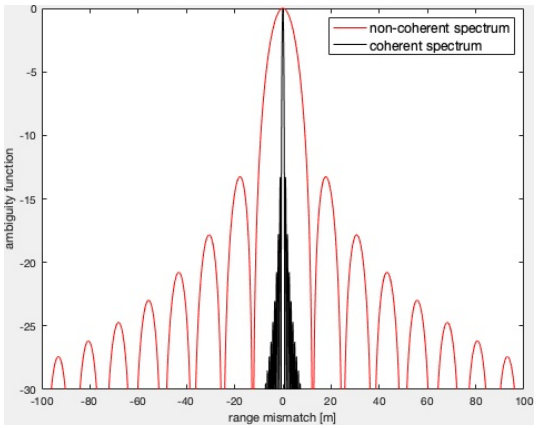

Figure 3-6 Impact of spectrum non-coherence on the range ambiguity function.

3.2.2.2 Spectrum phase coherence

The need for spectrum phase coherence is illustrated in Figure 3-6, which shows the range ambiguity function for a system with 400 MHz bandwidth and 3300 subcarriers. When there is full phase coherence, the ambiguity function is narrow, with a width of the main lobe of around 1.5 meters, indicating that different paths/objects that are separated at least 1.5 meter apart can be resolved. When the band is split up into 17 bands of around 24 MHz each and these bands do not preserve phase coherence, the red ambiguity function results. The main lobe has a width of around 25 meters, leading to a severe degradation in range resolution. In contrast to contiguity, phase coherence cannot be compromised.

3.2.2.3 Spectrum availability

The final spectrum aspect is related to availability. Referring to [HEX21-D31, Table 3-35], update rates vary from 10 kHz to fractions of a Hz. Use cases that combine (i) high update rates (e.g., augmented reality placing virtual objects in the real world) or a safety-critical nature (e.g., localisation of semi-autonomous ground vehicles) with (ii) large bandwidth requirements, demand proactively allocated time and spectrum resources, which may generate a penalty in data rate. The different demands in the time-frequency grid are visualised in Figure 3-7.

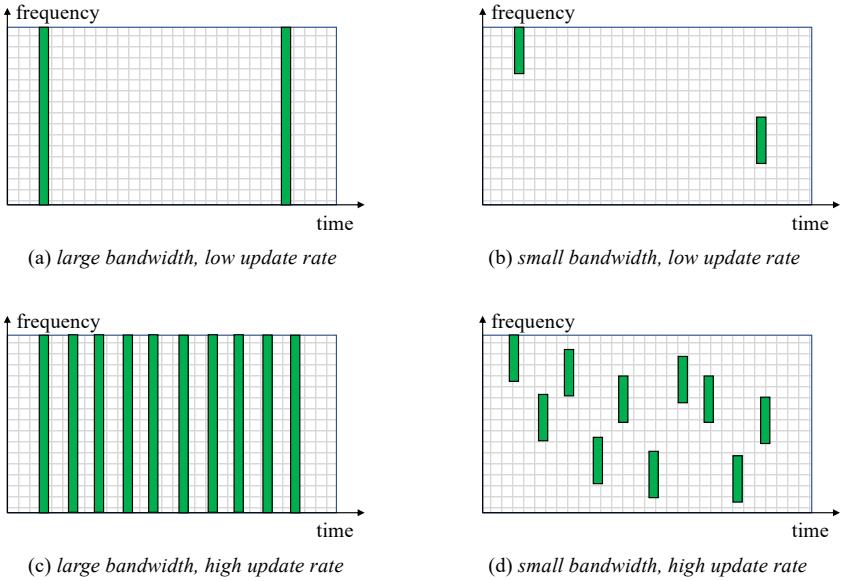

Figure 3-7 Localisation and sensing use cases have a variety of demands in terms of time and spectrum resources. The green boxes represent the resources allocated to support the localisation or sensing requirements. Use cases with high localisation accuracy requirement demand large bandwidth, while use cases with stringent latency requirements demand high update rate.

Applications with extreme requirements on localisation and sensing accuracy, such as those in the context of robotics or virtual reality, may have such extreme spectrum demands that the communication service is jeopardised. To mitigate this, the joint communication and sensing paradigm from Section 1.3.2 can be applied, so that the same spectrum at the same time can be used for both communication and sensing/localisation services. The allocation of spectrum resources is further explored in Section 3.2.3, where resource allocation is covered.

3.2.2.4 Adjacent channel leakage

At upper mm-wave and beyond, the RF hardware components used to generate the transmit signal are less ideal and tend to inflict more hardware impairments than at lower frequencies. For wireless communications this is typically handled by introducing larger guard bands between channels, or, alternatively, a performance degradation is accepted in the presence of interference. Sensing and localisation can more easily cope with degraded signal-to-interference-and-noise-ratio (SINR), since the effect of adjacent interference and noise can be mitigated by using longer integration times at the cost of increased latency. This assumes that the environment is changing slowly relative to the required integration time and that noise and interference are zero-mean.

Different parts of a frequency band, available for communication and sensing, are affected differently by adjacent channel interference. The band edges are normally subject to more interference than the centre of the band. Thus, since sensing is less sensitive to interference than communication, it could be possible to allocate channels on the band edge for sensing and use the centre of the band for communication.

3.2.3 Resource allocation

Given the allocated spectrum, time-frequency resources should be allocated to optimize the real-time performance of both localisation and sensing and enhance communication functionalities. In this section, these two facets are discussed. In this section, the whole analysis is focused on ISAC/JCAS, however, similar principles apply to the field of positioning.

3.2.3.1 Radio interface

ISAC/JCAS refers to the integration of sensing capabilities in communication networks. The success of this process, especially in terms of cost, heavily relies on the efficient and smooth reuse of the available and future communication spectrum and infrastructure. Towards this direction, it is important to harmonise as much as possible of the radio interface for radar sensing and communication. Thus, special care should be given to the underlying waveform used for communication and sensing, which determines the radio access to a large extent. As 4G and 5G adopted the OFDM and discrete Fourier transform spread-OFDM (DFTS-OFDM) waveform for their radio access network (RAN) operation and most likely 6G will also use these waveforms for most its allocated spectrum, complexity and cost reasons strongly motivate the use of OFDM-based sensing. Therefore, the focus of this subsection is on the potential radio interface, procedures, and scheduling algorithms used by a future 6G network that uses OFDM as the communication and sensing waveform.

A well-known advantage of OFDM is that it can form a two-dimensional grid of decoupled time and frequency resource elements (REs). This characteristic of OFDM can be used for implementing a wide range of flexible ISAC/JCAS systems. Focusing on the important elements of the underlying waveform of OFDM, two broad groups of ISAC/JCAS systems can be identified based on the way that radio resources are used. The first group includes systems where sensing and communication occupy different REs of the OFDM time-frequency (TF) grid. The other group of systems includes setups where there is no distinction between the REs used for sensing and communication. Even though there are several aspects that differentiate these two groups, they can both be implemented using the same OFDM circuitry, which results in a harmonised radio interface.

3.2.3.2 Procedures

A typical example of OFDM-based ISAC/JCAS of the first group, where sensing and communication takes place in disjoint REs, is given in Figure 3-8. In this figure, communication data and a train of pulses are allocated at the same time-frequency grid but in different REs. In Figure 3-8, W is the bandwidth allocated for radar sensing, T_{OFDM} is the OFDM symbol period, and T_{rep} is the repetition interval of pulse in a train of pulses. In such a system, the REs used for communication can be filled with constellation points of a given modulation and coding scheme (MCS). In contrast, the REs used for sensing can be filled with dedicate reference signals (RSs) for sensing or already existing communication RSs, for example RSs for channel state information (CSI) estimation. As discussed in [HEX21-D12] and based on a radar link budget analysis, the utilized bandwidth W, T_{rep}, and T_{OFDM}, determine the performance of a radar measurement in terms of ranging and radial velocity. Furthermore, the subcarrier spacing for a given bandwidth allocation determine the pulse repetition interval which determine the unambiguous (maximum) range. Also, in OFDM-based ISAC/JCAS, which uses only cyclic prefix and not a guard interval, the maximum range is also limited by the duration of the cyclic prefix, which needs to be longer than the maximum time of flight of a pulse. Finally, the time duration of the pulse repetition interval, combined with the cyclic prefix duration plus any delay due to processing, multiplied by the number of pulses in a train of pulses, determine a lower bound on the latency of a sensing procedure.

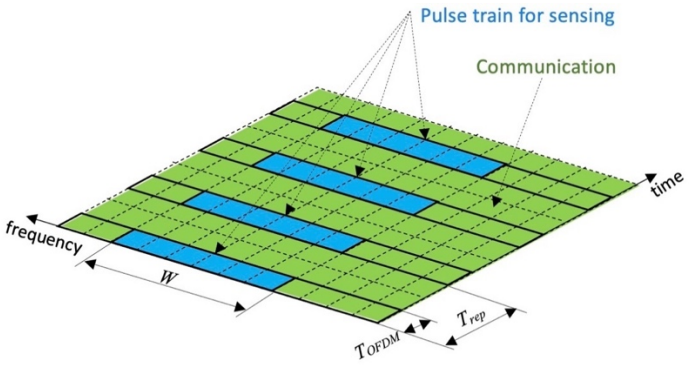

Figure 3-8 An example of resource allocation in an OFDM-based ISAC/JCAS system.

Clearly, in OFDM-based ISAC/JCAS, when sensing and communication are undertaken using disjoint REs, its performance is limited by the exact allocation of the REs used for sensing. One way to overcome this limitation, without reducing the volume REs used for communication, is to undertake sensing and communication using the same REs. In terms of complexity, the simplest approach to achieve this is to use the information-carrying modulated constellation points. This means that the sensing receiver should be aware of the transmitted data. This requirement can be satisfied intrinsically in monostatic sensing where the transmitting and receiving points are co-located. Such an example is given in Figure 3-9.a where BS senses a target. An example of bistatic sensing where the receiver is aware of the transmitted data is given in Figure 3-9.c where a transmitting remote radio unit (RRU) and a receiving RRU are connected to central processing unit. Obviously, the previous scenario can scale in multi-static sensing, as long as the existing RRUs are connected to a central processing unit.

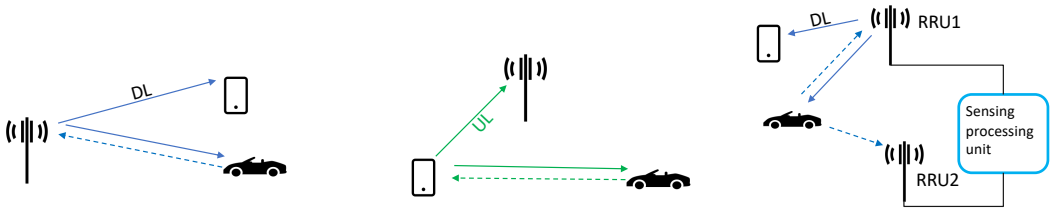

a. DL monostatic sensing b. UL monostatic sensing c. DL bistatic & monostatic sensing

Figure 3-9 Monostatic (a., b., and c.) and bistatic (c.) radar sensing using the information carrying modulated data.

An alternative approach to undertake sensing using the transmitted modulated data is based on the recovery of the transmitted signal in the intended JCAS receiver via the appropriate demodulation process. In this case, it is possible to form bistatic sensing between the communication transmitter and receiver. Such an example is given in Figure 3-9.b, where bistatic sensing can be performed both in the uplink and downlink.

In a point-to-point communication link, the objective is generally to maximize the transfer of data from the transmitter to the receiver in the shortest time possible. This means that, for a given SNR, the modulation order should be as high as possible. In contrast, this is not necessary the case for sensing. A transmitted signal generated using a high order modulation (HOM) has no flat spectrum and thus no perfect periodic auto-correlation function (ACF). In addition, the frequency-domain matched filtering (MF) of the received signals generated with HOM constellations results in high side lobes. This can be seen clearly in Figure 3-10, where the ACF of a signal generated using quadrature phase shift keying (QPSK) is compared against the ACF of a signal generated using 64-quadrature amplitude modulation (QAM). One possible solution is to avoid using HOM, resulting in lower spectral efficiency.

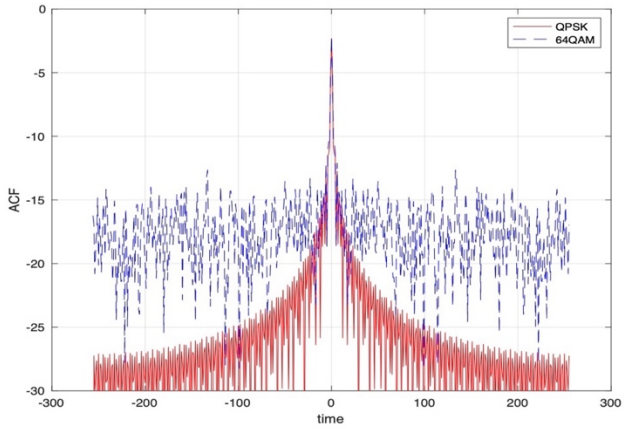

Figure 3-10 Autocorrelation function of a OFDM transmitted signal using QPSK and 64-QAM (300 subcarriers, 512 FFT size).

The previous conclusion motivates the search of alternative receivers than the classical MF for radar processing. Even though MF maximizes the receiver SNR, an alternative receiver might have a better behaviour in terms of side lobes. In this section, the behaviour of the well-known zero forcing (ZF) and minimum mean square error (MMSE) receiver are explored. Given that the received signal, in the frequency domain, is expressed as, $\mathbf{y} = \mathbf{h} \odot \mathbf{x} + \mathbf{w}$, where, $\mathbf{h} \in \mathbb{C}^{N_{sc}}$, is a vector that contains the frequency-domain channel taps; $\mathbf{x}$ is the transmitted signal in the frequency domain; $\mathbf{w}$ is the additive noise; $\odot$ stands for the Hadamard product; and, N_{sc} is the number of sub-carriers. Also, the frequency domain, the noise free: i) MF is expressed as, $\hat{\mathbf{h}} = \mathbf{x}^* \odot \mathbf{y}$; ii) ZF reception is given as, $\hat{\mathbf{h}} = \mathbf{x}^{-1} \odot \mathbf{y}$; while iii) MMSE reception is written as, $\hat{\mathbf{h}} = \mathbf{x}^*(\mathbf{x}^*\mathbf{x} + \sigma^2\mathbf{I}) \odot \mathbf{y}$, where σ^2 is the regularization factor. Focusing on the idealistic case of noise-free reception, Figure 3-11 presents the time domain output of MF, ZF and MMSE reception when the linear processing is undertaken in the frequency domain. This is done for the case of a transmitted signal generated using QPSK and a transmitted signal generated using 64-QAM. As shown in Figure 3-11.a, with MF reception high side lobes are created when 64-QAM is used. However, the observation of Figure 3-11.b and Figure 3-11.c shows that when ZF or MMSE reception is used, there is no difference between the use of QPSK and 64-QAM. From this, it can be concluded that ZF and MMSE reception have a better behaviour, in terms of side lobes, when compared to MF reception.

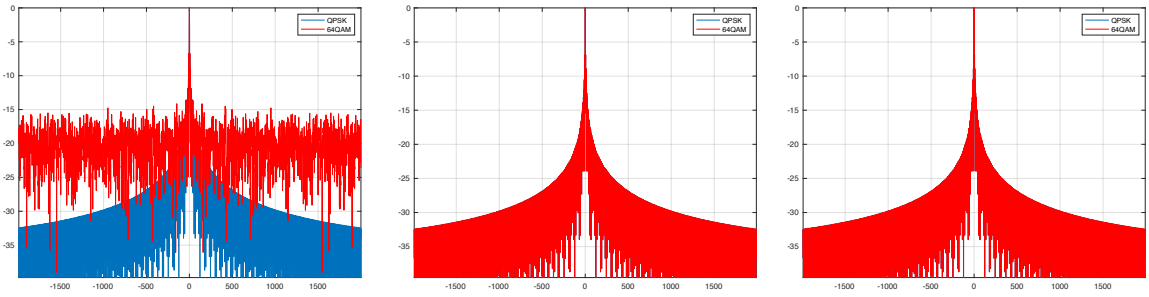

a. Matched filter receiver, no noise

b. Zero-forcing receiver, no noise

c. MMSE receiver, no noise

Figure 3-11 The output of MF, ZF, and MMSE reception (processing) for the idealistic case of noise-free signal reception. The red curves show 64-QAM, while the blue curves show QPSK.

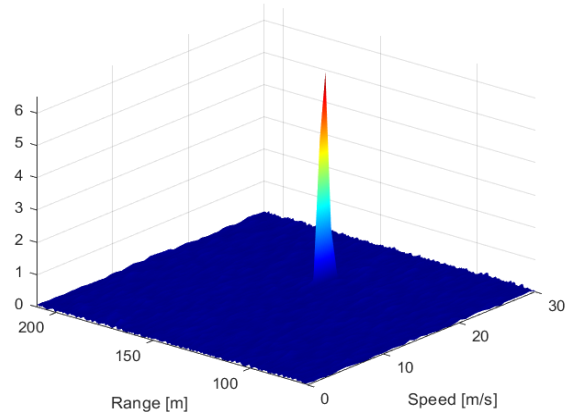

a) 64QAM, MF, SNR = -5dB

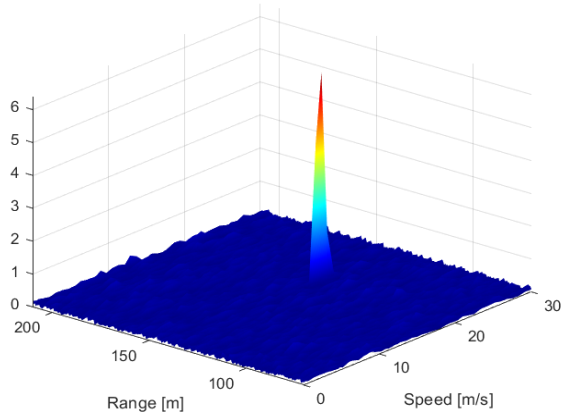

d) 64QAM, MF, SNR = -5dB

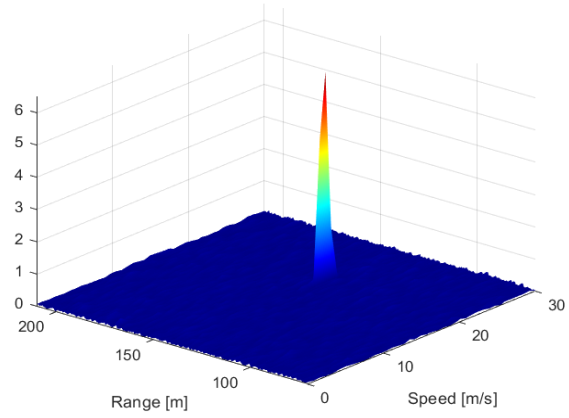

b) QPSK, ZF, SNR = -5dB

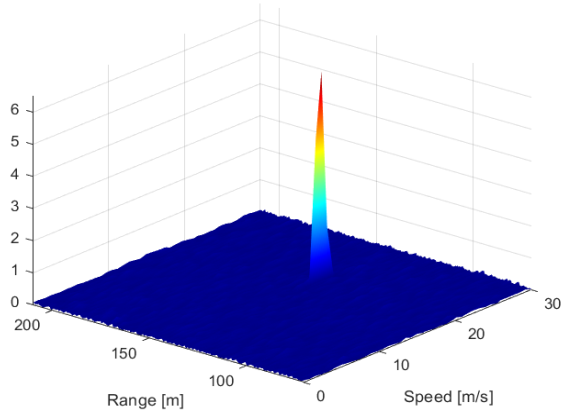

e) 64QAM, ZF, SNR = -5dB

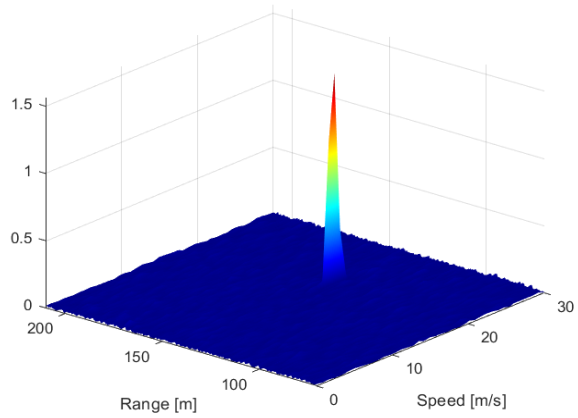

c) QPSK, MMSE, SNR = -5dB

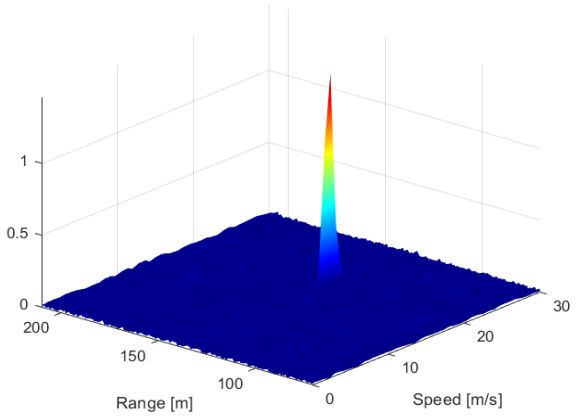

f) 64QAM, MMSE, SNR = -5dB

Figure 3-12 The effect of the use of HOM, in relative high SNR, in the Doppler-Delay grid in the receiver when MF, ZF, and MMSE reception is used.

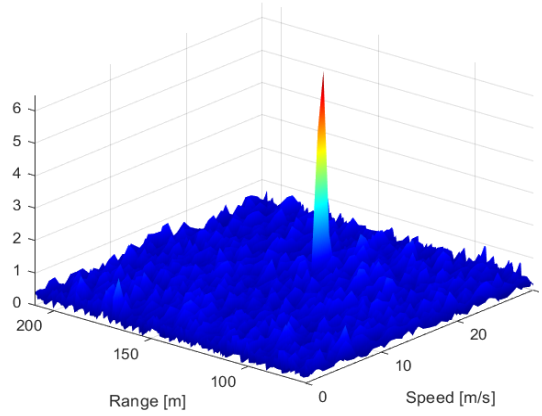

a) QPSK, MF, SNR = -20dB

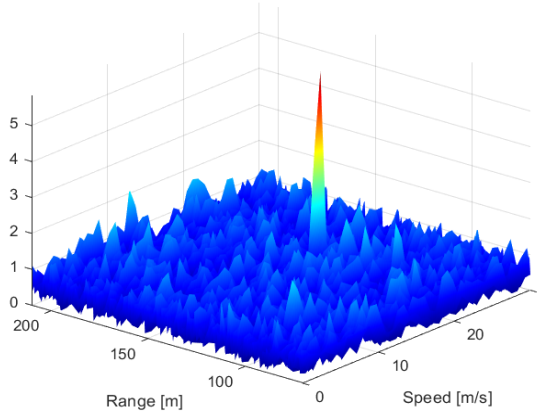

c) 64QAM, MF, SNR = -20dB

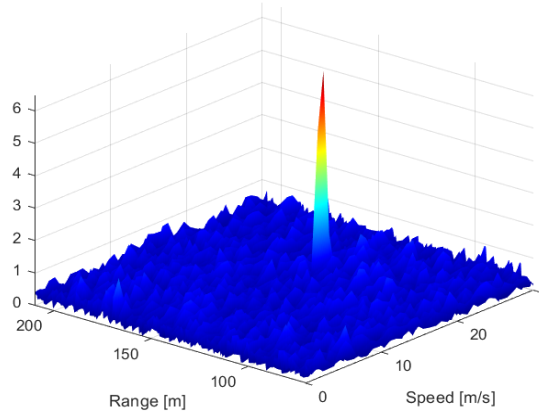

b) QPSK, ZF, SNR = -20dB

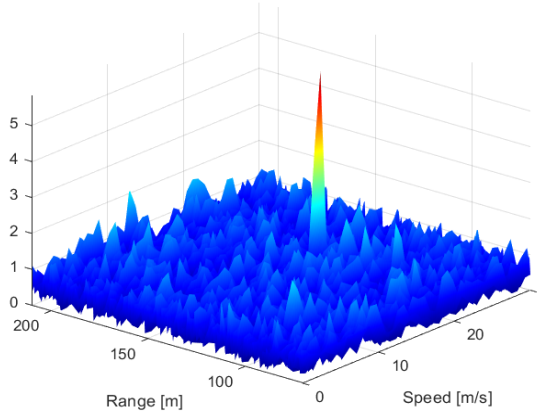

d) 64QAM, ZF, SNR = -20dB

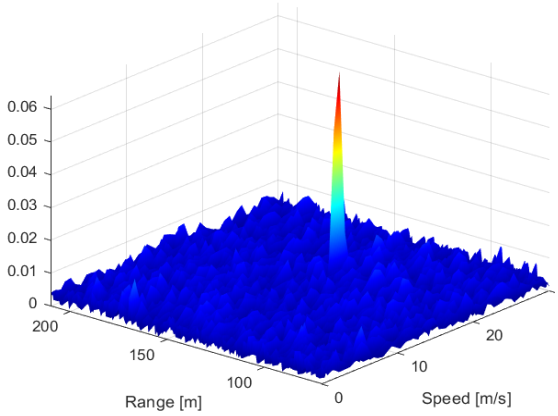

c) 6QPSK, MMSE, SNR = -20dB

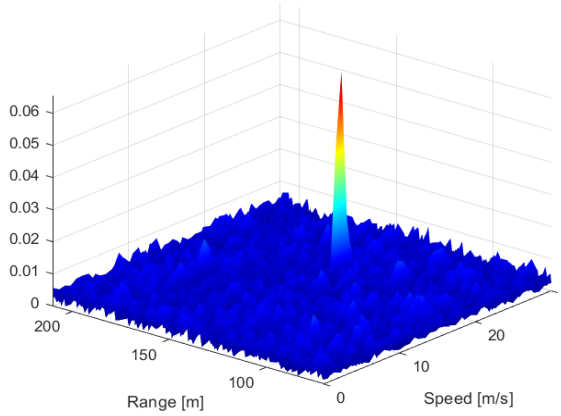

e) 64QAM, MMSE, SNR = -20dB

Figure 3-13 The effect of the use HOM, in relative low SNR, in the Doppler-Delay grid in the receiver when MF, ZF, and MMSE reception is used.

For drawing a complete conclusion, the performance of the previous receivers should be characterised under the presence of noise. For this reason, Figure 3-12 presents the Doppler-delay (DD) grid expressed in terms of range and velocity when the transmitted signal is again generated using QPSK and 64-QAM. The operating SNR is -5 dB, which, for the sake of this comparison, could be considered

as a relatively high SNR. Note that the SNR is defined per symbol (i.e., RE) meaning that QPSK and 64-QAM have different E_b/N_0, where E_b is the energy per bit and N_0 is the noise power spectral density. As can be seen in Figure 3-12.a, Figure 3-12.c, and Figure 3-12.e, when QPSK is used MF, ZF, and MMSE reception have the same effect as the DD grid. However, comparing the influence of MF when 64-QAM is used, some ripples start to form in the place where there is no target, because of the side lobes of MF. In contrast, for the case of ZF and MMSE reception, these ripples cannot be observed. This means that, in high SNR, ZF and MMSE have good behaviour in terms of side lobes.

The performance of MF, ZF, and MMSE reception is illustrated in Figure 3-13, for an SNR equal to -20 dB (low SNR). As shown in Figure 3-13.b, for the case of MF, for 64-QAM, there are strong ripples due to the strong sidelobes of MF reception. In contrast, as shown in Figure 3-13.d, for the ZF reception of 64-QAM, there are strong ripples. However, these ripples are not due to the strong side lobes but due to the noise amplification of ZF reception. Figure 3-13.f shows that for MMSE reception the use of 64-QAM does not create a bad behaviour in the DD grid.

Finally, from the previous analysis, the following conclusions can be drawn. First, HOM can have large side lobes with a MF receiver at high SNR. Second, HOM does not create side lobes with a ZF receiver, however, at low SNR there is noise amplification. Finally, the MMSE receiver performs similarly to ZF at high SNR, and similarly to MF at low SNR. MMSE seems to be the preferred receiver over all SNR range.

3.2.3.3 Scheduling in the space-time-frequency grid

Additionally, the complete localisation of a target in the three-dimensional space requires angular information in addition to the range and Doppler obtained usually from the DD grid. A simple approach to obtain the angular information of a target is via the appropriate beam-sweeping search. The beamwidth of the used beams determines the angular resolution. More specifically, a narrow beam created from a large antenna array corresponds to a better resolution at the cost of a longer beam-sweeping process. This motivates the consideration of the extension of the TF grid to include the space dimension. In this case, the resulting space-time-frequency (STF) grid, of size $N_b \times N_t \times N_{sc}$, becomes the main element where scheduling takes place. Here, N_b, N_t, and N_{sc} is the number of beams of given beamwidth, number of OFDM symbols, and number of subcarriers, respectively, used for a sensing procedure.

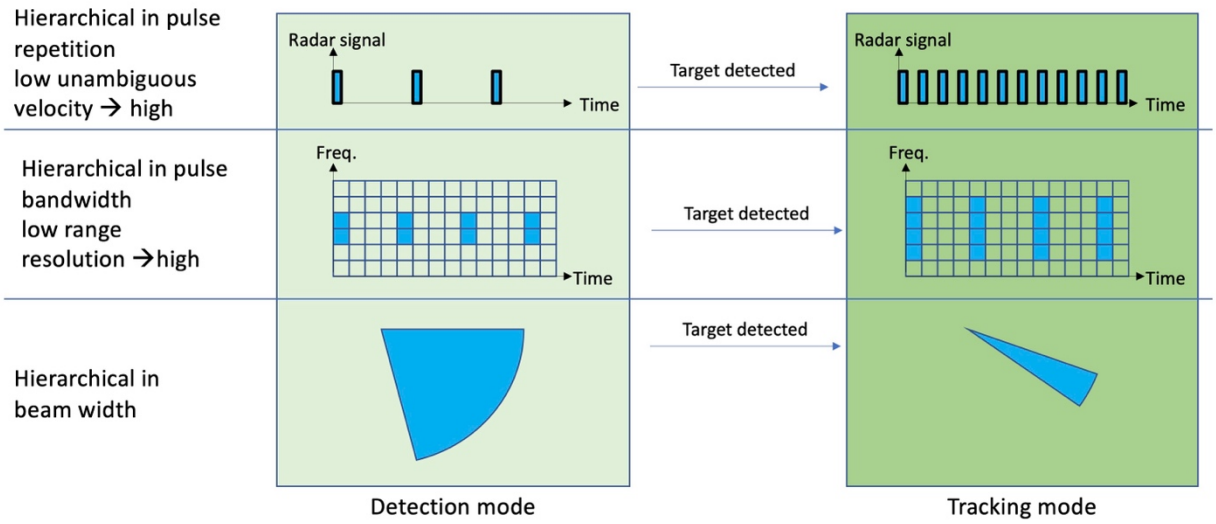

Figure 3-14 Principles of hierarchical radar sensing for scheduling in the STF grid.

Irrespective of whether sensing is taking place using dedicated RSs or the actual information-carrying signals, for a given sensing evaluation metric, the objective is to reduce overhead, i.e., to minimise the number of occupied points used for sensing in the STF grid. A simple and efficient approach to achieve this is the introduction of a detection and a tracking mode. In particular, the detection mode can be used for detecting targets using low overhead. The detection mode could be constantly on, or it could be

periodically activated. In contrast, the tracking mode should be only activated when a target is detected. Upon the activation of the active mode, the required resources in the dimension of interest of the STF grid are occupied and used for sensing.

Figure 3-14 presents the transition from the detection mode to the tracking mode for cases where more resources are needed in the time, frequency, and space dimension. In radar sensing, when a higher unambiguous velocity is needed, more resources need to be allocated in the time domain. In contrast, when higher range resolution is needed, more elements in the frequency domain need to be allocated. Finally, when higher angular resolution is needed, the value of N_b needs to be increased with the concurrent use of beams with narrower beamwidth. The previous framework is very flexible apart from the separate utilisation and scheduling of the space, time, and frequency resources, it allows the joint utilization and scheduling of two or three dimensions of the STF grid. This is possible with a dedicated scheduling algorithm.

3.2.3.4 Proactive resource allocation

An equally important aspect of resource allocation relates to the use of localisation and mapping information to optimize communication performance. Thanks to highly accurate mapping and localisation information, including (planned) trajectories of mobile/nomadic users, advanced resource allocation methods can be designed to achieve better system performance. Here, the resource could come from, time, frequency, as well as spatial domain.

For flexible resource planning, how to utilize sensing/localisation information, or its prediction, to fulfil the communication needs, in combination with trajectory, resource and spectrum planning through system simulations, is investigated in [HEX22-D72].

As one example, to solve the problem of avoiding dynamic blockage as well as channel aging, one can utilize context-information-assisted communications, as shown in Figure 3-15. With advanced sensors and localisation techniques, the BS could potentially predict the position of not only the UE, but also the blockers, and this information could be useful for dynamic blockage avoidance. Moreover, channel quality variations could be mitigated by using the recently proposed concept of predictor antenna (PrA) [GMD+21]. A PrA system refers to a setup with two groups of antennas deployed on the top of a vehicle, where the front antennas (called PrAs) sense and report back the CSI to the BS. Then, the receive antennas (RAs) followed behind the PrAs could use the CSI from PrAs when they reach the same positions at the PrAs. In this way, both prediction of blockage and the quality improvement of CSI lead to better system performance. Using recently proposed reconfigurable intelligent surfaces (RIS) instead of BS handovers could further increase the flexibility in spatial resource allocation and reduce the operation cost.

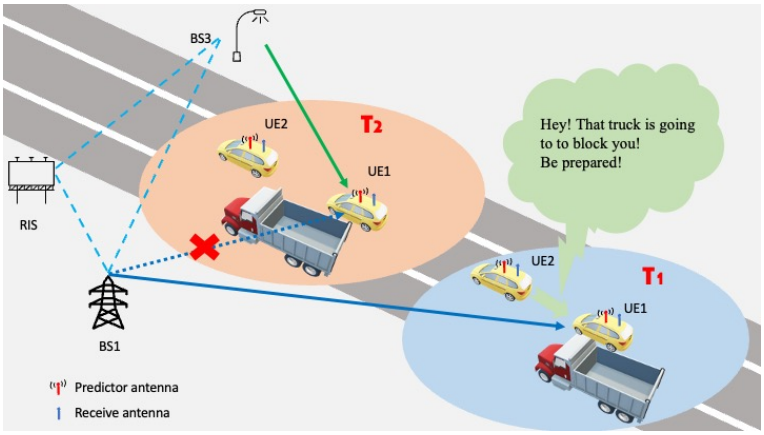

Figure 3-15 Better resource allocation with localisation and sensing assistance [GMA+22].

3.2.4 Infrastructure optimization

Limitless connectivity is one of the major goals in the next-generation wireless network, where the communication services will cover all the users in the urban and rural areas [MLH21]. However, coverage for localisation and sensing services is more challenging to be satisfied compared with communication. In the asynchronous scenarios without geometrical constraints, at least four BSs are needed for TDoA-based localisation, and at least two BSs with LOS paths are needed for angle-based localisation. In sensing scenarios, since tandem channels (e.g., transmitter (Tx) to the object and object to the receiver (Rx)) are involved, the received signal power is the bottleneck limiting the coverage. As a result, the infrastructure designed for communication may not be sufficient for localisation and sensing services.

A direct but costly solution is to increase the number of deployed BSs. However, it is impractical due to the coordination and deployment cost, and sometimes unnecessary as the service request usually has peak hours (e.g., commuting period on workdays) and off-peak hours. Several alternative solutions are promising (see also Figure 3-16):

1. *The deployment of low-cost anchors* [CKA+23a]. For localisation and sensing purposes, BSs with full communication capabilities may not be needed, and low-cost anchors that can transmit and receive (and probably with processing capability) are sufficient. These anchors could be roadside units tailored for localisation and sensing, or passive reconfigurable surfaces. Sidelink communications are needed to coordinate the services between the anchors and target devices such that the resource at the BS can be saved.
2. *The integration of terrestrial and non-terrestrial networks (NTN)* [HST19]. The advantages of adopting NTN for localisation and sensing lie in two aspects. On the one hand, a BS with a higher altitude provides better coverage (e.g., less blocked by the buildings in the urban area) and 3D localisation performance, especially on the height. On the other hand, the geometry constraints are less stringent. For example, a UAV carrying a BS can travel in three dimensions and is able to organize the network flexibly and adaptively. The role of non-terrestrial networks

Figure 3-16 Infrastructure optimization includes both the terrestrial network and the non-terrestrial network.

NTNs are expected to play an essential role in localisation and sensing for 6G. NTN refers to space-borne and aerial communication networks, such as satellites or UAVs. The integration of NTN in 6G communication systems provides several advantages, including increased coverage, positioning accuracy, and synchronization [KG21]. One of the main advantages of NTN in localisation and sensing is the ability to provide coverage in areas where terrestrial networks are not available or are difficult to access, such as remote or disaster-struck areas [PFS+22]. This is particularly important for applications such as search and rescue, disaster management, and precision agriculture. Additionally, NTN can provide a complementary coverage layer to terrestrial networks, helping to increase accuracy and reduce errors in localisation and sensing applications.

One of the key technologies that is enabling NTN to play a larger role in positioning and sensing is the use of *low-Earth orbit (LEO) satellites*. LEO satellites can provide a higher update rate and increased availability compared to traditional geostationary satellites. Several LEO systems are currently available such as e.g., Iridium, OneWeb, and Starlink (for broadband connectivity), Hiber, Myriota (for Internet of Things applications), and Iceye, HawkEye (for Earth observation and synthetic aperture radar applications [PFS+22]. In addition, LEO satellites also have the potential to provide precise localisation and sensing which is still not yet to be harnessed. Another important aspect of NTN in localisation and sensing is the use of UAVs as communication platforms. UAVs can be used to provide temporary coverage in emergency situations, or to provide coverage in hard-to-reach areas such as mountainous regions. Additionally, they can be used to provide additional sensing capabilities in areas with high traffic demands, such as stadiums or concert venues. UAVs can provide high-resolution imagery, environmental sensing, and other location-based services.

The integration of NTN for 6G requires careful consideration of various factors, which are also present in GNSS. One of the most critical factors is the synchronisation of the NTN with the terrestrial network. This is important to ensure that the positioning information provided by the NTN is accurate and consistent with the terrestrial network. Additionally, the Doppler effects and path loss caused by the movement of the satellites and the atmosphere must be considered [PFS+22].

3.2.4.1 Deployment optimization

All the mentioned solutions require dedicated infrastructure optimization to fully exploit the network potential for providing localisation and sensing services that satisfy stringent and diverse requirements, such as accuracy, latency, and processing speed. To meet these requirements, optimisation problems need to be formulated, which, in general, consists of an objective function and a set of constraints. The objectives include the system KPIs such as communication and localisation coverage, and the variables include BS positions, beamforming matrix, and more details can be found in [CSB+22]. Potential optimization problems for the mentioned three solutions can be summarized as follows:

- *Anchor layout optimization:* If the number of anchors (e.g., BSs or RISs) and service area are determined, the positions of anchors can be optimized based on the localisation coverage (e.g., percentage of area with Cramér-Rao bound (CRB) performance satisfying the requirements using a predefined codebook). Prior information of the target UEs (e.g., geometrical distribution of UEs) and environmental information (e.g., the geometry of the detection area and position of the blockage) can also be used to optimize the layouts and achieve the best localisation performance. For the BSs with antenna arrays or directional antennas, the orientation should also be optimized.
- *UAV trajectory optimization.* When the anchor positions can be controlled (e.g., UAV BSs), objective functions can be formulated as maximizing the determinant of the Fisher information matrix (FIM) over a finite time horizon, as the inverse of FIM prescribes a lower bound of the estimation error covariance of an unbiased filter [Tay79]. Performance measure of observability based on geometric conditions can also be utilized as a cost function, and a closed-form solution considering physical constraints is derived in [HST19].
- *Adaptive network configuration.* When requesting localisation and sensing services, multiple entities are envolved. However, not all the UE devices are able to process the measured data, and the BS might be crowded with data transmission and processing requests. For this reason, adaptively changing network configuration and providing computing, storage, and communication functionalities at the network edge helps not only in reducing the end-to-end delay, but also can alleviate the burdens on cloud servers and backhaul links [ASE+19]. In addition, UE devices with powerful computational capability could also be utilized in certain scenarios to guarantee the overall localisation and sensing performance of the system.

In summary, infrastructure optimization can provide the coverage and delay requirements for localisation and sensing. In addition, mobile BSs and the function configuration of different devices can provide extra flexibility in serving different scenarios (e.g., rush hours). Localisation and sensing information are both important for offline and online infrastructure optimization. For example, user

location distribution and map information are useful in the offline BSs / anchor deployment phase. While for online infrastructure optimization (e.g., deployment of mobile BSs), location estimation and dynamic prediction of all the available UEs are critical to minimize the defined optimal objective function. In general, infrastructure optimization is highly non-convex, and it is thus hard to obtain globally optimal solutions. Heuristic algorithms and learning-based methods could be alternative time-saving options to get satisfactory suboptimal results.

3.3 KVIs and implications

Key value indicators [HEX20-D11, HEX21-D12] for localisation and sensing regarding *trustworthiness*, *inclusiveness*, and *sustainability* complement the KPIs from Section 3.2. The KVIs are discussed and analysed in the following sections.

3.3.1 Trustworthiness

Trustworthiness for localisation and sensing plays an important role especially when the measurements are applied in critical use cases and scenarios. The trustworthiness for localisation and sensing measurements must be higher for use cases such as secure track and trace, secure location-based access control, or security gates [HEX22-D32] or within factory environments when collision avoidance between humans and machinery must be guaranteed for human safety. Other, less critical use cases, such as monitoring material flow or sensing weather conditions should also be trustworthy, but with less stringent requirements. Systems that aim for trustworthiness need to consider many aspects, for localisation and sensing we focus on *Security*, *Safety*, and *Privacy*.

3.3.1.1 Security

The term security can be considered in two different ways in the domain of localisation and sensing (see Figure 3-17): (i) localisation and sensing information used for security applications and (ii) securing the localisation and sensing process itself. Both dimensions are further elaborated below.

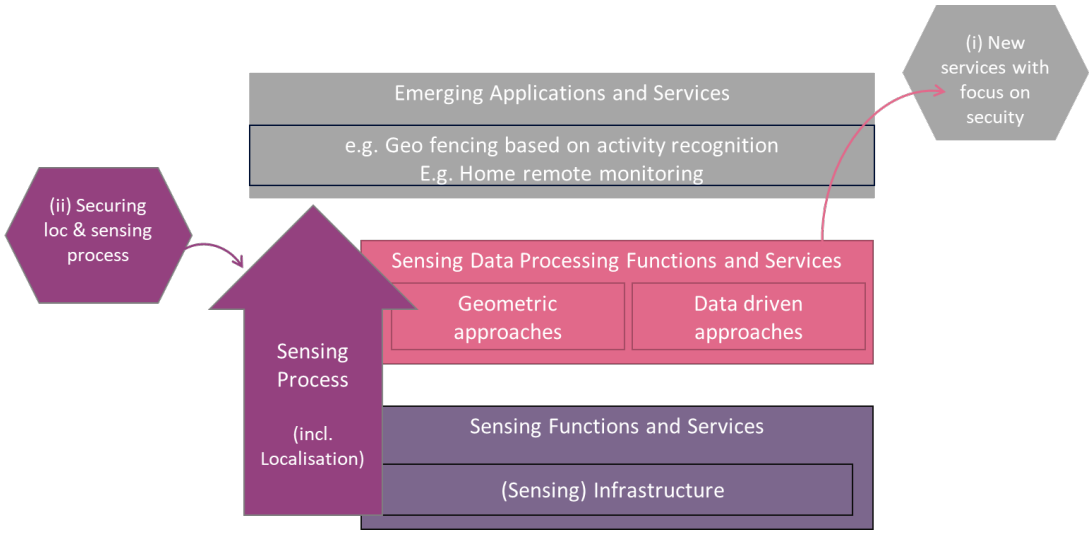

Figure 3-17 Overview of the two interpretations of the term security in the localisation and sensing domain.

Usage of localisation and sensing information to enable new emerging 6G (security) services and applications.

[HEX22-D32] lists several scenarios where localisation and sensing information can be used to enable new security use cases. One example is remote home monitoring for security by receiving alarms when movement or activity is detected when nobody is supposed to be at home. Another example is location-based access control. Geographic information / geo-locations are used to decide whether a person gets access granted to, for example, specific data or a specific IT system. Geo locations can be used directly

as decision parameters (if a certain person is at a certain position, then a specific action is triggered) on the application layer, or the geo-location could be included in a more sophisticated way in an end-to-end established cryptographic algorithm and protocol between the information provider and the information consumer. The latter geo-encryption is a special research area where systems and algorithms are designed to protect against location bypassing or, in parts, also against location spoofing [SD03]. These algorithms are independent of the localisation system source (GPS, Bluetooth, or a 5G localisation system). Next-generation mobile networks can deliver information, such as location, velocity, or orientation that could be used in such algorithms, but also, situational context gathered via sensing could be helpful in the future (current surrounding/environment sensed by the mobile network, such as urban environment, human-crowded area, etc.).

Securing the process of localisation and sensing

Depending on the security level demanded by certain use cases, applications and scenarios, requirements can be deduced for each security attribute. From the localisation and sensing perspective, security mechanisms on all layers are equally important as for communication that protect the system must against intentional harm or unauthorized access. An interesting aspect is how the system can support localisation and sensing *data integrity*. Cyber security for the communication system focuses on sending data from application to application in a secured/encrypted way. But in the case of localisation and sensing, meaningful data is generated out of measurements on signals travelling over the air. Such measurements can be an angle of arrival of a signal, or the time of arrival (at UE or base stations side), etc.

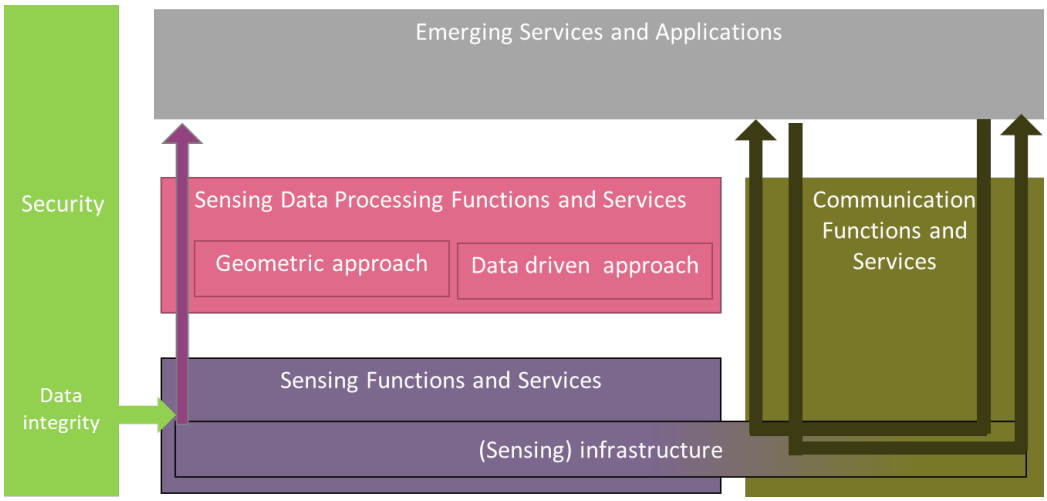

Figure 3-18 Difference between sensing and communication process (application to application for communication and infrastructure to application for sensing) and the security challenge for data integrity when sensing data is generated in the infrastructure layer.

Figure 3-18 shows that on an abstract level, communication over a network is bidirectional from application to application, but measurements for sensing and localisation are generated by the infrastructure of the network and have their origin on that layer. With SDR (software defined radio) mechanisms combined with open-source code becoming more common and cheaper, the risk of attacks becomes more likely. Depending on the measurements used, attack modes and mitigation features may differ. [SRR+22] focuses on ranging methods in OFDM systems. Here, certain attack modes can result in wrong distances between two communication units: distance enlargement via overshadowing symbols or carrier frequency offset attacks and distance reduction due to early detect late commit (ED/LC) effect. In ED/LC scenarios attackers for example reduce the distance measured by pre-emptively injecting signals that triggers an early signal detection at the receiver side. With no security features on PHY layer, the receiver has no means to detect such a falsification, which will lead consequently to a wrong position. The authors of [SRR+22] propose a solution called V-range which uses shortened OFDM symbols which the receiver uses for the integrity check of ToA estimates. This approach can work in the sub-6 GHz and mm-wave bands intended for 5G. For further work, it should

be systematically and thoroughly researched what attack modes and possible mitigation mechanisms exist per measurement type.

3.3.1.2 Safety

Safety may seem similar to the term security but there are distinct differences. While security refers to the protection of systems (and data) from intentional harm or unauthorised access (with focusing on preventing cybercrime attacks), safety refers to the protection of humans, equipment, or the environment from accidental or unintended harm through systems. Both aspects are important to consider and in practice they often may influence each other. As an easy example, consider a fire door: For safety it would be best if this door is always unlocked to let people escape easily in case of an emergency. For security reasons the door should always be locked to prevent unauthorized access to the building.

For safety, localisation and sensing can be used as supportive system to lower the chances for harming the environment, equipment, or humans. In the field of safety though, many requirements are reflected in standards and regulations monitored by different authorities. The difference for localisation and sensing being just a supportive system or a system which safety relies on will be explained in the following two paragraphs.

Localisation and sensing information can be used to support "safety use cases"

Safety applications exist in various domains. And usually, safety related applications aim for the goal of humans and the environment being protected from danger, risk, or injury. Depending on the application requirements, it may be necessary that system components or even the whole localisation and sensing system must be developed according to safety regulations to guarantee functional safety, explained in detail in the next section. An example where functional safety development and implementation is not necessarily required is managing streams of people. In addition to existing measures to prevent harm from mass panic (like fences or the maximum amount of people allowed in a certain area), knowing the position and movement patterns of people can help to predict aggregation and crowd building. Thus, allowing early prevention measures.

In factory environments, collision avoidance between humans and autonomous guided vehicles (AGVs) is currently achieved by attaching certified laser sensors that guarantee obstacle detection in the AGV's trajectories that when triggered lead to an automated stop of the AGV (to prevent harming people). If replacement of such sensors is desired by using a localisation system for AGVs and humans in order to prevent collisions, the localisation system needs to guarantee a similar failure free working mode as the certified sensors which will be explained in more detail in the next paragraph.

Where standard / non failsafe localisation can help in the collision avoidance scenario is to plan routes of AGVs according to humans' positions. If AGVs can avoid the routes with high human traffic the chances that the certified sensors detect human obstacle decrease.

Failsafe localisation and sensing system

In the factory / electronic devices and systems domain of, safety mostly refers to functional safety which comprises a set of regulations and standards that need to be followed while designing and building a failsafe system. Performing the localisation and sensing process must ensure that humans are not harmed, and regulatory aspects are followed (e.g., to not exceed allowed transmit power). Depending on the scenario and environment where it will be deployed, the safety integrity level required and the regulatory requirements for each country differ. Functional safety standards for electronic devices are for example ISO 13849 or IEC EN 61508. Standard safety aspects like for example electric and radiation safety which apply anyways for the mobile communication network must be also ensured for example for dedicated signals only used for localisation and sensing purposes.

However, a very challenging task that is special for localisation and sensing is the guarantee of the **position and sensing integrity** itself. Data integrity is important, both for security and safety. Security ensures data integrity against attack modes; safety needs to ensure data integrity by implementing certain safety measures to avoid wrong behaviour leading to falsified position and sensing data.

Position information, as an example, can be falsified by intentional attacks but also due to malfunctioning of the system or simply by physical effects like non-line-of-sight conditions. Integrity assurance mechanisms and receiver autonomous integrity monitoring (RAIM) already exist in global navigation systems (GNSSs) to strengthen the trustworthiness of the calculated position information for those applications [RHC+19].

Quantifying positioning integrity requires formulating an upper bound on the instantaneous positioning error, known as the protection level (PL), for each position coordinate individually or for two/three coordinates together, to ensure the desired level of confidence. Specifically, PLs determine a geometric region with a predefined shape, and they are computed in such a way that the probability of the true user position being outside of this geometric region is lower than the target integrity risk (TIR) - a very small number given by the underlying application.

To illustrate this, consider in Figure 3-19, the blue circle surrounding the estimated position in smartphone navigation, which changes its radius according to the real-time PL computed for the desired 99.99% confidence level in the position estimate. It is crucial that the computed PLs are sufficiently tight to maximize their utility across various applications.

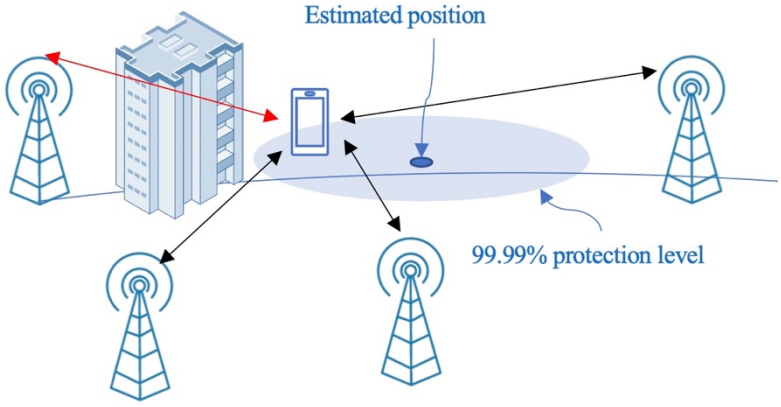

Figure 3-19 Example of integrity under non-line-of-sight conditions (red link). The size of the protection level depends on the target integrity risk and surrounds the estimated position.

3.3.1.3 Privacy

With sophisticated and accurate localisation and sensing, the topic of privacy becomes both more important and more challenging. There are two aspects of privacy that are considered: privacy of persons/users and privacy of assets.

User privacy

With localisation of UEs already available in current mobile networks, the conditions for protection of this data does not differ much. The protection level needs to follow country-specific regulations e.g., the General Data Protection Regulation (GDPR) regulation in the EU and the California Consumer Privacy Act (CCPA). Obviously, although localisation is an existing feature of current mobile networks, from a user perspective the conditions change drastically as localisation becomes much more accurate and hence more sensitive and more worth protecting [CBK+22]. Especially if there are still open issues regarding how data integrity can be ensured and attack scenarios handled, localisation data must be protected from misuse. The main new challenge comes with the sensing feature. With the new sensing feature, persons can be localised in a radar-like manner and, therefore, be tracked even without carrying any device. The identity of a sensed person is not easily determinable, but with additional context information (like movement patterns or social engineering), conceivable.

Asset privacy

Tracking of objects may not be traditionally in focus of privacy concerns, but if for example objects within factories are being located or sensed, this asset information is worth protecting. Asset or material flow may inherently contain process and/or automation information that shall not be revealed to unauthorised systems or persons.

3.3.2 Sustainability

The second KVI under consideration is sustainability. As with security, there are two facets to sustainability: (i) using localisation and sensing information to make services (including communication) more sustainable (e.g., more energy efficient compared to their conventional counterparts) and (ii) making localisation and sensing itself sustainable, using minimal resources.

Sustainability supported by localisation and sensing

This was discussed, in part in Section 3.2.3.4 (which dealt with proactive resource allocation in order to reduce overheads), and is further elaborated in Section 4.2.7, where the reduction in transmit power is considered. In addition to more sustainable operation of communication, the ability to sense and localise has broader sustainability implications, such as the ability to monitor pollution and weather [HEX22-D32], as well as the more general potential for earth monitoring [HEX21-D31]. More examples, where localisation and sensing have a high impact on sustainability are in the use case of massive twinning. Digital twins, independent of the domain (e.g., twins for manufacturing, twins for sustainable food production, or twins in context of immersive smart cities) include tracking or knowing the position of assets or humans often to optimise processes and to save material, waste, or energy per produced item. The same holds true for autonomous supply chains. To ensure worldwide tracking capabilities also NTN localisation comes into play.

Sustainable localisation and sensing

This has been discussed in detail in Section 3.2.3 and Section 3.2.4, which covered resource and infrastructure optimization. While the optimization generally considers the KPIs, there is an implicit consideration in terms of sustainability, as the allocated resources should be as small as possible, while still meeting the KPIs. By flexible and adaptive resource allocation, conservative designs can be avoided, and energy consumption reduced in comparison to not optimised network deployments. Deployment and operating cost can also be accounted for in the resource optimization processes, e.g., based on reduced-energy devices such as reconfigurable intelligent surfaces (RISs). More generally, the localisation and sensing design should consider the sustainability impacts including the power consumption and material life cycle assessment.

3.3.3 Inclusiveness

The goal of next generation mobile network is to ensure that 6G is available for all people across the world. To achieve that, it needs to be affordable and scalable, with coverage everywhere. So, one aspect of localisation and sensing about inclusiveness is to enable localisation and sensing for all those areas as well and ensure easy configuration and deployment. For localisation and sensing that comes with a re-use of communication signals, this might be easily achievable.

Another scenario where localisation and sensing play a more particular role in inclusiveness is on a much smaller scale. For example [WGP+18], with sensing], it might be possible in the future to recognize gestures of people who are not able to interact with systems (e.g., UEs) in a traditional way (by voice or typing on the keyboard/touchscreen). This could ensure another possibility of human-machine interaction. These novel HMIs are also discussed in [HEX22-D72]. In addition to such intelligent interaction, there is also intelligent monitoring, such as elderly monitoring, chronic patient monitoring, and infant care, which can all benefit from sensing information.

4 Final models and algorithms

Section 3 drew the big picture of the localisation and sensing ecosystem which comprises of the three functional layers: *Sensing layer, Sensing data processing layer* and the *Emerging services and application layer*. This chapter focuses on the technical work and results for selected aspects of each layer. For development localisation and sensing algorithms and to generate synthetic data, accurate models of the channel and hardware components are crucial. These are detailed in Section 4.1. The localisation and sensing algorithms themselves are described in Section 4.2, covering 6D localisation, monostatic sensing, bistatic sensing, ISAC (monostatic and bistatic), deployment optimization, and location-aided communication. This complex interplay between many services can be considered as one example of the new emerging services within the localisation and sensing ecosystem.

4.1 Channel and hardware models

Two types of models are important for localisation and sensing: first, the model of the propagation channel, which includes the information about the transmitters, receivers, and objects around. Second, the models of the hardware and their impairments.

4.1.1 Channel models

Channel models play a critical role in various aspects of communication system design from transmit waveform design to receiver algorithms. Accurate channel models are also needed for system and link simulations to evaluate KPIs. The channel models for sensing depend on the type of sensing system employed. For mono static sensing, both transmitter and receiver are co-located, and receiver uses the backscattered signals from the target for sensing. Assuming a LOS link to the target, the amount of the backscattered signal energy received depends among others, on the geometry of the exposed surface of the object to the transmitter and its reflectivity, which is commonly expressed using radar cross section (RCS). The received signal power from such a radar channel is defined by the radar equation [Sko80]

$$\boldsymbol{p_r = \frac{p_t G \sigma A k_a}{(4\pi)^2 R^4}},$$

Where p_t is the transmitted power, p_r is the received power, R is the distance between the transmitter and receiver, G, A, k_a denotes antenna gain, size, and efficiency respectively. Multistatic sensing, where transmitter(s) and receiver(s) are spatially distributed offers several benefits including better sensing coverage using widely deployed communication infrastructure. To provide extensive coverage, typical 6G systems will be deployed in low, mid, and high frequency bands. Apart from supporting traditional deployment scenarios like urban, semi-urban, and rural scenarios, the 6G deployments will also include newer scenarios arising from air-to-ground, industry, healthcare, etc. Channel models should be general and flexible in addressing the different bands and deployment scenarios for wider adaptability.

For low and mid band frequencies (<10 GHz), the 3GPP models defined in [36.901] provide a low-complexity parametric channel model. These models are extended to consider the elevation angles of the array to support 3D channel modelling in [36.873]. In addition, the channel models for the band between 0.5 and 100 GHz are provided in [38.901]. The 6G channels need to support high frequency bands (up to 300 GHz) with very wide bandwidths (several hundreds of MHz). They also need to support a wide range of deployment scenarios. In many of these scenarios, the distance between the transmitter and the receiver does not exceed the Rayleigh distance, resulting in the need for near-field channel models. There exist many measurement campaigns and modelling techniques for the higher frequency bands above 10 GHz. These include mmMagic [Magic22], NIST channel model [Nist22], QuaDRiGa [JRT+19], NYU WIRELESS [RSM+13], [MRS+15], [RMS+15]. A summary of the large-scale channel parameters such as path-loss, shadow fading, blockage, penetration losses, etc. in high bands is briefly described below.

The line-of-sight (LOS) pathloss typically follows the Friis formula, and the pathloss exponent changes very little with the increase in frequency. However, with non-line-of-sight (NLOS), the pathloss

exponent is higher than in LOS. The ray tracing measurements have indicated that the shadow fading losses at high frequency are larger (more than 10 dB in mmWave bands) compared to the low and mid frequency bands. Measurements also indicate that the delay and angular spread of the channel reduces with the increase in the frequency bands.

The variation of absorption or penetration loss with frequency, depends on the material; for example, for materials such as glass, the penetration loss does not vary significantly with frequency. However, for other materials such as concrete or brick, the penetration loss increases significantly with frequency [HJT+16,GSY+22]. Blockage can occur between the transmitter and receiver due to high penetration loss to many obstacles in the environment. As discussed in [HJT+16], there are two different types of blockages, dynamic blockage which occurs due to the movement of the objects in the environment and geometric blockage which occurs due to stationary static objects in the visual line between the transmitter and receiver. Figure 4-1 shows the dynamic blockage due to the random walk by a human at 2 m/s in an airport environment with UE and BS at a height of 1.3 m and 3.5 m, respectively, at 140 GHz [HEX23-D23]. Little or less dynamic regions in Figure 4-1 indicate the constant signal power at the receiver due to the stationary environment.

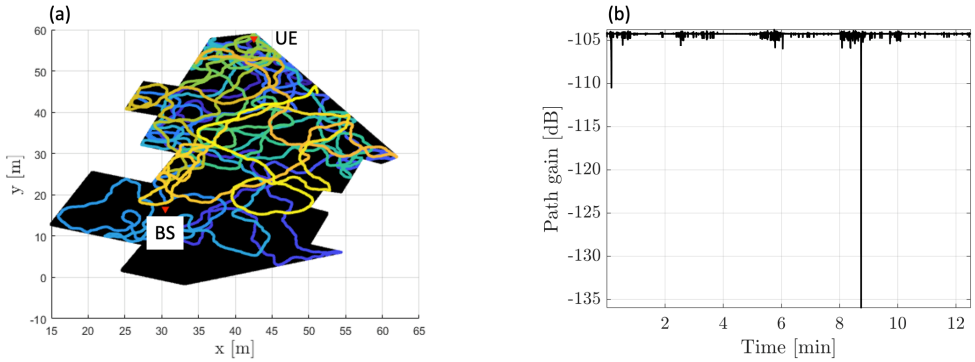

Figure 4-1 Example of dynamic blockage in an airport environment for human random walk.

The multi-path profile, which defines the small-scale fading information, is critical for sensing and localisation as it carries information about the targets and clutters in the environment. The small-scale modelling of these channels for low and mid bands using stochastic parametric channel models are available in [36.901]. The high frequency band operation with ultra-wide bandwidth is favoured in 6G for sensing and localisation as they provide very high resolutions in time and frequency. The usage of large dimension MIMO antennas provides very high angular resolution which increases the spatial resolution in sensing and localisation problems. However, the multipath channels at these frequencies are sparse due to the increased absorption at high bands, due to which receivers will observe reflections only from a few highly reflecting objects in the environment. Due to the large bandwidth of the signal, multiple regions of the same object could get resolved creating a cluster of multipaths per reflecting object. This is further illustrated in Figure 4-2.

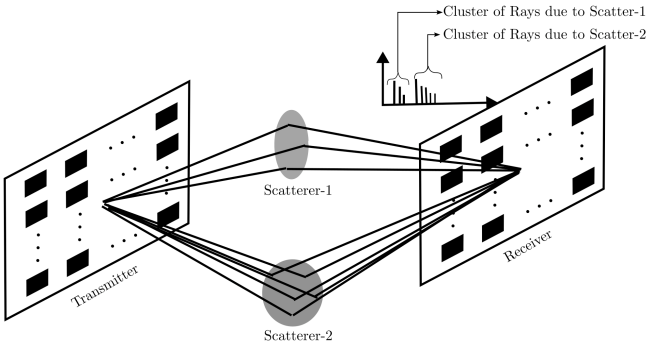

Figure 4-2 High frequency 6G channels are sparse, comprising cluster of reflections from few scatterers.

Deterministic channel models based on raytracing are commonly employed for modelling 6G channels at high frequency bands. However, these channel models are typically site-specific and do not generalize well towards other environments. Another approach to modelling these sparse 6G channels is to employ a stochastic geometric channel model like Saleh-Valenzuela (SV) channel and its variants [SV87] [LAH+19]. In these models, the multipaths typically arrive in the form of a cluster of rays, the power and inter-arrival times of the cluster/rays are drawn from parameterized distributions, which can be controlled to create various scattering environments.

Without loss of generality, OFDM transmission is considered as it is the de-facto modulation scheme employed in cellular communication. For an OFDM frame with N subcarriers and K symbols, the channel between the transmitter and receiver for a subcarrier, $n \in \{0, \dots, N-1\}$ and symbol, $k \in \{0, \dots, K-1\}$ can be written as

$$\boldsymbol{H}_{n,k} = \sum_{l=1}^{L} \alpha_l \boldsymbol{a}_{rx}(\theta_l)\boldsymbol{a}_{tx}^{T}(\phi_l) e^{-j2\pi n \Delta_f \tau_l} e^{-j2\pi k T_s \nu_l},$$

where L is the number of propagation clusters, α_l is the complex channel gain, $\boldsymbol{a}_{rx}$ and $\boldsymbol{a}_{tx}$ are the receive and transmit array responses, θ and ϕ denotes the AoA and AoD, τ and ν denote the delay and Doppler associated with the propagation path respectively [WS22]. While the communication receiver is interested in demodulating the transmitted symbols from the channel impaired signal, the sensing receiver needs to estimate the geometric information from the channels such as angles, delays and Doppler. Several measurement campaigns were conducted in Hexa-X to understand the channel effects at 6G high frequency bands. These studies can provide an understanding of various aspects of the channel at higher mmWave bands such as path loss, delay spread, angular spread, etc. These measurements, which are available to the public, can enable engineers to choose appropriate parameters for the above-discussed channel model [PHC+21]. For more details related to the channel modelling activities in Hexa-X, the reader is referred to [HEX23-D23].

Several extensions to the channel model discussed above could include aspects such as beam-squint and near-field propagation. As 6G moves towards wideband signals at high frequency bands, the array responses tend to become frequency-dependent, creating a beam-squint effect, where beams have different directions depending on the frequency. Extending current spatial channel models to consider the effect of beam-squint is an interestingly important area of research. Complementing the beam-squint effect is the near-field effect. The far-field assumption can be employed in channel modelling when the distance between a transmitter and receiver is sufficiently large. However, to overcome the severe path-gain losses at high frequencies, large antenna arrays are key, as they provide large aperture gains. As the size of the antenna array D increases, the near-field region, i.e., the region around the transmit and receive antennas with distances d less than $2D^2/\lambda$, could become prominent, and wave-front curvature should be considered. Hence the current far-field models should be extended towards a hybrid model considering both near- and far-field effect, especially in cell-free MIMO scenarios.

In all the above discussions ideal hardware in the transmitter and receiver are assumed. However, as the operating frequency increases, the transceivers become less than ideal due to the hardware imperfections. These aspects need to be taken care of, and modelling the systems is discussed in the next section.

4.1.2 Hardware models

In this section, the channel model is extended to consider the hardware impairments (HWIs), such as phase noise (PN), carrier frequency offset (CFO), mutual coupling (MC), power amplifier nonlinearity (PAN), array gain error (AGE), antenna displacement error (ADE) and in-phase quadrature imbalance (IQI) [Sch08].

4.1.2.1 Benchmark model without hardware impairments

For convenience, a pure LOS channel under a stationary scenario is considered, with a BS transmitting in downlink to a UE. The HWI-free channel matrix for the kth subcarrier can be expressed as

$$\mathbf{H}_k = \alpha d_k(\tau)\boldsymbol{a}_{\mathrm{B}}(\boldsymbol{\varphi}_{\mathrm{B}})\boldsymbol{a}_{\mathrm{U}}^{\mathrm{T}}(\boldsymbol{\varphi}_{\mathrm{U}}) \ ,$$

Where α is the complex channel gain to be identical for different subcarriers, $d_k(\tau) = e^{-j2\pi k\Delta_f \tau}$ (Δ_f is the subcarrier spacing) as a function of the path delay τ, while $\boldsymbol{a}_{\mathrm{B}}(\boldsymbol{\varphi}_{\mathrm{B}})$ and $\boldsymbol{a}_{\mathrm{U}}(\boldsymbol{\varphi}_{\mathrm{U}})$ are the BS and UE steering vectors as a function of the AoA and AoD. By concatenating all the received symbols into a column, the received symbol block is obtained as $\mathbf{y} = [\boldsymbol{y}_1, \ldots, \boldsymbol{y}_g, \ldots, \boldsymbol{y}_G]$, where $\boldsymbol{y}_g$ can be expressed as

$$\mathbf{y}_g = \alpha\left(\boldsymbol{w}_g^{\mathrm{T}} \boldsymbol{a}_{\mathrm{B}}(\boldsymbol{\varphi}_{\mathrm{B}}) \boldsymbol{a}_{\mathrm{U}}^{\mathrm{T}}(\boldsymbol{\varphi}_{\mathrm{U}}) \mathbf{v}_{\boldsymbol{g}}\right) \mathbf{d}(\tau) \odot \mathbf{x}_g + \boldsymbol{n}_g \,,$$

In which $\mathbf{d}(\tau) = [\mathrm{d}_1(\tau), \ldots, \mathrm{d}_K(\tau)]^{\mathrm{T}}$, $\mathbf{x}_g$ and $\boldsymbol{n}_g$ are the signal and noise vectors for the g-th transmission, respectively. In addition, $\mathbf{v}_{\boldsymbol{g}}$ and $\boldsymbol{w}_{\boldsymbol{g}}$ denote the precoder and combiner, respectively.

4.1.2.2 Hardware impairments and their models

The effects of MC, PAN, AGE, ADE, PN, CFO, and IQI, as shown in Figure 4-3 [CKA+23b], can now detailed. Note that the impairments such as PN, CFO, MC, AGE, ADE, and IQI exist both at the transmitter and the receiver, while the PAN appears only at the transmitter. The HWIs are usually compensated offline during calibration or online with dedicated signals and routines, depending on whether the impairment is static or time-variant. Both offline and online methods will have residual errors, which can be modelled as random perturbations around the nominal values. The impact of these residual errors after calibration is discussed. For online methods, these random realizations correspond to different times for a specific device, while for offline methods, these random realizations should be interpreted as corresponding to an ensemble of devices. The imperfections of analogue-to-digital converter (ADC), digital-to-analogue converter (DAC), low-noise amplifier and mixer are not considered.

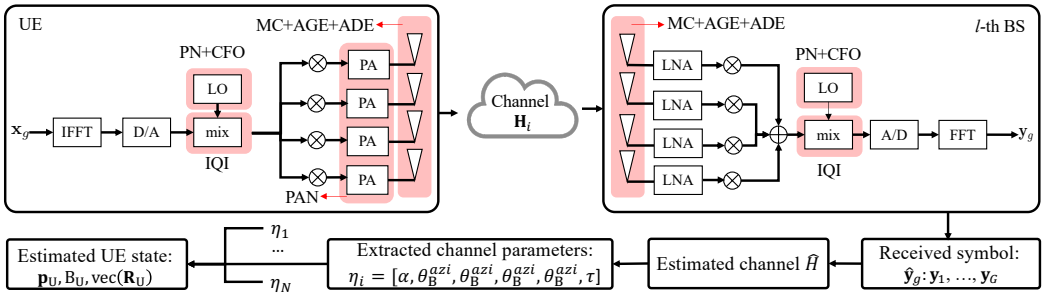

Figure 4-3 Block diagram of the hardware impairments considered at transmitter and receiver (highlighted in shaded regions). When the localisation algorithm does not have ideal knowledge of the generative model, it operates under model mismatch.

Phase noise and carrier frequency offset

Non-ideal local oscillators (LOs) in the up-conversion and down-conversion processes add PN to the carrier wave phase. The variance of the phase noise process increases linearly with time and at a rate depending on the quality of the oscillator. In addition, when the down-converting receiver LO does not perfectly synchronize with the received signal's carrier [MT21], CFO occurs. In general, both PN and CFO are estimated and compensated by the receiver [HAE20], so only the residual PN and residual CFO at the receiver are considered. An example of one realization of PN and CFO is shown in Figure 4-4. Note that the residual CFO ϵ is fixed, while the PN and residual PN are different for all the subcarriers symbols.

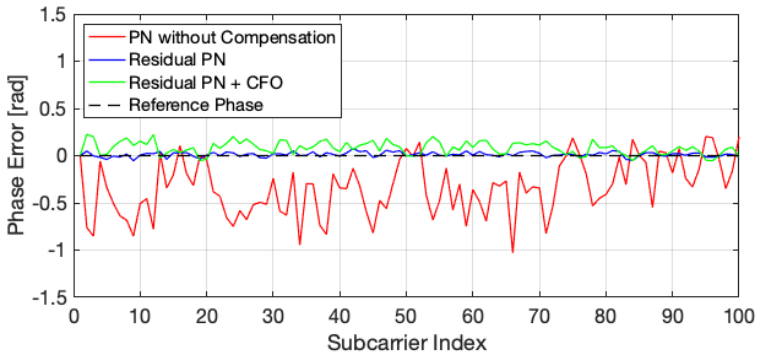

Figure 4-4 Visualization of phase errors caused by (a) PN without compensation, noise STD $\sigma_{\mathrm{TPN}} = 0.1745$ (10^{o}); (b) Residual PN, noise STD $\sigma_{\mathrm{PN}} = 0.0436$ (2.5^{o}); (c) Residual PN and CFO, $\sigma_{\mathrm{PN}} = 0.0436, \epsilon = 0.05$.

Mutual coupling

MC refers to the electromagnetic interaction between the antenna elements in an array [YDX+09]. For a UPA, the MC model as in [YL08] is adopted by assuming the antenna is only affected by the coupling of the surrounding elements, as shown in Figure 4-5. Note that MC affects both the transmitter and the receiver array.

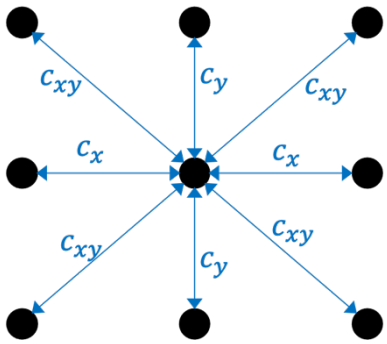

Figure 4-5 Illustration of mutual coupling for a uniform planar array. Each antenna is affected by the MC of the surrounding 8 antennas, and this influence descends with the distance between the adjacent antennas (e.g., $|c_{\mathrm{xy}}| < |c_{\mathrm{x}}|, |c_{\mathrm{xy}}| < |c_{\mathrm{y}}|$).

Power amplifier nonlinearity

For the PA nonlinearity, a Q-th order memoryless polynomial nonlinear model from [CKA23] is considered, where both the effects of digital predistortion and power amplifier are modelled, and non-oversampled signals are used as input to PA for tractable localisation performance analysis. Note that the PA affects the time domain signals and each antenna at the Tx has a separate PA, and the PA model in [CKA23] does not consider the out-of-band emissions (only the in-band distortion). For simplicity, the models are the same for different PAs, and one example of the effect of PA nonlinearity is shown in Figure 4-6.

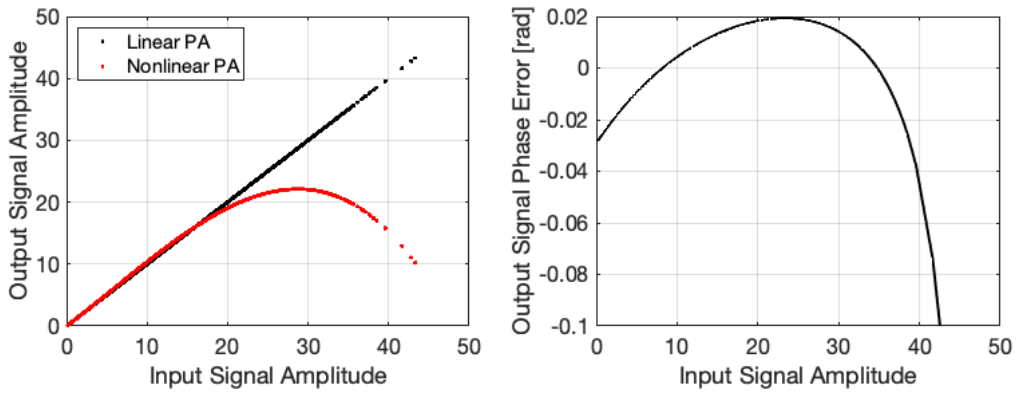

(a) (b)

Figure 4-6 Illustration of the effect of PA on the transmitted signals (1e4 complex numbers with random phases and amplitudes), in terms of (a) amplitude [V] and (b) phase [rad].

Array calibration error

The AGE, which models the perturbations of the array element response, and the ADE, which models the perturbations in the array element spacing, are considered in the array calibration error. The complex excitation coefficient of the n-th antenna at direction $\boldsymbol{\varphi}$ is defined as [BJJ+18] $b_n(\boldsymbol{\varphi}) = (1+\delta_g)e^{j\delta_p}$, where $\delta_a \sim \mathcal{N}(0, \sigma_{\mathrm{AA}}^2)$ and $\delta_p \sim \mathcal{N}(0, \sigma_{\mathrm{AP}}^2)$ are the relative amplitude error and phase error, respectively. Regarding the displacement error, the n-th antenna position is assumed to have a displacement on the 2D plane of the local coordinate system as $\tilde{\mathbf{z}}_n = \mathbf{z}_n + [0, \delta_{n,y}, \delta_{n,z}]^{\mathrm{T}}$, where $\mathbf{z}_n \in \mathbb{R}^3$ is the ideal position of the nth antenna in the local coordinate system, $\delta_{n,y}, \delta_{n,z} \sim \mathcal{N}(0, \sigma_{\mathrm{ADE}}^2)$ are the displacement error. The steering vector is then modified as $\boldsymbol{a}(\boldsymbol{\varphi}) \rightarrow \mathbf{b}(\boldsymbol{\varphi}) \odot e^{j\frac{2\pi}{\lambda}\tilde{\mathbf{Z}}^{\mathrm{T}}\mathbf{t}}$, where $\tilde{\mathbf{Z}} = [\tilde{\mathbf{z}}_1, \ldots, \tilde{\mathbf{z}}_N]$ contains the geometry information of all the antennas. The array calibration error is fixed for a certain array and varies across different devices.

In-phase and quadrature imbalance

IQI operates on the time domain signal, the transmitting and receiving symbol vectors can be modified as [GAI+20] $\mathbf{x}_g \rightarrow \alpha_{\mathrm{U}}\mathbf{x}_g + \beta_{\mathrm{U}}\mathbf{x}_g^*$, $\mathbf{y}_g \rightarrow \alpha_{\mathrm{B}}\mathbf{y}_g + \beta_{\mathrm{B}}\mathbf{y}_g^*$. The effect of IQI on the received symbols is shown in Figure 4-7.

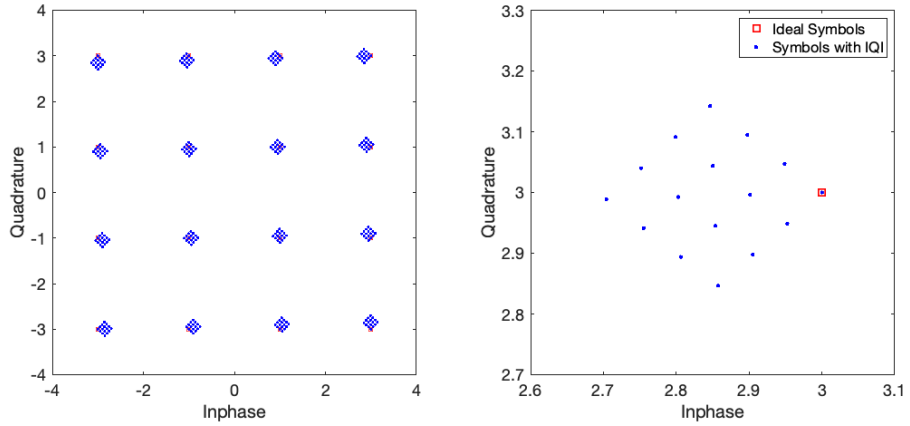

(a) (b)

Figure 4-7 Illustration of (a) the effect of IQI on the transmitted signals ($\alpha = 0.95, \beta = 0.05$), and (b) full constellation of QAM-16 zoomed in around one signal symbol (right).

To summarize, an ideal model without any HWIs was defined, which is used for algorithm development and evaluation. With HWIs introduced, the impaired model is used as the true (generative) model. In

the simulation results in later sections, the performance impact of using the ideal model to process data generated by the true model are evaluated.

4.2 Algorithms for localisation, sensing, and their integration with communication

Hexa-X has proposed and evaluated a variety of algorithms for localisation and sensing based on the models from Section 4.1. These models are reported here and associated to [HEX21-D31, HEX22-D32], where appropriate. An overview of these algorithm is provided in Figure 4-8.

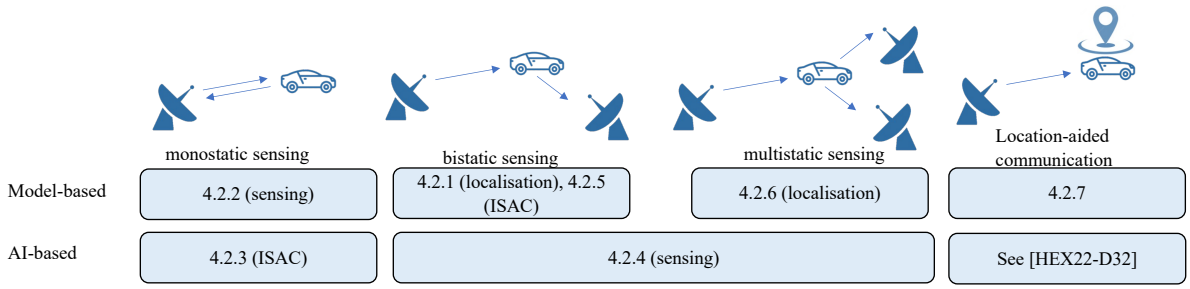

Figure 4-8 Overview of the contributions on algorithms. The numbers refer to the corresponding sections in this deliverable.

4.2.1 6D localisation and bistatic sensing

Motivation and background

The problem of 6D single-BS localisation and synchronization of an unsynchronized multi-antenna user has been reported in [Ch. 3.1, HEX22-D32], where it was shown that at least 1 NLOS path (with reflection from a scatterer at a favourable position) is needed together with the LOS, to obtain the 6D state of the UE. The study of localisation coverage indicates that having 2 NLOS paths in addition to LOS, renders the problem identifiable for most geometric configurations. The ability to solve the 6D localisation depends crucially on the availability of LOS to the BS, which is not necessarily always present, especially in dense urban areas. This motivates the research on 6D localisation in obstructed LOS scenarios, in which only NLOS paths between the BS and user are present.

It is worth highlighting that the work reported here has a connection to the signal design solution presented in [HEX22-D32]. In particular, the problem of downlink spatial signal design (i.e., BS precoder optimization) for mmWave localisation has been studied. This section focuses on the receiver side algorithms for location and orientation estimation. Hence, the study in [Ch. 3.1, HEX22-D32] complements the one reported here, leading to an end-to-end 6D localisation system.

Model and methodology

The considered scenario is a downlink mmWave MIMO OFDM system with a multi-antenna BS at a given position and orientation, and a multi-antenna UE, with unknown position, orientation, clock offset to the BS. The UE orientation is modelled by an unknown rotation matrix, that maps the global coordinate frame to the local coordinate frame of the UE. The rotation matrix is a unitary matrix belonging to the spatial orthogonal group, denoted by SO (3). The LOS path is blocked, but there are at least 4 NLOS paths available, as shown in Figure 4-9. The paths are considered resolvable, due to the large available bandwidth and antenna apertures. Less than 4 NLOS paths are not enough for the localisation problem to be identifiable. Moreover, it is assumed that the NLOS paths correspond to single-bounce reflection points at unknown positions. In practice, multi-bounce paths may also exist. Those paths can be identified and excluded from the localisation scheme, e.g., using iterative [LJW+22] or progressive [HRY+22] methods, since they adversely affect localisation accuracy. This is because the number of measurements each multi-bounce NLOS path gives (5, i.e., angle and time measurements) is less than the number of unknowns (at least 6 unknowns, i.e., the 3D positions of the

corresponding first and last incidence points on the propagation path). Therefore, without a priori map information, localisation scheme cannot benefit from the multi-bounce NLOS paths.

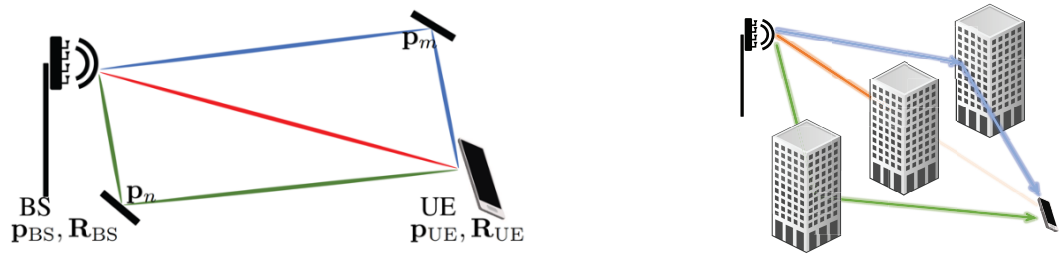

Figure 4-9 6D localisation with LOS (left) and under a blocked LOS condition (right).

Following the layers described in Section 3.1.1, a two-stage localisation scheme is adopted where the problem is decomposed into a channel parameters estimation routine, followed by a localisation routine [CSB+22]. The channel estimation routine determines the marginal posterior densities of the channel parameters (in the form of estimates and the associated uncertainties), based on the observations. The localisation routine uses the output of the channel parameters estimator to determine the 6D state of the UE. The focus of this research is on the 6D localisation from the estimated channel parameters.

The localisation problem is then given by a maximum likelihood estimation (MLE), which is solved by gradient descent, starting from an initial estimate, provided by an ad-hoc estimator [NSJ+23]. The ad-hoc estimator is based on a least square (LS) optimization problem.

Results

The root-mean-square-error (RMSE) of 3D position and 3D orientation estimation vs. the total transmit power of the MIMO OFDM system are considered as the performance indicators for the proposed localisation scheme. Assuming that there is a channel estimator operating close to the CRB of the channel parameters, one can plot the CRB of localisation parameters, on top of the performance curves of both ad-hoc and MLE schemes as a benchmark (the simulation parameters can be found in [NSJ+23]).

Analysis of Figure 4-10 and Figure 4-11 shows that both MLE and ad-hoc estimators improve by increasing the transmit power and follow the corresponding orientation error bound (OEB) and position error bound (PEB). The saturation of performance in ad-hoc estimates is due to the resolution of sampling of SO (3). The gap between the performance of ad-hoc estimation and CRB is negligible for a large range of transmit powers, and that can even be tightened using MLE. The tightness of MLE to the CRB for a practical range, show the efficiency of the proposed estimation algorithms.

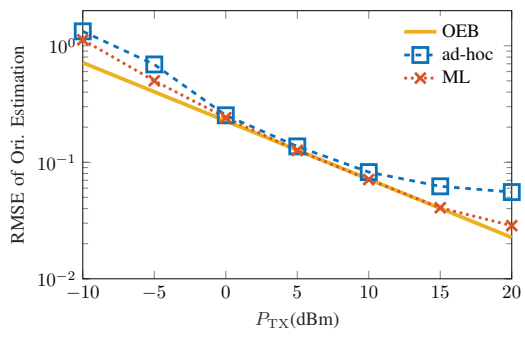

Figure 4-10 RMSE of UE orientation estimation vs. transmit power without LOS and *M=4* NLOS paths.

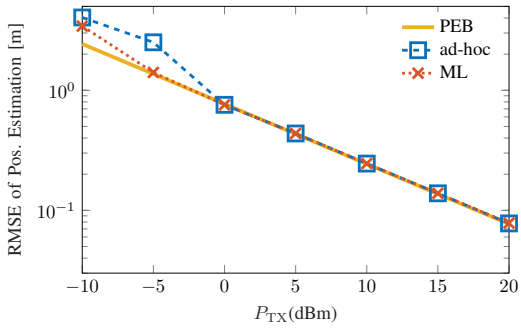

Figure 4-11 RMSE of UE position estimation vs. transmit power without LOS and *M=4* NLOS paths.

For comparison, Figure 4-12 and Figure 4-13 show the corresponding results in case the LOS path is present and only 1 or 2 NLOS paths are available. The results indicate that the LOS path is valuable for single-BS 6D localisation, but not strictly needed.

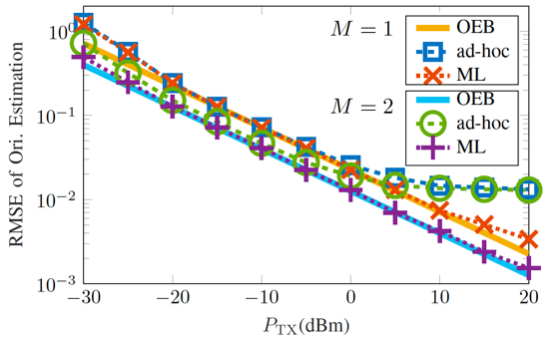

Figure 4-12 RMSE of of UE orientation estimation vs. transmit power with LOS and *M=1,2* NLOS paths.

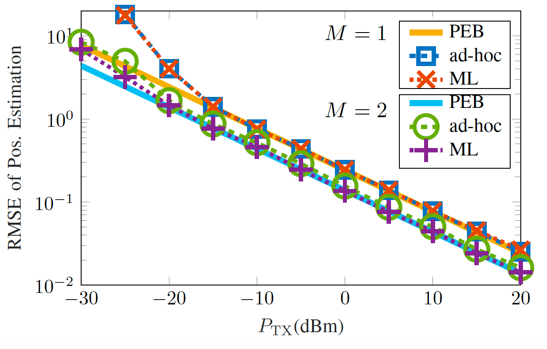

Figure 4-13 RMSE of UE position estimation UE vs. transmit power with LOS and *M=1,2* NLOS paths.

Conclusions

Evaluation of a 6D localisation scenario at mmWave frequencies (or higher) with a single BS transmitting OFDM signals and a multi-antenna UE showed the feasibility of localisation under the presence of at least 4 NLOS paths. The localisation routine, given the estimated channel parameters, consists of an MLE for which the initialization is provided by ad-hoc estimates obtained from geometrical arguments.

4.2.2 OFDM monostatic ISAC/JCAS

Motivation and background

OFDM has been a popular choice as ISAC/JCAS waveform for monostatic sensing applications due to its widespread use in cellular communication standards as well as its promising performance and flexibility in radar operation [SW11], [PPG22]. As 6G networks are envisioned to operate at high carrier frequencies, reaching sub-THz bands (e.g., 140 GHz), hardware impairments (especially, PN), can create serious performance bottlenecks for OFDM-based ISAC/JCAS systems. The reason is that PN becomes more severe with increasing carrier frequency due to deteriorating oscillator non-idealities at high frequencies [CLE22], [SNM+14]. Compared to other types of hardware impairments (such as MC, PAN, CFO and IQI), PN represents the most challenging to deal with due to its rapidly time-varying behaviour, which necessitates dynamic compensation strategies. In the literature, PN estimation and compensation methods for OFDM communication systems have been extensively studied in the last two decades, leading to various time-domain [ZTS07], [LY17] and frequency-domain compensation algorithms [MRW+11], [PRF07], [CLE22]. However, the impact of PN on the sensing performance of OFDM ISAC/JCAS systems and the related PN mitigation strategies for sensing have remained largely unexplored. This can be attributed to the fact that at carrier frequencies considered up to and including 5G NR (both FR1 and FR2), PN has a negligible impact on delay-Doppler estimation accuracy and the relevant use cases for radar do not require extreme levels of accuracy (cm or mm-level).

As envisioned use cases and applications in 6G networks impose tight requirements on sensing accuracy [URB+21], PN requires rigorous investigation in monostatic sensing with OFDM ISAC/JCAS systems, to both understand its impact on the sensing performance and develop mitigation (and, in certain cases, exploitation) algorithms. The aim of this section is to describe a system and signal model for the monostatic sensing receiver of an OFDM ISAC/JCAS system under the impact of PN, formulate the sensing problem of interest and propose an approach to estimate PN, together with target parameters (delay and Doppler), and mitigate its effect on sensing performance.

The problem tackled here represents an extension of the joint communication and sensing problem in [Ch. 4.3, HEX21-D31] to the case with non-ideal oscillators impaired by PN in the monostatic dual-functional transceiver. In [Ch. 4.3, HEX21-D31], the trade-offs between radar sensing accuracy and communications rate have been investigated in the absence of oscillator PN. This section aims to focus on the sensing performance under PN, while the impact of PN on the communication performance is

studied in [Ch. 4.2.2, HEX23-D23]. Another relation to other Hexa-X deliverables can be found in [Ch. 3.2.2, HEX22-D32], where the effect of intercarrier interference (ICI) on OFDM radar sensing has been explored in high-mobility scenarios and mitigation strategies have been developed. While ICI is a static and deterministic impairment whose severity depends on subcarrier spacing, carrier frequency and speed of targets in the environment [Ch. 3.2.2, HEX22-D32], PN in general constitutes a more serious challenge than ICI for radar sensing as it is a stochastic impairment with rapidly time-varying nature resulting from oscillator imperfections.

Model and methodology

As shown in Figure 4-14, an OFDM ISAC/JCAS system is considered, which consists of (i) an ISAC/JCAS transceiver containing, on the same hardware platform, a conventional OFDM transmitter (Tx) and a co-located radar receiver (Rx) for monostatic sensing; (ii) a remote communication Rx. An important distinction between radar and communication channels in such ISAC/JCAS applications with monostatic sensing transceiver is that the PN statistics in the radar Rx depend on radar channel parameters (i.e., target delays) due to up- and down-conversion with the same oscillator, while the PN statistics in the communication Rx have no relation to communication channel parameters due to the use of an independent oscillator at the communication Rx. In [Ch. 4.2.1, HEX23-D23], PN models have been presented for mmWave and sub-THz communication systems. In this deliverable, PN models are derived for monostatic sensing in ISAC/JCAS transceivers. As is shown below, such PN models have differential nature and thus delay-dependent statistics, different from those in [Ch. 4.2.1, HEX23-D23].

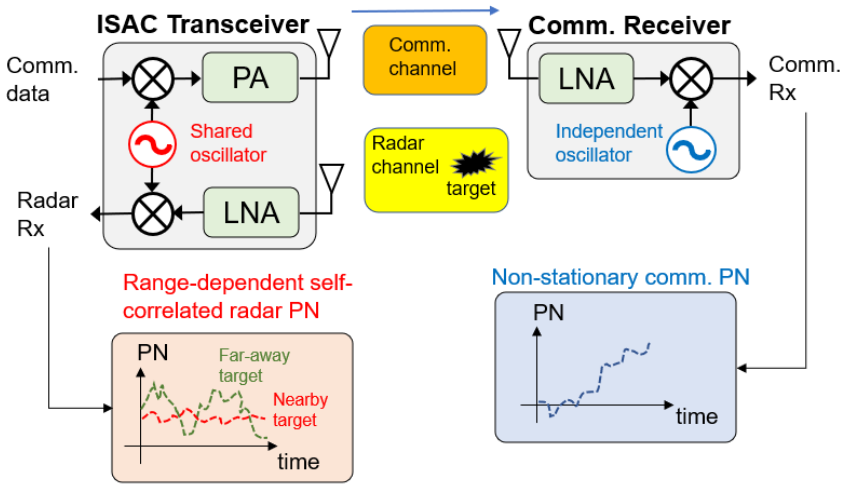

Figure 4-14 OFDM ISAC/JCAS system with monostatic radar transceiver under the impact of PN.

Considering an OFDM frame with N subcarriers and M symbols, the problem of interest for radar Rx in Figure 4-14 is to jointly estimate delay, Doppler and the multiplicative PN matrix of size N-by-M from an N-by-M fast-time/slow-time observation matrix, taking into account the statistics of PN samples. Assuming the existence of a single target, the N-by-M observation matrix can be expressed as follows:

$$Y = \alpha W \odot F_N^H \left(X \odot b(\tau) c^H(\nu) \right) + Z$$

where α, τ, ν represent complex channel gain, round-trip delay and Doppler shift of the target, respectively, W denotes the N-by-M multiplicative PN matrix, $\odot$ is the element-wise product, F_N is the N-by-N unitary DFT matrix, X is the N-by-M complex data symbols matrix, $\boldsymbol{b}(\tau)$ and $\boldsymbol{c}(\nu)$ represent, respectively, the frequency-domain and time-domain steering vectors of size N-by-1 and M-by-1, and $\boldsymbol{Z}$ is the N-by-M additive noise matrix. In this problem, α, τ, ν and W are unknowns to be estimated, while $\boldsymbol{X}$ is known to the radar receiver due to the co-located monostatic sensing architecture, as seen from Figure 4-14.

The proposed approach to solve this challenging sensing problem consists of the following three stages:

- Derivation of range-dependent PN statistics in the radar receiver.
- Hybrid MLE/maximum a-posteriori (MAP) estimator of delay, Doppler and PN parameters based on the PN statistics.
- Iterated small angle approximation (ISAA) algorithm to optimize the MLE/MAP cost function.

Range-dependent PN statistics

Since the Tx and radar Rx shares the same oscillator for up-conversion and down-conversion, respectively, the radar Rx observes a *differential/self-correlated PN* given by

$$\xi(t,\tau) = \phi(t) - \phi(t-\tau)$$

obtained as a result of conjugate multiplication of the time-delayed target echo with the transmit signal itself. This leads to a self-correlated PN process described by the difference between the original PN process and its version shifted in time by the round-trip delay of the target. Hence, the statistics of the PN in the radar receiver are *delay-dependent*. The statistical characterization of the PN can be written as $\xi(t,\tau) \sim N(0,\sigma_\xi^2(\tau))$, where the form of the delay-dependent variance depends on the type of oscillator. For free-running oscillators (FROs) and phase-locked loop (PLL) synthesizers, there are standard expressions (assuming the existence of only white noise sources in the oscillator [Dem06], [CB06]), $\sigma_\xi^2(\tau) = 2\,\pi f_{3dB}|\tau|$ (for FRO) and $\sigma_\xi^2(\tau) = 2\,\frac{f_{3dB}}{f_{loop}}(1 - e^{-2\pi f_{loop}|\tau|})$ (for PLL). The sampled version of the PN process has the delay-dependent statistics: $\xi = N\big(0, R(\tau)\big)$, where the covariance matrix structure differs between FROs and PLLs. Here, the PN covariance matrix is a symmetric Toeplitz-block Toeplitz matrix. Figure 4-15 shows the first row of this matrix (i.e., covariance profile) for different target delays and types of oscillators, revealing the delay-dependency of the PN statistics.

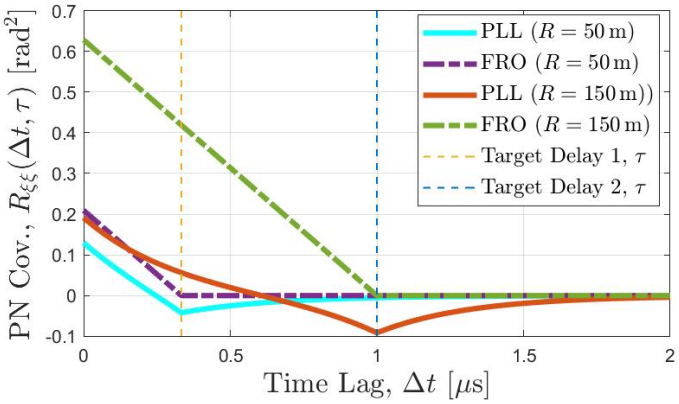

Figure 4-15 Covariance profile of the delay-dependent PN statistics for different target delays and oscillator types.

Hybrid MLE/MAP estimator

Given the PN statistics, the hybrid MLE/MAP estimator is derived to estimate the deterministic gain, delay and Doppler parameters and the random PN matrix. There are two challenges associated with the implementation of this estimator:

- A-priori unknown PN statistics: Since the PN statistics depend on the unknown target delay, it is not possible to estimate the multiplicative PN matrix and compensate for its effect on the observations before estimating target parameters. Hence, sensing and PN estimation should be performed simultaneously.
- Nonlinearity of PN: PN appears nonlinearly in the observation-related part of the estimator cost function, while it appears linearly in the prior-related part due to its statistics being Gaussian. This leads to a high-dimensional non-linear optimization problem with many local minima.

To overcome the above challenges, an algorithm is proposed, as described next.

Iterated small angle approximation (ISAA) algorithm

To circumvent the nonlinearity of PN, an iterated small angle approximation (ISAA) algorithm is developed that invokes the small angle approximation (SAA) $e^{j\theta} \approx 1 + j\theta$ around the current PN estimate at each iteration. This enables progressive minimization of estimation error through successive residual PN estimations. Additionally, to deal with the a-priori unknown (delay-dependent) PN statistics, an alternating optimization strategy is proposed to update PN and delay/Doppler parameters in an alternating fashion. In a nutshell, the ISAA algorithm works as follows: (i) Initialize the PN estimate to be all-zeros and find the corresponding delay-Doppler estimates; (ii) At each iteration: Given the latest delay-Doppler estimate, update PN estimate by finding residual PN through SAA around the current PN estimate. Given the latest PN estimate, update delay-Doppler estimate. (iii) Continue until convergence (e.g., negligible change in delay-Doppler estimates).

Results

To evaluate the performance of the proposed sensing algorithm in the presence of PN for both FROs and PLLs [KWK22], simulations have been carried out using the following parameters: a carrier frequency of 140 GHz, a total bandwidth of 50 MHz (limited for computational reasons in this simulation study), 256 subcarriers with 195.31 kHz spacing, 10 OFDM symbols, an OFDM symbol duration of 5.12 us (with an additional 1.28 us cyclic prefix). The following three benchmark schemes are considered, including the proposed algorithm:

- ISAA: The proposed ISAA algorithm.
- 2-D FFT: The optimal delay-Doppler estimation method for OFDM radar in the absence of PN.
- 2-D FFT (PN-free): 2-D FFT applied on the (hypothetical) PN-free observations (to provide a genie-aided baseline that can help quantify the PN-induced performance gaps).

Besides the RMSE performances of the above schemes, theoretical limits are also plotted using the CRB analysis (CRB and CRB (PN-free), respectively, for observations with and without PN). In the simulations, a target with range 30 m and velocity 4 m/s is considered and an oscillator with 3-dB bandwidth 200 kHz and loop bandwidth 1 MHz (in the case of PLL) is used.

(a) (b)

Figure 4-16 and Figure 4-17 show the range and velocity estimation performances with respect to SNR for FRO and PLL architectures, respectively. It is observed that the proposed algorithm can successfully mitigate the impact of PN in range estimation and exhibit performance very close to that achievable without PN, both for FRO and PLL architectures. The same observation is also valid for the corresponding theoretical bounds. This indicates that almost perfect recovery of PN-induced performance degradations in ranging is possible in monostatic OFDM radar. In addition, the performance of the standard 2-D FFT method saturates above a certain SNR as it does not consider the existence of PN, which suggests that PN can create bottlenecks for emerging 6G sensing applications with stringent accuracy requirements (cm and mm-level). Moreover, looking at the velocity RMSE results, PN causes severe performance losses in velocity estimation, especially for FRO architectures. This results from high correlation of PN in fast-time (which can be exploited to compensate for its effect in range estimation) and its low correlation in slow-time (which makes it difficult to estimate and compensate for PN in slow-time, leading to poor Doppler estimation). In the case of PLL, performance loss is less severe compared to FRO because PN has non-zero correlations for PLL across consecutive OFDM symbols through the use of feedback loops in the oscillator.

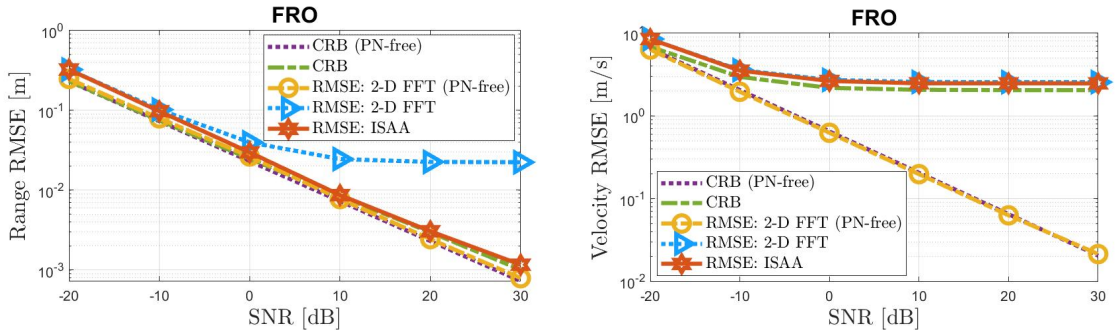

(a) (b)

Figure 4-16 Range and velocity estimation performances with respect to SNR for FRO architectures.

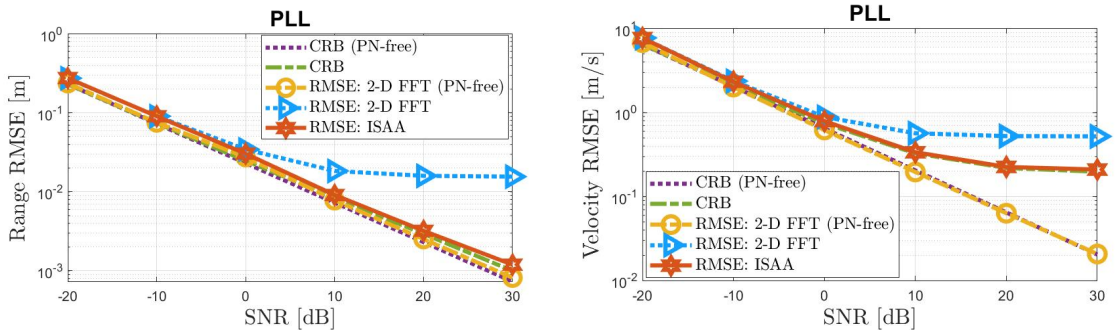

(a) (b)

Figure 4-17 Range and velocity estimation performances with respect to SNR for PLL architectures.

Figure 4-18 demonstrates the ranging performance with respect to oscillator quality (3-dB bandwidth for FRO and loop bandwidth for PLL) for a fixed SNR of 20 dB. The proposed MAP-ISAA algorithm is robust against worsening oscillator quality, while the accuracy of the standard FFT algorithm becomes worse as the 3-dB bandwidth increases or loop bandwidth decreases. Together with Figure 4-16 and Figure 4-17, this result shows that PN can be effectively mitigated in range estimation under a wide range of operating conditions. The reader is referred to [KWK22] for more results and detailed interpretations.

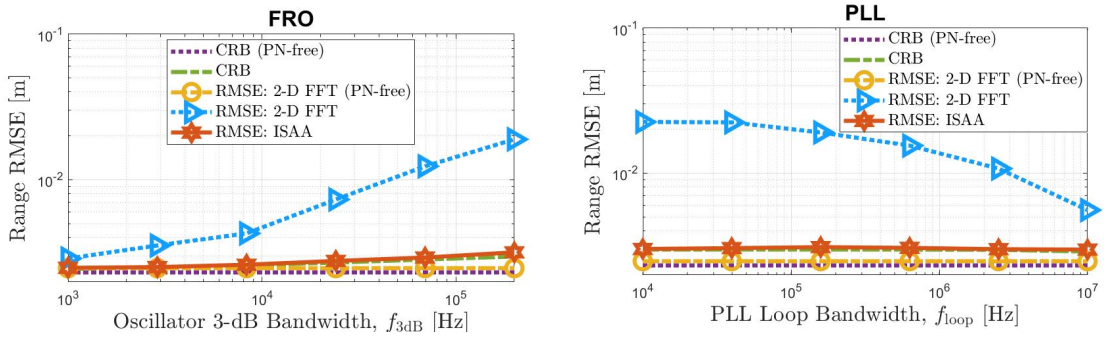

(a) (b)

Figure 4-18 Range estimation performance with respect to oscillator quality for fixed SNR for FRO and PLL architectures.

Conclusions

An OFDM-based monostatic ISAC/JCAS system has been considered in the face of oscillator PN. In particular, the problem of estimating delay, Doppler and multiplicative PN matrix in the monostatic radar receiver has been formulated and a solution approach based on iterated approximation of the

hybrid MLE/MAP cost function has been proposed, taking into account the delay-dependent PN statistics in the radar receiver. Key take-aways from the results can be listed as follows:

- Range vs. velocity accuracy under PN: Due to high (low) correlation of PN in fast-time (slow-time), the impact of PN on ranging accuracy can be almost entirely mitigated, whereas velocity accuracy is severely degraded by PN.
- FRO vs. PLL – impact of oscillator type: PLLs lead to less severe performance losses in velocity estimation than FROs because there exists non-zero correlation between consecutive OFDM symbols (i.e., slow-time correlation).
- Scenarios where PN induces significant degradation: PN-induced performance losses are more pronounced at higher SNRs and for oscillators with higher 3-dB bandwidth and smaller loop bandwidth.

4.2.3 AI-based monostatic ISAC/JCAS

Motivation and background

As previously mentioned in this deliverable, 6G networks are severely affected by hardware impairments. Classical model-based approaches suffer from performance degradation under model mismatch, or they become too complex to solve. Data-driven designs relying on machine learning can adapt to the impairments, given that they do not assume any underling model. Machine learning for ISAC/JCAS has been studied in different scenarios [MSW+22], [SFY+22], [WLH+22]. However, these methods often lack interpretability and require high training complexity.

Model-driven machine learning emerges as a trade-off between model-based and data-driven methods. In this approach, the structure of the model-based methods is exploited, but some of the components are still allowed to be optimized based on data [SWE+20]. Moreover, the learnt components can be initialized based on the model-based assumptions, thus starting from a reasonably well-performing point. Model-driven machine learning has found a wide range of applications in communications [HJW+19], [SFE+21], [YL22], due to the extensive models available.

In this section, end-to-end model-driven machine learning for ISAC/JCAS is applied. The goal is to extend the previous work reported in [HEX22-D32] to account for randomized prior information of the target AoA and to reduce the training time. An architecture with parameter sharing is proposed to perform 2 tasks simultaneously: (i) precoder designing at the transmitter and (ii) target AoA estimation at the receiver. A comparison between (i) model-driven machine learning, (ii) neural-network-based learning and (iii) the best-known baseline is made under hardware impairments and complexity constraints.

Model and methodology

The problem formulation is summarized in Figure 4-19. A monostatic sensing transceiver equipped with a uniform linear array (ULA) is considered, which is also used as communication transmitter. The transmitter is divided into an encoder, that maps the information messages to complex symbols and a beamformer, that steers the antenna energy into a particular direction. The received sensing signal depends on the target presence. If it is present, the signal reflected from the target is received, otherwise only noise is received. The communication receiver has a single antenna, and it is assumed to be always present. The signal at the communication receiver is independent of the target's presence, and CSI is also received. In both cases, a LOS link is considered between transmitter and target, and between transmitter and communication receiver. The location of the target and the communication receiver is random in each transmission. Some a priori angular information about target and communication receiver locations is available at the transmitter.

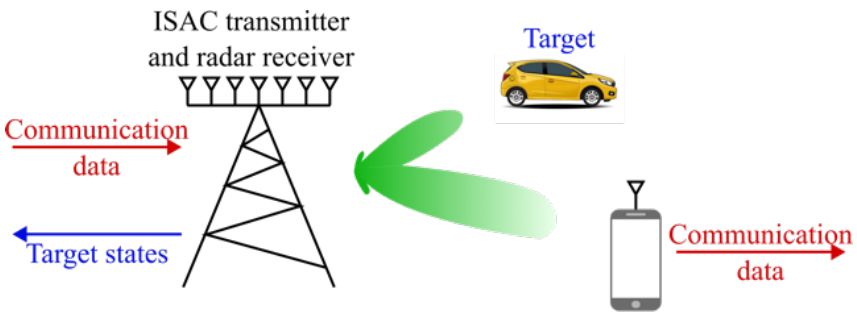

Figure 4-19 Considered monostatic ISAC/JCAS scenario.

A model-based transmitter is designed resorting to the beampattern synthesis approach in [AEL+14], [TSF+17]. The model-based radar receiver was derived as the maximum a-posteriori ratio test (MAPRT) detector [GCH20]. The model-based communication transmitter was selected using M-quadrature amplitude modulation (M-QAM), and the communication receiver as a maximum likelihood estimator, given some channel state information.

Following the model-based design, an ISAC/JCAS architecture for model-driven learning is developed, as summarized in Figure 4-20. The goal is to learn a matrix of steering vector of the ULA transmitter for different angles, such that it can adapt to imperfections in the spacing of the antenna elements. Since the communication receiver is already optimal given the CSI (even in the presence of impairments), the matrix was trained just based on the radar link. However, supervised end-to-end learning was used to optimize the elements of the matrix. Thus, a radar receiver based on differentiable operations was designed.

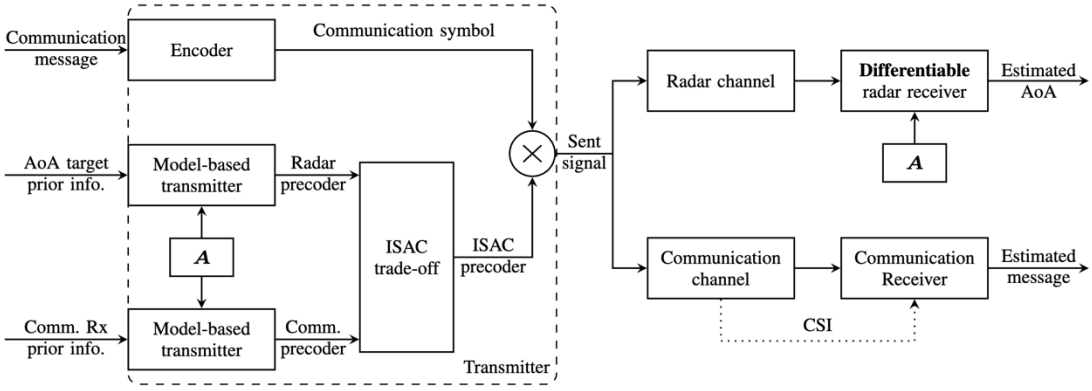

Figure 4-20 Block diagram of the ISAC/JCAS model-driven approach. The matrix A is optimized via model-driven learning. The radar receiver was designed based on differentiable operations so that the gradient can be computed in an end-to-end manner.

Results

Here the most important results of the model-driven approach of Figure 4-20 are presented (for more results, see [MHK+22]). In Figure 4-21 the performance in terms of probability of detection and angle estimation is depicted. The spacing between the antenna elements in the ULA is considered nonideal and normally distributed around the ideal value. In addition, the case of complexity limitations for both neural-network-based and model-driven learning is studied. In general, machine learning techniques outperform the conventional model-based method. Furthermore, when complexity is limited, model-driven learning still has similar performance, whereas neural-network-based learning severely degrades.

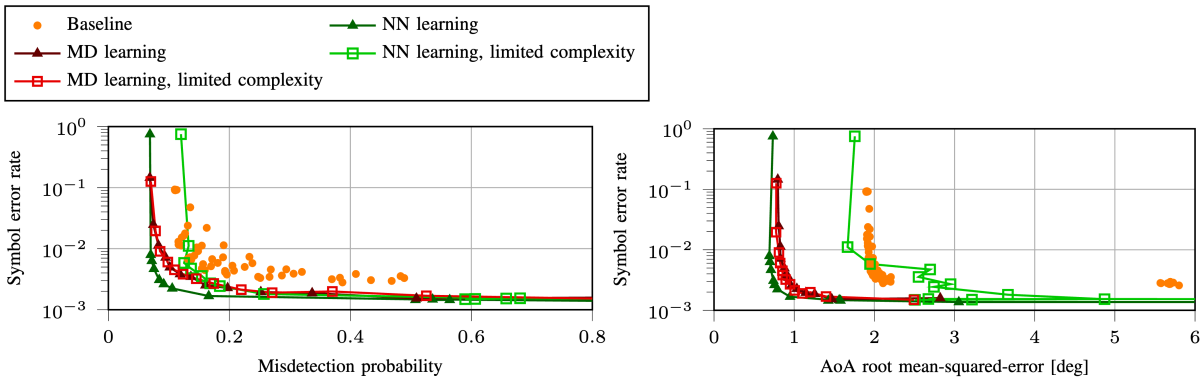

Figure 4-21. Monostatic ISAC/JCAS results under hardware impairments.

In Figure 4-22, machine learning methods are tested to an unseen scenario during training, where model-driven learning is shown to generalize better than neural-network-based learning to unseen data since it exploits the model-based structure of the steering vectors.

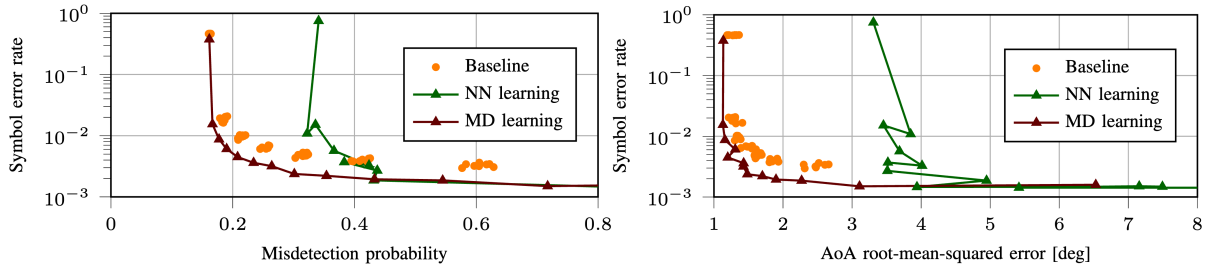

Figure 4-22 Results under hardware impairments with low complexity constraints. The target lies in an angular sector that is not included in the set of training angular sectors.

Conclusions

In this section, a model-driven approach for ISAC/JCAS has been developed. This approach outperforms model-based knowledge under the presence of hardware impairments, similar to neural-network-based learning. However, when complexity is constrained, model-driven learning yields better performance than neural-network-based learning, especially when tested with different data from training.

4.2.4 AI-based multi-static ISAC/JCAS

Motivation and background

The 6G systems will be deployed in low (< 1 GHz), mid (1-10G) and high frequency bands (>10 GHz). At high frequency 6G systems will operate in frequencies which will overlap with traditional radar bands, thus enabling 6G communication systems to be employed for sensing. Multiple 6G base stations can be employed in the sensing activity to form multi-static sensing. The high-frequency operation of 6G will enable high-dimension MIMO coupled with the wide bandwidth operation of these systems can provide high resolution in angle, range, and Doppler domains [YXX+19], [WSC+21], [BBP+22]. This enables both conventional radar type processing such as estimating its parameters such as velocity, range, etc. but also in non-radar type sensing where the sensing includes identifying the contextual information. In [HEX21-D31] a method to identify the landscape around the UE is proposed wherein the path-loss information is captured in a multi-static way towards inference on the landscape. In [HEX22-D32] an extension to contextual sensing towards detecting indoor human activity was proposed where the main goal was to employ active sensing by exploiting the connection between the UE and BS to transfer sensory data (such as inertial sensor data) for detecting the human activity.

In this work, the focus is on the sensing of passive targets using AI-based methods. Sensing here involves detecting the presence of the target and estimating its parameters, such as position. Targets by themselves will not aid in any form of the sensing process and hence called passive targets. Vision-

based target sensing is very common and can be employed in several use cases. Even though vision-based methods provide highly accurate passive sensing of targets, they compromise privacy and security. They also do not work well in low light conditions, and since new cameras need to be installed, the cost is increased with coverage. Sensing piggybacked on the omnipresent cellular communication will provide enhanced sensing coverage at a low cost. Adding a sensing service on top of the 6G communication system will enable several use cases, such as intruder detection, equipment tracking, etc.

There exist several works, such as [Alq17], [YND+17], and [MZW20], where Wi-Fi wireless signals have been used for passive sensing. In these methods, channel statistics of mid-band frequencies (2 – 10 GHz), such as received signal strength indication (RSSI), Doppler shifts, etc., are used to sense targets. These studies are not applicable for 6G channels operating in high bands (>10 GHz) since 6G channels are sparse with clustered multi-paths which pertains to highly reflective scatterers in the environment. Typically, these channels are modelled using geometric clustering models such as SV channel models [SV87], [LAH+19].

In the following, AI-based methods to sense the passive targets using communication infrastructure, as shown in Figure 4-23 is discussed. AI methods for detection and estimation of the position of the passive targets by exploiting the perturbations in the SV cluster-based geometric channel model is discussed. The resolution, coverage, and position uncertainty using the proposed methods for various indoor deployments are analysed.

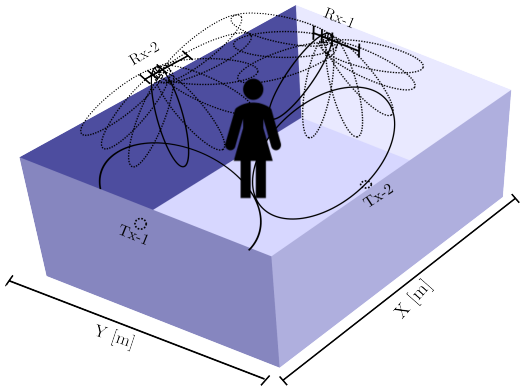

Figure 4-23 Passive indoor sensing using communication infrastructure.

Model and methodology

6G channels at high frequencies (above 20 GHz) are sparse. These channels have multipaths in the form of clusters with each cluster mapping to a highly reflective surface in the environment as shown in the Figure 4-2. A deployment consisting of a single low-cost transmitter having omni-directional anchor UE and L BS acting as receivers, each having a ULA with N_r antennas with each element separated by a half wavelength is considered.

During default state, that is, when the target is not present in the room, then the CSI between the transmitter and the l-th receive device is given by

$$\boldsymbol{h_l^{null}} = \sum_{v=1}^{N_{cl}} \sum_{u=1}^{N_{rays}} \boldsymbol{\beta_{l,u,v} a_{rx}(\phi_{l,u,v}) G(\psi_{l,u,v})},$$

The values N_{cl} indicates the number of clusters and N_{rays} indicates number of rays in that cluster. The u-th ray of the v-th cluster at the l-th receiver will have a complex gain, AoA and angle of departure (AoD) given by $\beta_{l,u,v}$, $\phi_{l,u,v}$ and $\psi_{l,u,v}$ respectively. The transmit gain pattern and receive array pattern is denoted by G and a_{rx} respectively.

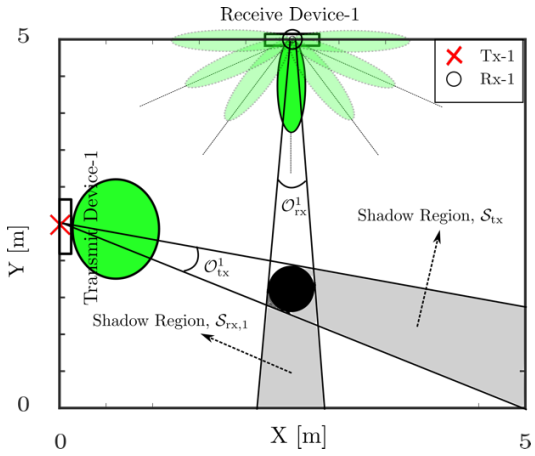

Figure 4-24 $L+1$ Convex shadow regions caused during alternate hypothesis.

The presence of the target in the scene perturbs each of the L links uniquely between the transmitter and receiver. Due to the high frequency operation, it is assumed that target completely blocks the rays, and there is no diffraction or reflections. This results in $L+1$ convex shadow regions $S_{tx} \subset \mathbb{R}^2$ and $S_{rx,l} \subset \mathbb{R}^2$ behind the target as given in the Figure 4-24. Therefore, during alternate hypothesis, the CSI is given by

$$\boldsymbol{h_l^{alt}} = \sum_{v=1}^{N_{cl}} \sum_{u=1}^{N_{rays}} \boldsymbol{\beta'_{l,u,v} a_{rx}(\phi_{l,u,v}) G(\psi_{l,u,v})}$$

where $\beta'_{l,u,v}$ is zero if the ray corresponds to the reflection from the scatter corresponding to the shadow region shown in the Figure 4-24 [YH22].

In order to sense the perturbation in CSI towards passive target detection, a shallow convolution neural network (CNN) based AI pipeline called CsiSenseNet is trained. The tuning of this network is done in such a way that the network yields good performance, and, at the same time, it can be implemented in embedded platforms. The network is shown in the Figure 4-25. The target detection and position estimation part of the CsiSenseNet shares several layers except the last two layers shown in the green shaded and blue shaded areas for target detection and position estimation, respectively.

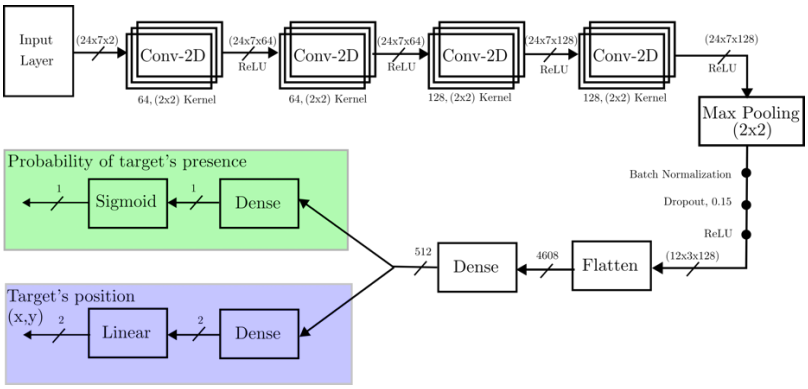

Figure 4-25 AI pipeline for passive target detection and position estimation.

The CSI data is converted into 2D frames, wherein CSIs for a given beamforming direction from L links are concatenated in horizontal dimension and all the concatenated CSIs at different beam forming directions are concatenated in the vertical dimension as given in the equations below.

$$\boldsymbol{h_{\theta_i}} = \left[\boldsymbol{h_{1,\theta_i}} \middle| \boldsymbol{h_{2,\theta_i}} \middle| \ldots \middle| \boldsymbol{h_{L,\theta_i}}\right] \in \mathbb{C}^{\boldsymbol{LN_r}},$$

$$\boldsymbol{H} = [\boldsymbol{h_{\theta_1}^T} | \boldsymbol{h_{\theta_1}^T} | \ldots | \boldsymbol{h_{\theta_{N_b}}^T}]^T \in \mathbb{C}^{\boldsymbol{LN_r\, X\, N_b}}$$

where $\boldsymbol{h}_{\theta_i}$ is the aggregated CSI in direction θ_i and | is the concatenation operation. N_b indicates the number of beamforming directions employed [YH22].

An indoor deployment in a room of 25 m^2 area with single transmit device and L receive devices (BSs) each having an ULA with $N_r = 8$ antennas is considered. Each receiver has beamforming capability to scan between $-\pi/2$ to $+\pi/2$ using $N_b = 7$ beams as shown in Figure 4-24 with L=1. For target detection, an AI pipeline is trained using the different realization of channel H using a simulator for both hypothesis (null and alt). The labelled training set $(H_i, hyp_i) \mid i = 1,2,\dots M$ is used to train the target detection part of the AI pipeline shown in Figure 4-25 to minimize the binary cross entropy loss. Similarly, position estimation part of the network is trained using the training set $(H_i, p_i) \mid i = 1,2,\dots M$, where p_i is the true position of the target for the alternate hypothesis channel realization H_i. The position part of the CsiSenseNet is trained to minimize the L2 regression loss.

Results

MFM simulator [Rob21] is used to create three deployment scenarios with number of receivers, $L = 1,2$ and 3. The channel model for alternate hypothesis is modified as discussed above. To simplify the CSI computation during alternate hypothesis, all the rays within the occlusion angles, $\mathcal{O}_{tx}^{1}$ and $\mathcal{O}_{rx}^{l}$ are blocked.

Resolution Analysis: The relation between the size of the object with the accuracy of detection, $\mathcal{P}$ for the proposed AI method is analysed. To assess the performance, CsiSenseNet is trained by quantizing the room into 0.0625 m^2 bins and generating 2000 CSI realizations for each hypothesis having object of different sizes in them. The average performance for placing the target of various sizes at 1000 random positions for different deployments with $L = 1,2, and\ 3$ is as shown in the Figure 4-26 [YH22].

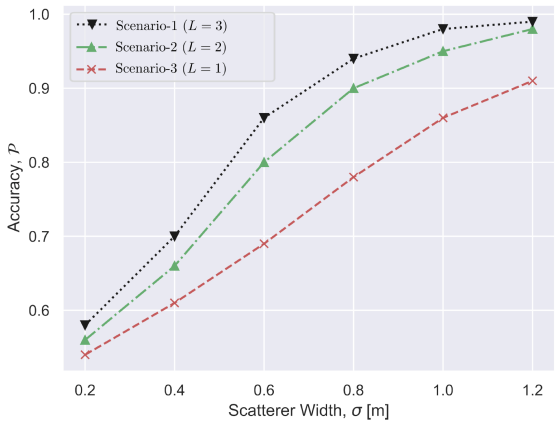

Figure 4-26 Accuracy of detection variation with the size of the target for different deployment.

Coverage Analysis: The detection accuracy variations in the 2D space of the room are analysed. The detection accuracy not only depends on the size of the target, but also on the position where the target is present. Coverage is better for targets closer to the nodes or larger sized. The coverage analysis for the proposed AI methods for different deployments with number of receivers $L = 1,2\ and\ 3$ is shown in Figure 4-27 [YH22].

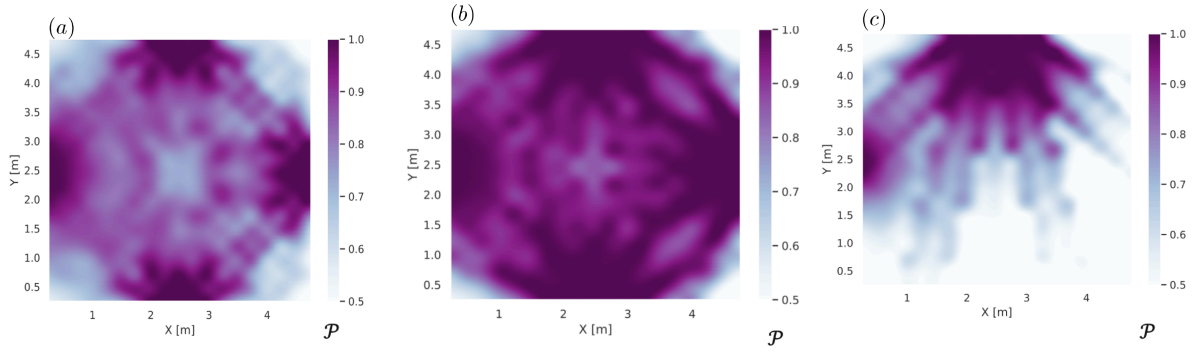

Figure 4-27 Coverage analysis for different deployment and sizes. (a) Coverage for L=3 and scatter width, rho=0.5 (b) Coverage for L=3 and target width, $\sigma = 0.5\,m$ (b) Coverage for L=3 and target width, $\sigma -= 0.8\,m$ (c) Coverage for L=1 and target width, $\sigma = 0.8\,m$.

Position estimation: In order to assess the performance of the CsiSenseNet towards position estimation, the AI agent is trained with data from 2000 CSI realizations by placing the target in the centre of each quantized bins of 0.0625m2. Then various sized targets are dropped at 1000 random positions to evaluate the performance. The performance of the proposed algorithm is shown in Figure 4-28 using the CDF ($F_{\epsilon}(\epsilon)$) of the L2-error, ϵ, mean of the L2-error, μ_{ϵ} , and the 90-percentile, Δ_{ϵ}^{90} [YH22].

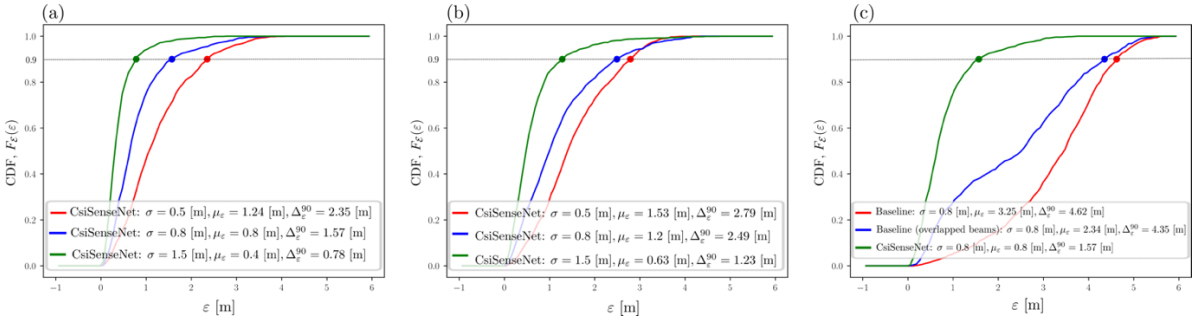

Figure 4-28 Performance analysis of CsiSenseNet for Position estimation. (a) and (b) are performance for L=1 and L=3 and (c) compares the performance of the CsiSenseNet on L=3 deployment with baseline algorithm.

In Figure 4-28-(c) the performance of the CsiSenseNet is compared with the baseline method. In the baseline method the position is estimated by triangulating beamforming angles with maximum attenuations [YH22].

Conclusions

Passive target detection using vision-based methods is commonly employed and they provide highly accurate target detection. However, these methods suffer from degraded performance when it comes to privacy, security, coverage, and cost [YH22]. When passive sensing is piggybacked on the communication infrastructure it reduces cost, increases privacy, and enhances coverage. However, to accomplish good performance in terms of accuracy of detection and parameter estimation, efficient algorithms are needed. A shallow CNN-based AI pipeline called CsiSenseNet for passive target detection and position estimation is proposed.

The proposed methods indicate that the sensing resolution (i.e., size of the target that can be faithfully detected) can be improved by having a deployment with many receivers, as shown in Figure 4-26. Results indicate that human-sized target ($\sigma = 0.8\,m$) can be detected with more than 90 percent accuracy with two receivers. The coverage study indicates that the larger objects have good coverage and coverage along the beamforming direction of the receiver is better as indicated by Figure 4-27. The analysis of position estimation indicates that the position uncertainty for a given sized target can be reduced by having more receivers. The proposed estimation method outperforms the angle-based baseline methods, as shown in Figure 4-28.

4.2.5 Bi-static ISAC/JCAS

Motivation and background

One of the major drawbacks when considering a monostatic ISAC/JCAS system which has co-located transmission and receive antennas, is the mutual interference that cause by the communication and sensing signals that share the same antenna [BTL+19]. Even though most of the existing research on ISAC/JCAS considered the system as full duplex, in practical scenario achieving full duplex communication is highly challenging. Therefore, this interference can degrade the performance of both functions, leading to reduced communication throughput and degraded sensing parameter estimation accuracy. In a bi-static ISAC/JCAS system, the sensing signal is transmitted and received by separate antennas, which can significantly reduce the mutual interference and improve the accuracy of sensing

parameter estimation. Hence, ISAC/JCAS in bi-static or multi static setup is worthy to investigate considering it as a practical solution to overcome this problem.

In [JVG+22], the joint design of the transmitter and radar with user receivers was addressed, resulting in a general resource allocation problem. However, neither radar-centric nor communication-centric designs could achieve a scalable trade-off between the two functions. Authors in [PPG22] considered a joint sensing and communication model where the modulation symbol is precoded by the communication and sensing beamforming vectors to serve both purposes. In [LML+18] a transmit beamforming design was proposed that utilized the communication waveform as a radar sensing waveform. However, these works had a loss of degrees of freedom for sensing when the number of communication users was small. To address this, [LHS+20] proposed to jointly optimize both communication and sensing waveforms, making full use of antenna array degrees of freedom. In [LLL+22] the CRB is introduced as a measure of sensing performance Instead of minimizing the mismatch between desired sensing waveforms and used it in the ISAC/JCAS joint waveform design.

The focus of this work is on a development of an ISAC/JCAS beamforming in a multi-user and multi-target MIMO network, with particular attention paid to the optimization of the target estimation performance as measured by the CRB for unbiased estimators. The proposed problem considers the per-user SINR constraints as the communication performance guaranteeing metric and further constraint on transmit power budget limit.

Model and methodology

The considered scenario is a mmWave MIMO OFDM bi-static ISAC/JCAS system, with two multi-antenna BSs that are inter-connected via backhaul links. Each BS serves a street which is perpendicular to each other and assumes that the wireless channel between BSs is obstructed. At a given time, one BS (BS1) works as the ISAC/JCAS transmitter, while the other BS (BS2) acts as the sensing receiver that receives the reflected signals from the sensing targets. Due to the backhaul link, it is assumed that the transmitted signal is known to the sensing BS. Let N_t and N_r denote the number of antennas at the transmit and sensing BSs respectively. Both transmit BS and sensing BS comprise of uniform linear array (ULA) with half-wavelength separation. BS1 communicate with K single-antenna UEs while detecting L stationary point targets distributed within the environment. Above-described system setup is shown in Figure 4-29.

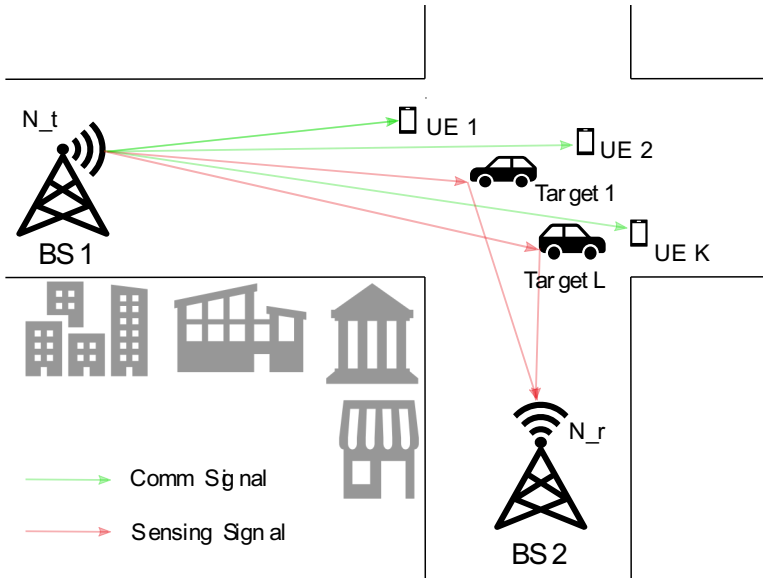

Figure 4-29 Bi-static ISAC system of two MIMO BSs, K single antenna UEs and L sensing targets.

At the transmit BS, both the communication and sensing functionalities operate simultaneously by joint beamforming. Let $\boldsymbol{s_c} \in \mathbb{C}^{\boldsymbol{K}}$ contains K unit-power data symbols intended for the K users, where each data symbol for the i-th communication user is denoted as $s_i \in \mathbb{C}$. The sensing signal is denoted as $\boldsymbol{s_s} \in$

$\mathbb{C}^{N_t}$ and assume orthogonal to communication signals, $\boldsymbol{s_c}$. Hence, the total transmit signal is written as $\mathrm{s} = [s_c, s_s]^T \in \mathbb{C}^{(K+N_t)}$. Let $\mathrm{W} = [W_c, W_s] \in \mathbb{C}^{N_t \times (K+N_t)}$ denote the transmit beamforming matrix to be design, where $W_c = [w_1, w_2, \dots, w_K] \in \mathbb{C}^{N_t \times K}$ is the communication beamformer for K communication users and $W_s \in \mathbb{C}^{N_t \times N_t}$ is the beamforming matrix for sensing. Therefore, the signal $\mathrm{x} \in \mathbb{C}^{N_t}$ transmitted by BS1 can be expressed as, $\mathrm{x} = \sum_{k=1}^{K} w_k s_k + W_s s_s$.

Without loss of generality, the following assumptions are assumed to be satisfied by the transmit signals. The communication signals intended for different users are uncorrelated, i.e., $\mathbb{E}\{s_i s_j^H\} = 0$ for $i \neq j$, and $\mathbb{E}\{|s_i|^2\} = 1$. The sensing signals sent from different antennas are uncorrelated with each other, i.e., $\mathrm{E}\{s_s s_s^H\} = I_{N_t}$. (These waveforms can be generated by pseudorandom coding.)

By transmitting x from BS1, the received signal $y_k \in \mathbb{C}$ at the receiver of the communication user k is $y_k = h_k^H x + z_c$ where, $z_c \in \mathbb{C}$ is an additive white Gaussian noise (AWGN) with the variance of σ_c^2, $h_k \in \mathbb{C}^{N_t}$ represents the communication channel between BS1 and the k-th communication user which is assumed to be known to both BSs. Further substituting x in previous equation, received signal of the communication user k is represent as, $y_k = h_k^H w_k s_k + \sum_{j \neq k}^{K} h_k^H w_j s_j + h_k^H W_s s_s + z_c$ where, the first term is the desired signal for the k-th communication UE, while the second term and the third term are the interference caused by the signals to the other UEs and the sensing signals, respectively. Thus, the signal-to-interference plus noise ratio (SINR) at the k-th communication UE can be expressed as,

$$\gamma_k = \frac{\left|h_k^H w_k\right|^2}{\sum_{j \neq k}^{K} \left|h_k^H w_j\right|^2 + \left|h_k^H R_s h_k\right|^2 + \sigma_c^2}$$

where, $\mathrm{R_s} = \mathrm{W_s} W_s^H$ denotes the sensing covariance matrix.

The received echo signal $\mathrm{y_s} \in \mathbb{C}^{\mathrm{N_r}}$ at the receiver of the BS-2 due to the transmitted signal x reflected from the sensing targets is given by $y_s = G\mathrm{x} + z_s$, where $\mathrm{z_s} \in \mathbb{C}^{\mathrm{N_r}}$ is an AWGN with the variance of each entry being σ_s^2, $\mathrm{G} \in \mathbb{C}^{\mathrm{N_r} \times \mathrm{N_t}}$ represents the target response matrix and can be further expressed as, $G = \sum_{l=1}^{L} \rho_l b(\phi_l) a^H(\theta_l)$ where L is the number of targets, $\rho_\mathrm{l}, \theta_\mathrm{l}$ and ϕ_l denote the reflection coefficient, azimuth AoD, and azimuth AoA associated with the *l*-th target. $\mathrm{a}(\theta_\mathrm{l})$ and $\mathrm{b}(\phi_\mathrm{l})$ are the transmit array response vector and receive array response vector respectively.

From the perspective of target sensing, the parameter estimation accuracy is of the main interest in the work, the CRB is adopted to evaluate the performance of the target sensing for the beamforming design. Assuming M as FIM with respect to estimation parameters, the CRB for the G is the inverse of FIM, M which can be expressed as, $\mathrm{CRB}(G) = tr(M^{-1})$. Hence, transmit beamforming optimization problem which optimizes the sensing performance while guaranteeing the per-user communication throughput satisfying the total power constraint can be expressed as,

$$\min_{\{w_k\},\, R_s \succcurlyeq 0} tr(M^{-1})$$

$$\text{s.t. } \gamma_k \geq \Gamma_k, k = 1, \dots, K$$

$$\sum_{k=1}^{K} \|w_k\|^2 + tr(R_s) \leq P_T$$

where Γ_k is the SINR threshold of the k-th communication user and $\mathrm{P_T}$ is the maximum transmission power of the BS1.

Assuming no prior information about the sensing targets, response matrix G is estimated instead of estimating individual parameters of G. In this scenario the FIM M with respect to vectorized G is reduced to $\frac{1}{\sigma_s^2} R_x^T \otimes I_{N_r}$, where $\mathrm{R_x}$ is the sample covariance matrix of x given by $R_x = xx^H$. Therefore, objective function of above optimization problem, CRB for the G will be reduced to $\sigma_s^2 N_r tr(R_x^{-1})$.

Results

To evaluate the performance of the presented beamforming optimization solution for bi-static ISAC system, simulations were carried out using numerical tools. Bi-static system considers here work in 28 GHz carrier frequency and the transmit array is an ULA with 16 elements while the receive array is ULA with 20 elements. The total available transmit power is 30 dBm while the variance of both communication and sensing channels are 0 dBm.

To check the trade-off between target estimation MSE and per user SINR threshold for single target scenario, simulations were carried out fixing number of communication users in the system. Target estimation MSE calculated from the optimization problem against the per user SINR threshold when the number of communication users are K=12 and K=6 is plotted in Figure 4-30.

It can be clearly seen from the graph that sensing parameter estimation performance is degrading as the per user SINR threshold is increasing. It is mainly due to allocating more power towards communication user direction compared to the sensing signal. It is clearly observed that as the number of users increase, the system performance degrades rapidly compared to the moderate number of users i.e., K=6 in this scenario.

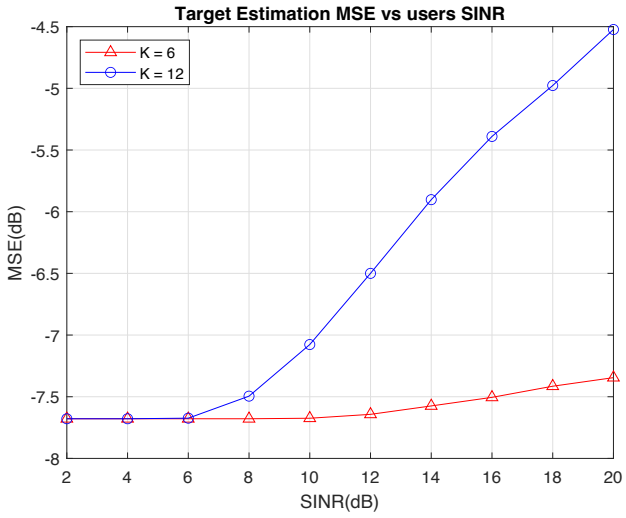

Figure 4-30 Trade-off between target estimation MSE and per user SINR threshold for single target scenario, when the number of communication users are K=6 and K=12.

Similarly, to check the trade-off between target estimation MSE against number of communication users for single target scenario, simulations were carried out fixing the per user SINR threshold value in the system. Target estimation MSE calculated from the optimization problem against the number of users in the system when per user SINR threshold at 10 dB and 20 dB is plotted in Figure 4-31.

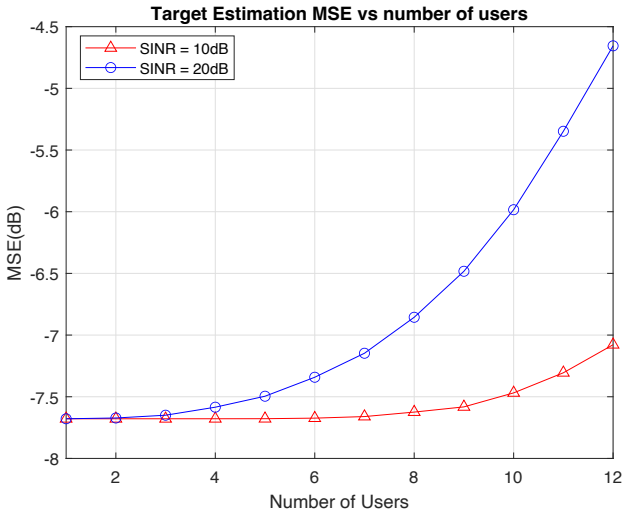

Figure 4-31 Trade-off between target estimation MSE against number of communication users for single target scenario, when per user SINR threshold is at 10 dB and 20 dB.

As mentioned earlier, this graph also proves that as the number of users increases, there is a noticeable decrease in estimation performance. However, when the required SINR threshold is around 10 dB, the variation of the MSE is not that significant even though the number of users is increased. Hence, this system performs well when modest number of communication users and SINR threshold is configured for operation.

Conclusions

The mutual interference caused by communication and sensing signals sharing the same antenna in a monostatic ISAC/JCAS system can degrade the performance of both functions. While most existing ISAC/JCAS research assumes full-duplex communication, achieving it in practice is challenging. A bi-static or multi-static ISAC/JCAS system with separate transmit and receive antennas can significantly reduce mutual interference and improve sensing parameter estimation accuracy. This work proposes an ISAC/JCAS beamforming solution for a multi-user and single target MIMO network that optimizes target estimation performance while satisfying per-user SINR and transmit power budget constraints. Currently this work is extended to detecting multiple targets and target's channel parameter estimation. In the future, different scenarios are to be considered.

4.2.6 Coverage analysis for extended reality

Motivation and background

Extended reality (XR) comprises virtual reality (VR), augmented reality (AR), mixed reality (MR) and it is expected to be the emerging immersive application in the future communication systems [BMM+20]. Due to the high data rate and high-accuracy localisation performance requirement, the related XR applications need to be supported by the mmWave (30-100 GHz) and even the THz frequency band (0.1-10 THz). Although promising localisation results are shown in these works and new localisation-aware mobile network deployment solutions are proposed [ASB+22], the coverage issue is rarely discussed, which is a practical issue in real localisation scenarios. This coverage is more pronounced when 3D orientation of the UE is considered (i.e., 6D localisation) due to the antenna array equipped at the UE side. As a result, by exploring the spatial structure of the sub-arrays (SAs) (i.e., 3D array) in an array of SAs system, the connectivity can be enhanced and the coverage with regards to both communication and localisation KPIs can be improved.

Model and methodology

Consider a far-field downlink scenario with M BSs and one UE, as shown in Figure 4-32-(a). The positions and orientations of the BSs are known in a global coordinate system (GCS). Each BS is equipped with a planar array and is connected to an independent radio frequency chain (RFC). By

adopting a 3D array of SAs structure, the array of the UE consists of N planar SAs arranged in a 3D space with fixed relative positions and orientations, as shown in Figure 4-32 and Figure 4-33. Each SA is connected to an independent RFC. Both localisation (i.e., determining the position and orientation of the UE) and communication functions are considered in this system.

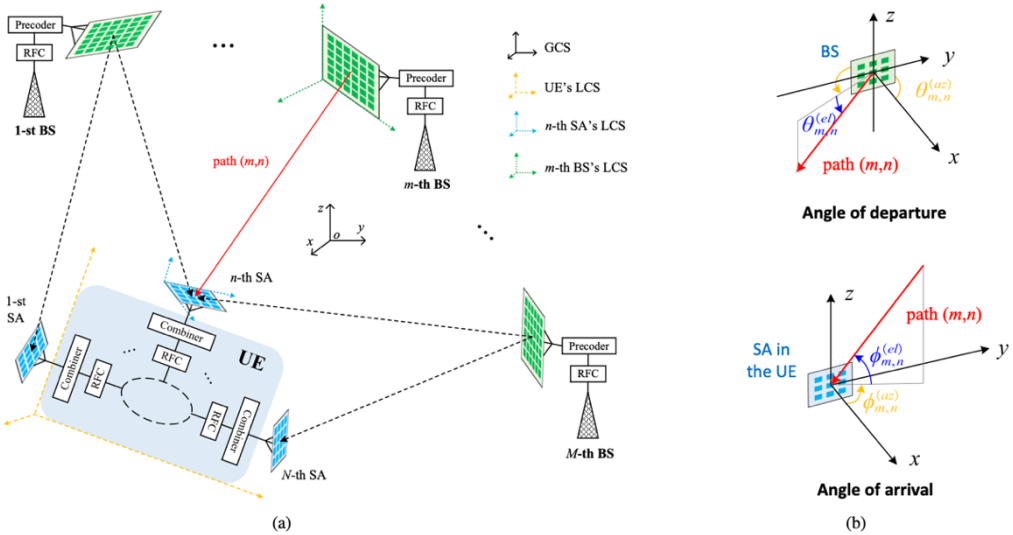

Figure 4-32. Illustration of the considered geometric model. (a) A downlink MIMO wireless system with multiple BSs and one UE equipped with a 3D array. (b) The geometry of the azimuth and elevation components of the AoD and AoA.

In THz wireless communication systems, the LOS path plays a dominant role [SNA+20]] while the multipath fading effect also exists due to the scattering on aerosols in the atmosphere [BPA19]. A commonly used model for THz wireless propagation captures the LOS path through a deterministic model and generates the multipath components using random processes of known distributions [TSC+21]. As experimentally validated by [PBA21], Rice distribution that models both LOS and NLOS components can achieve a good fit to empirical measurement data in an indoor THz wireless environment. Therefore, a Rician fading model is used to characterize the statistics of the considered THz channel, which contains all the geometric information (e.g., AoA, AoD, and delay) of the signal propagation path. Based on the channel model, the localisation error bound for 3D position and 3D orientation estimation can be derived. Sequentially, the localisation coverage can be defined as the probability that the PEB/OEB is lower than a threshold ξ_p/ξ_o when the UE is at random positions with a random orientation [ZBC+22].

Results

Two different array configurations (2D and 3D) are evaluated, each configuration with 6 SAs. For the 3D array, each SA is placed at the centre of a side of a $0.1 \times 0.1 \times 0.1\text{m}^3$ cube. On the other hand, the 2D array has all the SAs placed on a plane. Figure 4-33 shows the two array layouts where the cube is tiled into a plane. To evaluate the performance of the two array configurations, an indoor scenario with two BSs as shown in Figure 4-34 is considered, where the UE is placed inside a $20 \times 20 \times 5\text{m}$ indoor space (i.e., $-10 < x < 10, -10 < y < 10, 0 < z < 5$).

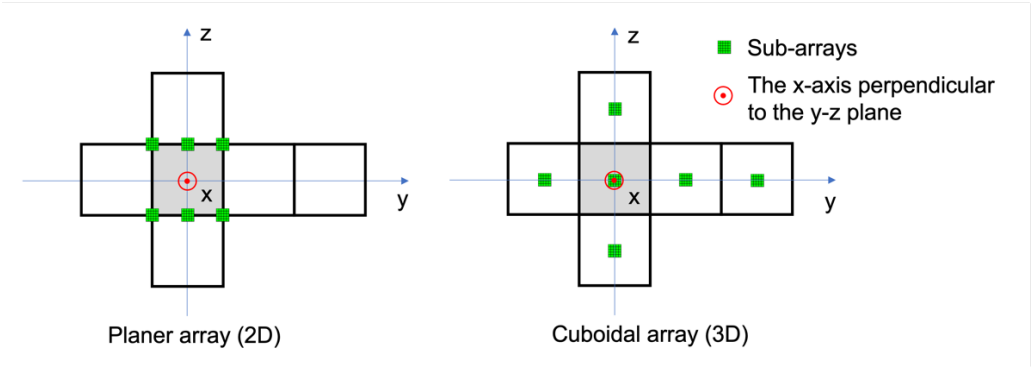

Figure 4-33 Illustration of the planar (2D) and cuboidal (3D) array layouts by tiling the cube into a plane.

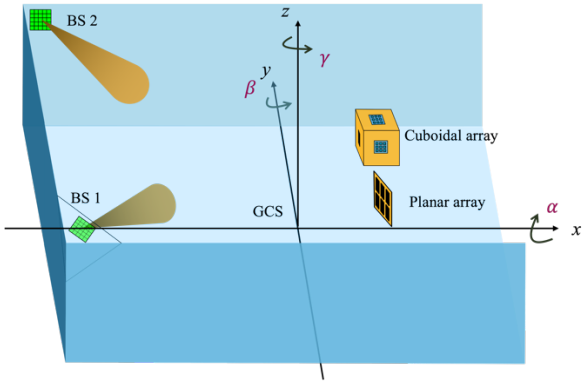

Figure 4-34 The indoor scenario considered in simulations.

The localisation coverage of the 2D and 3D array configurations are evaluated. To this end, the UE position and orientation are generated using a uniform distribution, namely, $x, y \sim U(-10, 10)$, $z \sim U(0, 5)$, and $\alpha, \beta, \gamma \sim U(0, 5)$. The PEB and OEB samples are collected to attain an empirical CDF. To give a compact view of the PEB/OEB's threshold with the coverage in different order of magnitude, the complementary cumulative distribution function (CCDF) is shown, by performing two simulations: (i) M = {2, 3, 4} BSs in a system with a fixed antenna directivity. From Figure 4-35 and Figure 4-36 it is observed that the planar array (dashed curves) suffers from limited coverage for all cases. As explained earlier, this is due to the lack of LOS with enough BSs in some specific UE orientation. Take the 4 BSs, $\theta = 180^{\circ}$ case with a coverage of 70% (outage of 30%) for example, a PEB within about 0.028 m using the cuboidal array is attained, while the planar array gives a PEB within about 0.173m. The same result holds in most of the range of the threshold ξ_p/ξ_o, revealing that the cuboidal (3D) array can achieve better coverage than the planar (2D) array in the practical range of threshold. Besides, from Figure 4-35 it is seen that under the same threshold, the more BSs that are deployed, the lower the outage and thus the higher the coverage that can be obtained for both 2D and 3D arrays. From Figure 4-36, it is seen that increasing the antenna directivity (i.e., decreasing θ) would improve the localisation coverage in the low ξ_o area but degrade the localisation coverage in the high ξ_o area. This is because a more directional antenna increases the antenna gain and thus produces a lower PEB and OEB in the covered space, which results in the higher coverage in the low ξ_o area. However, at the same time, a narrower beam also causes the shrinkage of the covered space, which results in the coverage limit in the high ξ_o area.

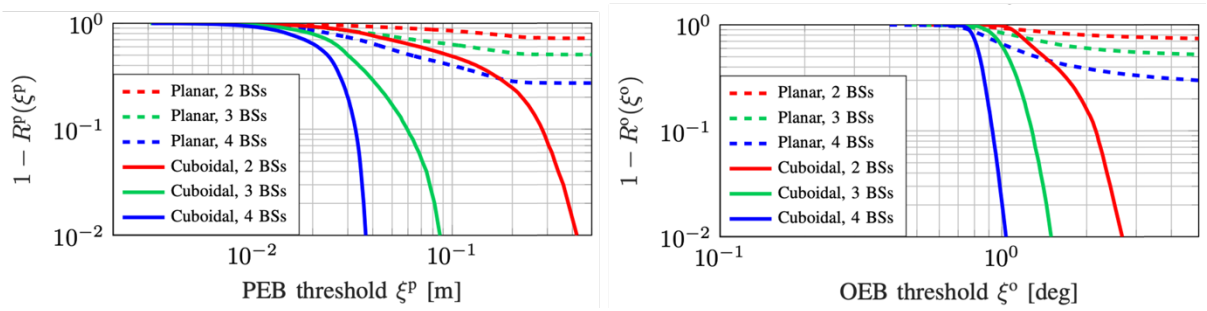

Figure 4-35 PEB and OEB coverage of the two types of arrays under {2,3,4} BSs with antenna directivity $\vartheta = 180^{\mathrm{o}}$.

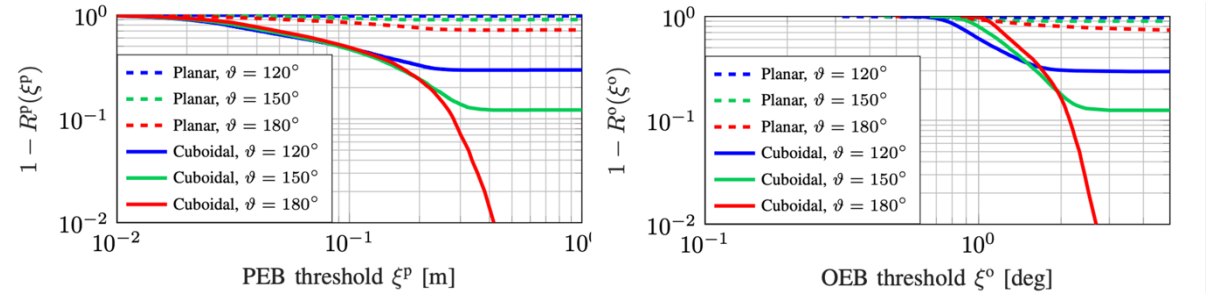

Figure 4-36 PEB and OEB coverage of the two types of arrays under antenna directivity $\vartheta = \{120^{\mathrm{o}}, 150^{\mathrm{o}}, 180^{\mathrm{o}}\}$ with 2 BSs.

Conclusions

A downlink, far-field sub-THz band MIMO wireless system is considered with multiple BSs and one UE equipped with a 3D array over a Rician fading channel. By deriving the localisation error bound in terms of PEB and OEB, the planar and 3D array configurations were analysed and compared with regards to the coverages of these metrics. The numerical results revealed a higher coverage for 3D array in both localisation and communication KPIs given a suitable threshold, and minor performance loss in certain areas compared with the planar array. The results are instructive for the BS placement optimization, array design of the THz localisation and communication systems, which can be potential future research directions.

4.2.7 Location-aided communications

Motivation and background

With 4G and 5G, wireless networks have made great progress in serving stationary/low mobility devices. At high speeds, however, there are still various issues to be solved. To connect everything at any time and any place, as one of the main objectives of 5G and beyond, vehicle-to-anything (V2X), in general, Internet-of-Vehicle (IoV) [GMA+22] communication plays an important role as the passengers in their vehicles expect the same quality-of-service (QoS) as they experience at home. With levels 3-5 of self-driving vehicles and the probable standardization of mobile integrated access and backhaul (IAB) in 3GPP Release 18, considerably higher rates may be required compared to those provided by LTE. Here, following 5G NR, there may be a need for using mmWave communications via small-cell deployments.

Although mmWave communication supports high data rates, it can be significantly affected by the penetration loss, along with severe path loss and beamforming mismatch. Blockage becomes more problematic for high mobility IoV systems, e.g., in highways or rural areas, due to the lack of good reflectors (e.g., buildings) and the mobility of vehicles. Beamforming mismatch was highlighted in [HEX23-D23] as an important challenge for mmWave communication and the necessity for side information (such as location information) was pointed out to perform initial beam access.

Recently, as one contribution to [HEX22-D32], [GMA+22] proposes a dynamic BS handover scheme for blockage avoidance using additional large-scale predictor antennas [GMP+21] mounted on top of vehicles. However, deploying extra BSs/antennas may not be commercially viable, and requires backhauling/handover with possible failures/delays. More importantly, deploying a BS/IAB along a highway/inter-city road may not be feasible if electricity connection is missing.

Instead of deploying additional BSs, one may consider the concept of RISs, as a low-power alternative solution. With a proper deployment, RISs can cover different areas of the highways/inter-city roads, which makes it possible to bypass dynamic blockages with no need for handover, backhauling, and wired energy supply of regular BSs, which would consume higher power with larger overheads.

In [GMA+22b], the potentials and challenges of RIS-based IoV communications were studied in highways/inter-city roads with dynamic blockage pre-avoidance. The work concentrated on two key challenges of RIS in high-speed IoV networks, namely, channel state information at the transmit side (CSIT) acquisition and imperfect beam reflections. To reduce the CSIT acquisition overhead, a large-scale fading-based service region prediction scheme is proposed. Here, the service regions of different RISs, based on the location information, are learnt by the network beforehand for predicted dynamic blockages positions. In this way, without instantaneous CSIT, the BS can exploit the vehicle and the dynamic blockers speed information to pre-select the RISs in different time slots. Then, the hardware aspects such as the transceiver impairments and phase noise effects leading to imperfect reflections are studied and the performance of the RIS-based scheme with multiple candidate techniques is compared.

Model and methodology

To enable multi-RIS IoV communications, one needs to reduce the RIS selection and configuration overhead as well as the sensitivity to the vehicles speed. For this reason, a large-scale based RIS pre-assignment (LSRPA) scheme is proposed in which the UEs and the blockers speed/position information is utilized along with the large-scale channel properties to predict and pre-select the RIS of interest, among multiple ones.

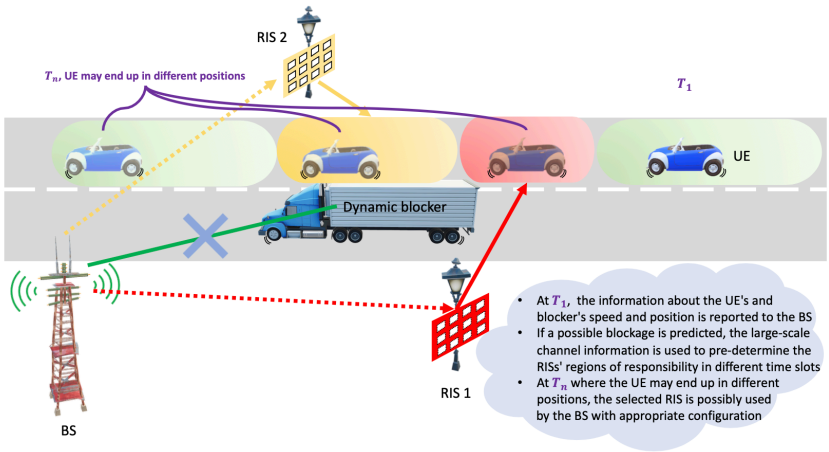

Figure 4-37 The proposed blockage pre-avoidance scheme in RIS-aided IoV networks.

Consider the cases with either a macro or a small BS along a highway/inter-city road, as illustrated in Figure 4-37. The LSRPA scheme follows the following procedure. At time slot T_1, if the vehicular UE detects a dynamic blockage, e.g., by a truck, it estimates the speed and the position of the blocker, e.g., using cameras, lidars. Then, along with its own speed/position information, the UE informs the BS about the speed and the position of the dynamic blocker (As an alternative approach, each vehicle can inform the BS about its own speed/position information). Knowing the blocker speed/position information at T_1, the BS predicts the blocker position at Slot T_n. Then, the BS utilizes the large-scale channel condition, i.e., the average performance which has been learned over time for the different blocker positions, to find the appropriate regions of interest to be covered by different RISs in different time slots. Then, the BS exploits the UE speed/position information provided at T_1 to predict the UE position at Slot T_n and pre-select the appropriate path towards the UE, either through direct BS-UE

connection or via an RIS-assisted link. Finally, at Slot T_n, only the instantaneous CSIT of the pre-selected path, and not all possible paths, is acquired and the BS/RIS beamforming is adapted accordingly.

Results

Considering the cases with one BS and two or three RISs with perfect and imperfect reflection efficiency, in the following, the performance of the LSRPA scheme is evaluated, in comparison with other alternative techniques. Typical RIS setups, as in, for example, [ZRS+21] are used, and the RIS beamforming is performed using [3, Algorithm 1]. As the metric of interest, the throughput (defined as the total number of successfully decoded bits per total transmission duration) is evaluated. Both sub-6 GHz (2.8 GHz) and mmWave (28 GHz) bands are considered and different numbers of RIS elements (10-500), are shown in Figure 4-38. The effect of the hardware impairments is studied. To evaluate the efficiency of the LSRPA scheme, it is compared with different alternative methods, listed in Table 4-1.

Table 4-1. Evaluation methods for location-aided communications.

Name of the method	Details
Proposed LSRPA scheme	Utilizing RISs for dynamic blockage pre-avoidance.
Additional BS	An additional BS is deployed to bypass the blockage with more cost.
Network controlled repeater	It is a normal repeater with beamforming capabilities. More expensive but has active signal amplification.
Benchmark	An ideal case where BS search for all possible links with perfect CSIT.
Random phase	LSRPA method without optimizing the RIS phase.
No RIS	The UE is served by BS direct link without the help from RIS.

Here, throughput is presented as a function of the BS transmit power with dynamic blockage. The BS and the UE are equipped with 16 and 4 antennas, respectively. The RISs have 200 elements. The transmit power at the repeaters is set to 32 dBm. With transceiver impairment, the proportionality coefficients, which describe the severity of the distortion noises at the transmitter and the receiver, are set to 0.005 (see [XWW+21] for the details of the hardware impairment model). The BS-RIS 1/repeater 1 and BS-RIS 2/repeater 2 hop distances are set to 200 m and 126 m, respectively. The hop distance between the BS and the additional BS and RIS 3 are 1500 m and 150 m, respectively. Finally, the results of sub-6 GHz refer to the case that the BS switches to sub-6 GHz with no RIS. Except for the results of sub-6 GHz with 20 dB VPL, 2.8 GHz frequency and 5 MHz bandwidth, the rest of the results are obtained with 40 dB VPL, 28 GHz frequency and 10 MHz bandwidth.

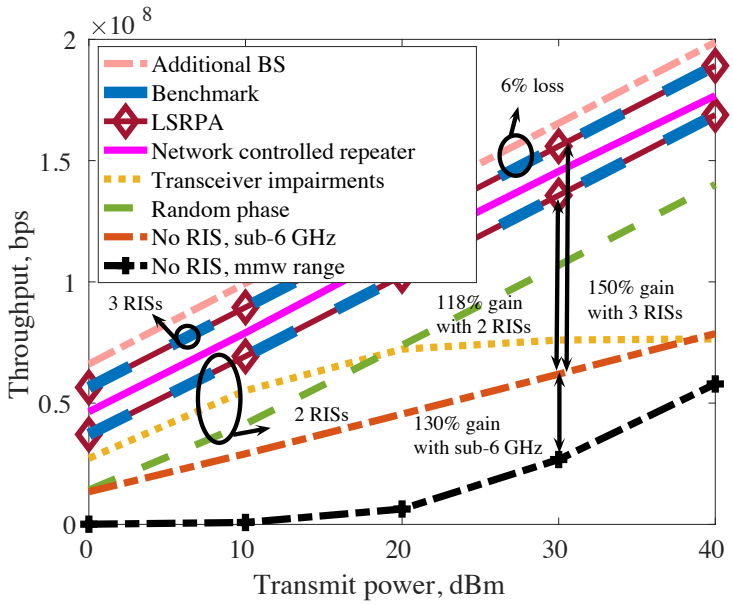

Figure 4-38 Location-aided communication performance evaluation, from [GMA+22b].

A few interesting insights can be drawn from the results:

- The proposed LSRPA scheme can reach the same performance as the benchmark, with lower overhead, thanks to the utilization of location information.
- The performance loss is not high compared to additional BS cases for both 2 and 3 RISs.
- Hardware impairments and random phases could degrade the performance drastically.
- Sub-6GHz is better when using a direct path thanks to lower penetration loss.

Conclusions

The potentials and challenges of RIS-assisted communication for blockage pre-avoidance in moving networks were studied. As demonstrated, RIS pre-selection and blockage prediction gives a chance to make the network performance more robust against dynamic blockages with an acceptable CSI acquisition overhead, compared to exhaustively estimate all RIS channels.

5 From theory to practice

In this section the effects of hardware impairments on localisation and sensing measurements are investigated. There are also results presented from measurements performed with a demonstration setup focusing on AoD estimations and ISAC.

5.1 Impact of hardware impairments

Most localisation and sensing works rely on idealized models of the received signals as a function of the channel parameters (angles, delays, Dopplers) induced by the propagation environment, based on the assumption of deterministic and sparse channels in high-frequency systems. However, in sub-THz bands for 6G communications, pilot signals can be distorted due to the presence of HWIs. Consequently, when algorithm derivation is based on a mismatched model (i.e., without considering the HWIs in the channel model), the localisation performance is unavoidably affected. In this section, an OFDM-based system is considered and the impacts of various HWIs on the received observations based on the HWI models mentioned in Section 4.1.2 are evaluated. It is assumed that the localisation and sensing algorithms have no knowledge about these residual HWIs. The degradation of performance is quantified by the misspecified Cramér-Rao bound (MCRB) [FGG+17], and the impact of individual impairments are also discussed.

5.1.1 The effect of hardware impairments on sensing

5.1.1.1 Analysis of impact of hardware impairments on bistatic sensing

In this section, the effects of each hardware impairment namely, PN, IQI, and PA are analysed through simulations for range estimation in a bistatic sensing scenario. The simulation setup is based on the 5G NR CP-OFDM grid with 120 kHz subcarrier spacing, 400 MHz bandwidth, and 16-QAM modulation. The environment consists of a transmitter and a receiver, plus two other reflections from the walls according to Figure 5-1. Both transmitter and receiver are equipped with a linear antenna array of 8 antenna elements, and free path loss model is used for the LOS path and reflections. The range spectrum is depicted based on 2-D FFT on the grid without applying any further windowing.

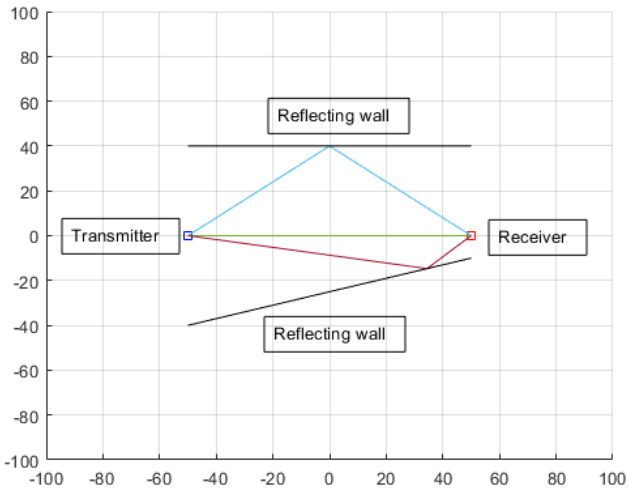

Figure 5-1 Simulation environment for evaluating the impact of HWIs on bistatic sensing.

The effect of each HWI represents itself as added distortion to the received signal and increases the noise floor in the range spectrum as indicated in Figure 5-2, Figure 5-3, and Figure 5-4. The theory behind this phenomenon can be explained by Bussgang theorem [BUS52]. Suppose that the input-

output relation for a nonlinear system is defined as $\boldsymbol{z} = \boldsymbol{F}(\boldsymbol{x})$. Based on the Bussgang theorem, in a MIMO scenario the input-out relation can be expressed as

$$\boldsymbol{z} = \boldsymbol{F}(\boldsymbol{x}) = \boldsymbol{B}\boldsymbol{x} + \boldsymbol{D}$$

Where **B** is a matrix of the form of

$$\boldsymbol{B} = \boldsymbol{C}_{zx}\boldsymbol{C}_{x}^{-1}$$

Where $\boldsymbol{C}_{zx}$ and $\boldsymbol{C}_{x}$ are cross-correlation and auto-correlation matrices, and **D** is the distortion matrix uncorrelated with $\boldsymbol{x}$. This distortion represents the increase of noise floor. This model can be applied for all HWIs without loss of generality.

The increase of noise floor level can be problematic in case of a multi-target scenario with different radar cross-sections for different targets, as the weak reflections corresponding to smaller radar cross sections may fall below the noise floor and masked out. Even in case of not being masked out, still the higher noise floor affects the detection algorithms, for example in constant false alarm rate (CFAR) detector, the higher noise floor directly affects the threshold for detection that can filter out weak reflections.

As can be seen in the Figure 5-2 and Figure 5-3, the target at 128 meters is masked out in case of applying the HWIs effect for PN and IQI. In Figure 5-4, the effect of PA nonlinearity is depicted for two different cases of 0% input back-off (IBO), and 20% IBO. By applying 20% IBO, the nonlinearity effect is suppressed to some level that the difference between the highest target peak and the lowest target peak decreases by 0.5 dB. In this way, it shows how the suppressed nonlinearity effect contributes to the detection. When targets have less difference in spectrum magnitude, the CFAR detection scales the detection threshold in a way that turns out to higher probability of detection for weak targets. On the other hand, increasing too much on IBO decreases the total received power which can lead to lower SNR, so the choice of IBO should be optimized by considering the system settings and thresholds for the detection in the CFAR detector.

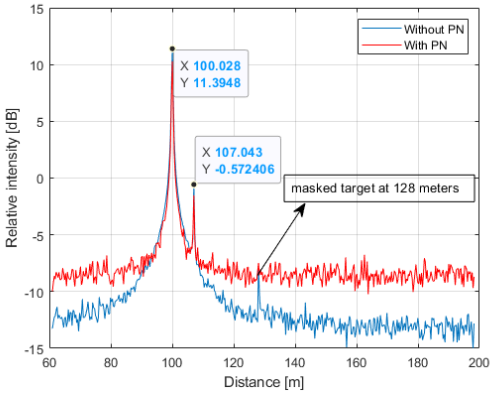

Figure 5-2 Range spectrum map considering the effect of PN.

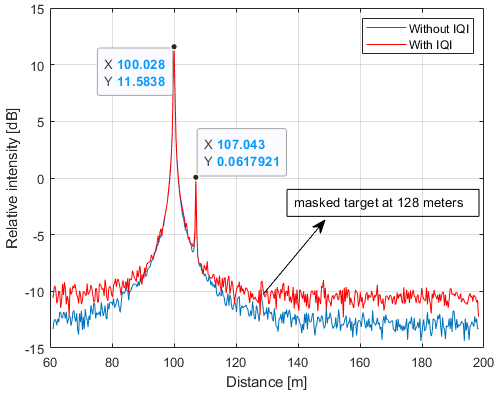

Figure 5-3 Range spectrum map considering the effect of IQI.

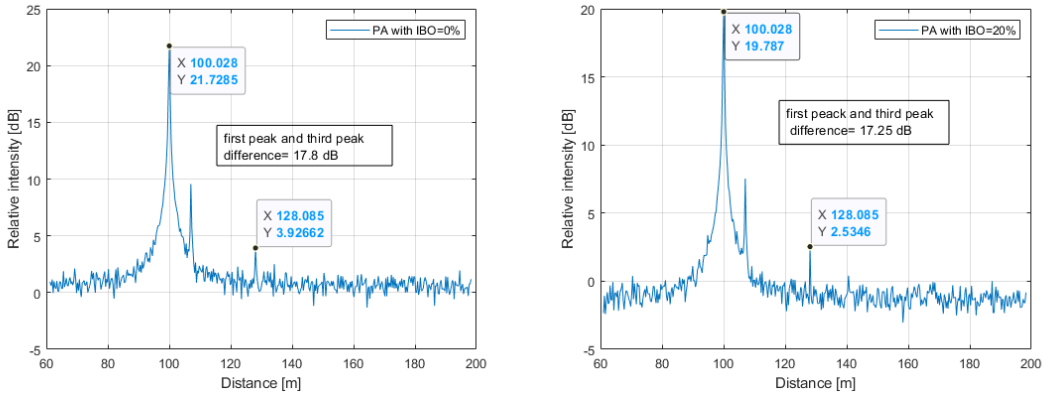

Figure 5-4 Range spectrum map considering the effect of PA.

5.1.1.2 Analysis of impact of phase noise on monostatic sensing

In this part, the same ISAC/JCAS setup as in Section 4.2.2 is considered and the MCRB analysis [FGG+17] is employed as a tool to theoretically quantify the impact of PN on monostatic sensing when the sensing receiver is unaware of PN, i.e., when the receiver applies standard algorithms without taking into account the presence of PN [KME+22]. The following theoretical bounds are evaluated:

- CRB (PN-free): The deterministic CRB on delay-Doppler estimation in the absence of PN provides a hypothetical baseline to reveal PN-induced performance gaps.
- CRB: The hybrid CRB on delay-Doppler estimation in the presence of random PN quantifies the sensing performance when the sensing receiver is aware of PN and has the knowledge of its statistics.
- Lower bound (LB): The LB on delay-Doppler estimation, obtained as a result of the MCRB analysis [FGG+17], quantifies the sensing performance when the receiver is unaware of PN.

Simulations have been conducted using the following parameters: a carrier frequency of 140 GHz, a bandwidth of 30.72 MHz, comprising 256 subcarriers with 120 kHz subcarrier spacing. Each OFDM symbol has a duration of 8.91 µs, comprising the data part (8.33 µs) and the cyclic prefix (0.58 µs). In addition, a target with range 50 m and velocity 4 m/s is considered and an oscillator with 3-dB bandwidth 100 kHz and loop bandwidth 1 MHz (in the case of PLL) is used.

Figure 5-5 and Figure 5-6 show the theoretical bounds on range-velocity estimation with respect to SNR and target range for FRO architectures, respectively. It is seen from the LB curves that the mismatch between the true model with PN and the assumed model without PN (i.e., the PN-unaware receiver) leads to large performance losses in range and velocity estimation, which are especially more pronounced at high SNRs and far-away targets. The reason is that the variance of the delay-dependent PN process increases with target delay [KME+22]. In addition, at low SNRs, the dominant factor affecting the sensing performance is additive noise (thermal noise), while at high SNRs, the effect of PN becomes more significant than that of additive noise, leading to performance bottlenecks.

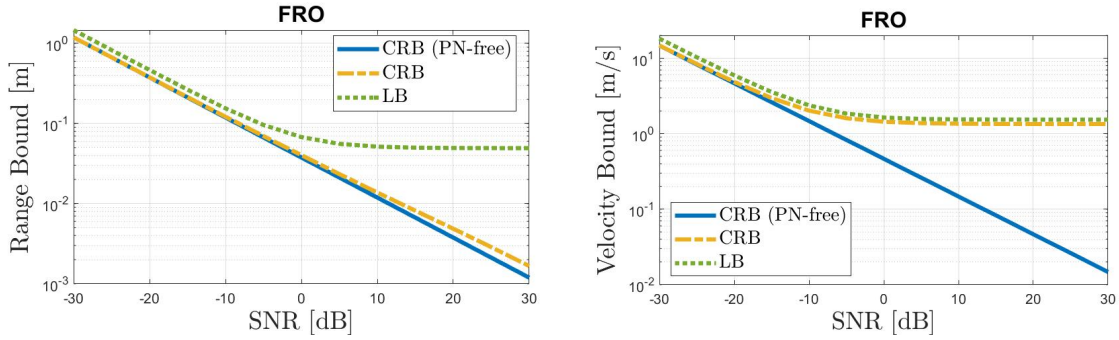

Figure 5-5 Theoretical bounds on range and velocity estimation under the impact of PN, as a function of SNR.

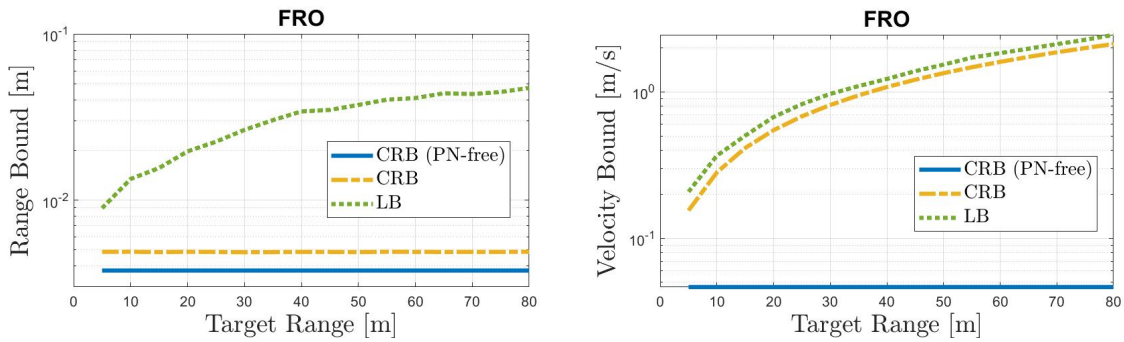

Figure 5-6 Theoretical bounds on range and velocity estimation under the impact of PN, as a function of target range.

In Figure 5-7, the theoretical bounds are plotted with respect to PLL loop bandwidth. It is observed that ignoring PN can lead to an order of magnitude degradation in ranging accuracy. For velocity estimation, the gap between the LB and the CRB is less pronounced compared to range estimation, indicating that the effect of PN on velocity estimation is difficult to mitigate since the correlation of PN across OFDM symbols is very low thus cannot be exploited for PN estimation and compensation.

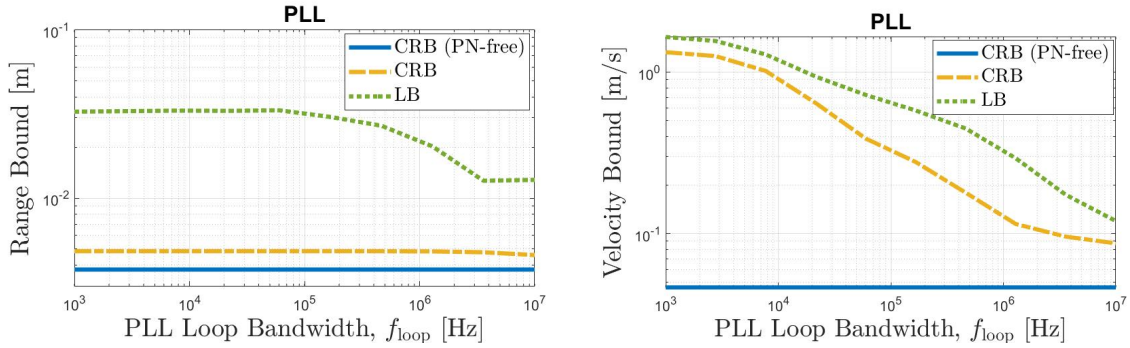

Figure 5-7 Theoretical bounds on range and velocity estimation under the impact of PN, as a function of PLL loop bandwidth.

5.1.2 The effect of hardware impairments on localisation

Based on the channel models with HWIs described in Section 4.1.2, simulations to evaluate the effect of HWIs on localisation are performed (the details of simulation parameters can be found in [CKA+23b]).

5.1.2.1 Channel estimation results

For convenient analysis, one specific realization of the HWIs for the system is adopted. The results of channel parameters estimation using the ESPRIT (estimation of signal parameters via rotational invariance techniques) method [RK89] (circle, square, and diamond markers) and the MMLE (mismatched MLE) (solid curves) are shown in Figure 5-8-(left). The estimators are benchmarked by the CRBs of the ideal/mismatched model (CRB-MM, dashed curves) and the LB using a mismatched model (dotted curves with cross markers). Note that the average transmit power P is calculated without considering the nonlinearity of the power amplifier (calculated before the PA). When the transmit power P is low, the LB (of using a mismatched model) has a similar performance as CRBs. This indicates that in low transmit power, the mismatched model will not significantly affect the performance, as the expected accuracy is low and limited by the noise. With the increase of transmit power, the contribution of MCRB decreases due to an increased SNR, and eventually, the mismatched localisation is lower bounded by the absolute lower bound (ALB). This indicates that the localisation performance can no longer be improved by increasing transmit power, which cannot be ignored in the scenarios require high-accuracy localisation performance. Regarding the estimators, the ESPRIT (using a mismatched

model) provides low-complexity results with limited performance in delay estimation. However, the refined results using an MMLE can reach the LB (solid curves align well with the dotted curve).

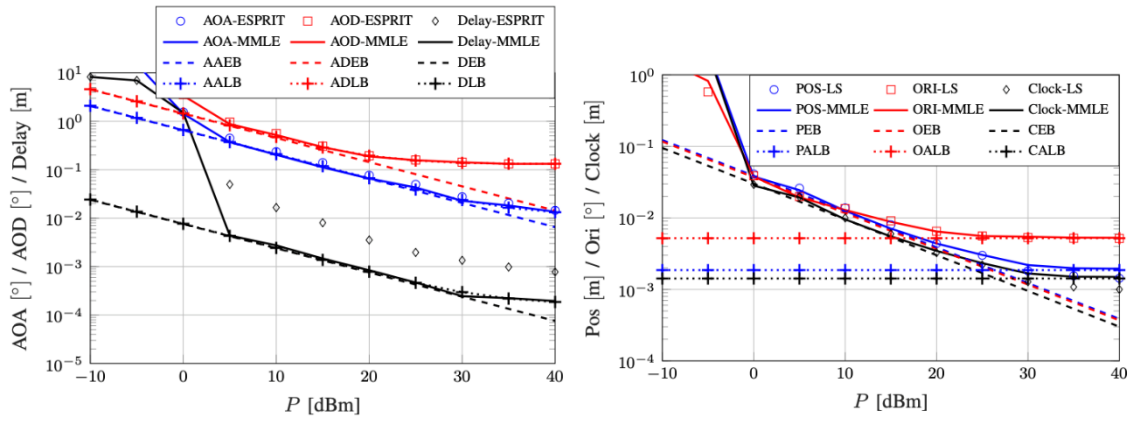

(a) (b)

Figure 5-8 The effect of HWIs on localisation. (a) Comparison between channel parameters estimation results (ESPRIT and MMLE) and different lower bounds (CRB of the MM and the LB of the mismatched estimator) in terms of AoA, AoD and delay. (b) Comparison between localisation results (position, orientation, and clock offset estimation) and different lower bounds (CRB of the MM and the LB of the mismatched estimator).

5.1.2.2 Localisation results

Based on the estimated channel parameters, the UE position and orientation can further be calculated. Like the channel estimation results, two estimators (LS and MMLE) and two bounds (CRB and LB) are evaluated. The results for localisation are shown in Figure 5-8-(b). The figure shows that at low transmit powers, the LB and CRBs coincide, implying that the HWIs are not the main source of error. At higher transmit powers (10 dBm for OEB, and 20 dBm for PEB), LB deviates from the CRBs, and the positioning performance is thus more severely affected by HWIs. The MMLE in high SNR is close to the ALB, indicating the validity of the MCRB analysis. Now that the validity of the bounds has been established, in the following the effect of HWIs on localisation is evaluated based on the bounds. First the impairments are studied individually, then the impact of the waveform type is evaluated, and finally, the impairment levels are varied.

5.1.2.3 The effect of individual impairments

To understand the effect of different types of HWIs, the LB for AoA, AoD, and delay estimation are studied by considering one type of HWIs at a time. The results are shown in Figure 5-9 for (a) PN, (b) CFO, (c) MC, (d) AGE, (e) ADE, and (f) IQI. The effect of PA is discussed in Figure 5-10. Considering the HWIs defined as random variables with a fixed impairment level, multiple hardware realizations are performed with a fixed pilot signal, and all the resultant LBs are plotted in the shaded regions. The results show that different types of the HWIs affect angle and delay estimation differently. The PN, CFO, and IQI introduce noise on the symbols across different subcarriers and hence affect delay estimation. Since the phase change introduced by CFO affects the phase changes across beams, angle estimation will also be affected. Instead of affecting the phase changes between different subcarriers, the MC, AGE, and ADE distort the steering vectors and therefore have a more significant effect on the angle estimation. For all the HWIs, the negative effect on the performance occurs when the transmit power is high.

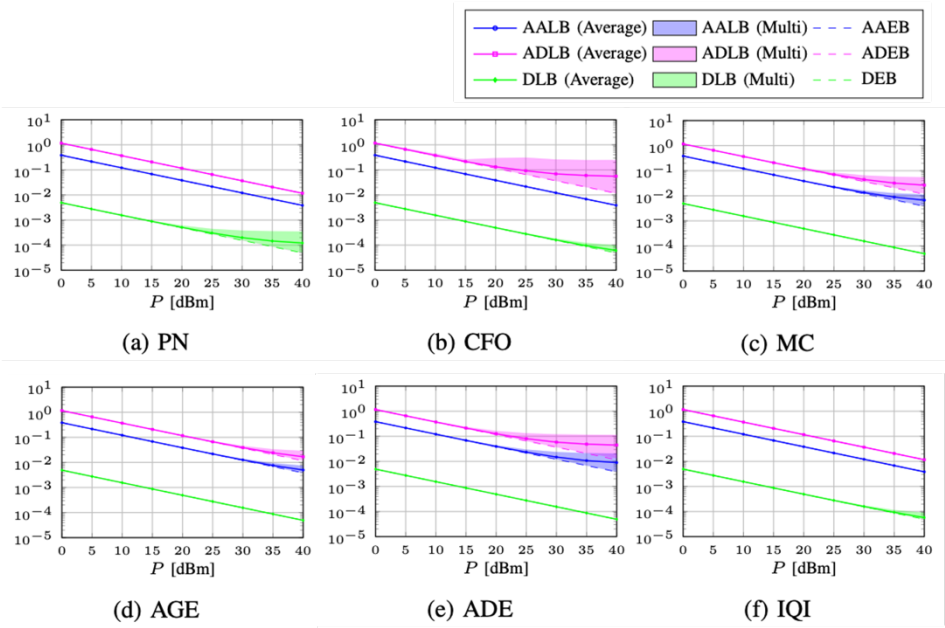

Figure 5-9 LBs of channel parameter estimation under different types of impairment with multiple realizations: (a) Phase noise, (b) Carrier frequency offset, (c) Mutual coupling, (d) Array gain error, (e) Antenna displacement error, (f) IQ-imbalance. The y-axis represents angle in degrees and delay in meters.

High peak-to-average-power ratio (PAPR) is one of the critical issues in implementing the OFDM signals, and a promising alternative is to use DFT-S-OFDM. When increasing the transmit power, the PAN is more likely to happen, as can be seen in Figure 5-10-(a). The delay estimation suffers more from the nonlinear distortion because of the clipping of transmit signal, which distorts the uniformity of phase changes across the subcarriers. The effect on angle estimation is less pronounced (at the same level of transmit power) since different antenna elements experience similar distortions with identical PAs adopted in this work. The random OFDM symbols and the FFT version of the benchmark symbols (a special case of DFT-S-OFDM by choosing an identity mapping matrix) are compared, and the results are shown in Figure 5-10-(b). Due to the reduced PAPR by DFT-S-OFDM, the localisation performance can be improved, as shown in the right figure, at the expense of reduced data rate by the spreading factor employed in DFT-S-OFDM [Mie19].

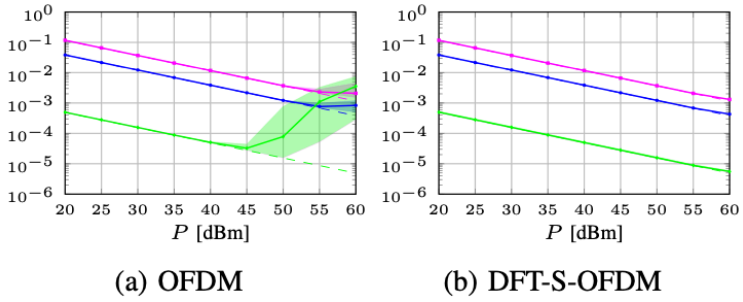

Figure 5-10 The effect of PA on channel parameters estimation using (a) OFDM, and (b) DFT-S-OFDM. The legend is the same as Figure 5-9.

In summary, the simulation results showed that PN and IQI have a stronger effect on delay estimation, while MC, AGE, and ADE have a more significant effect on angle estimation. The CFO and PAN affect both angle and delay, where the former one depends on the sweeping strategy and number of transmissions, and the latter's factor is determined by the transmit power or amplitude of the signals.

5.2 Over-the-air demonstration

In this section, the setup and of the experiment and their results for mmWave localisation and sensing are presented. The objectives of these experiments are to (i) understand the practical limitations (in particular the impact of hardware impairments) of localisation and sensing; (ii) report the achievable performance with a real hardware platform. The demonstration setup consists of a Xilinx Zync Ultrascale+ RFSoC ZCU111 evaluation kit, 2 SiversIMA semiconductors EVK06002 57-71 GHz radio evaluation kits and a PC for data processing. The waveform used for the measurements is an OFDM signal based on the 5G new radio (NR) standard, modified to have a subcarrier spacing of 960 kHz. Two different waveforms have been used with different bandwidths, one with 400 MHz bandwidth and the other one with 800 MHz.

5.2.1 Localisation

The localisation measurements have focused on how to improve the AoD estimation using derivative beams. Figure 5-11 provides an illustration of the measurement setup and the definition of AoD. Here, the measurements at the Rx are processed to estimate the AoD from the Tx array, which could in principle be combined with range estimates to estimate the location of the Rx. As a first step the beams had to be created and characterised. This was done using the demonstration setup with the Tx radio mounted on a turntable, and a power meter for measuring the received signal. The Tx radio is equipped with a 16-element uniform linear array with 2.5 mm inter-element spacing and the carrier frequency is 69.12 GHz. The Tx and the Rx were mounted three meters apart surrounded with absorber material, as can be seen in Figure 5-12. Each beam was characterised for directions in the range ±60º with measurement steps of 1.8º. In Figure 5-13 the measurement results for the boresight beam and its corresponding derivative beam are presented.

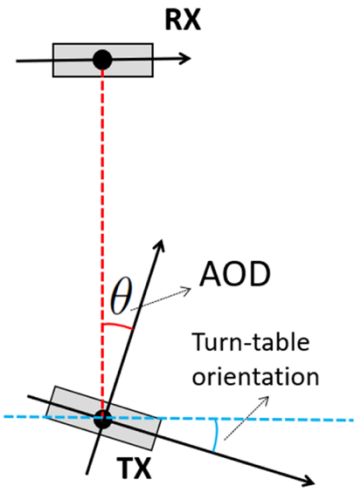

Figure 5-11 Bird-eye view illustration of the setup for AoD measurement experiments, showing the definition of turn-table orientation and AoD.

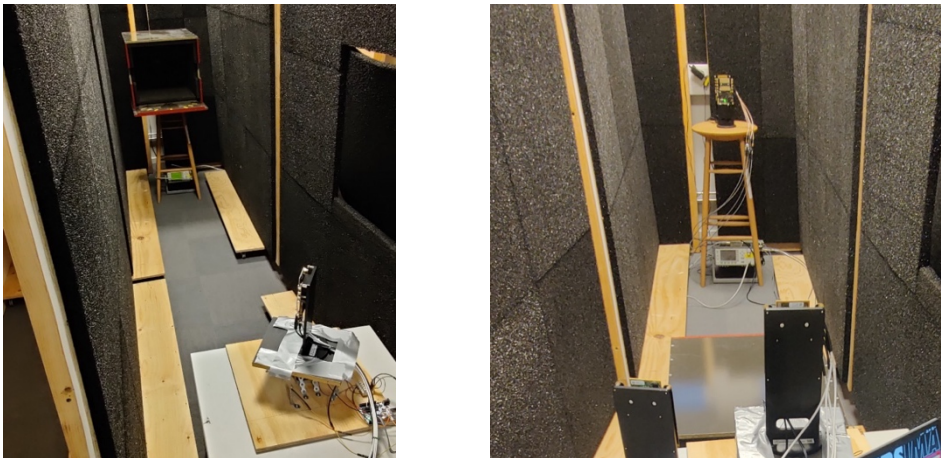

Figure 5-12 Setup used for beam (left) and AoD (right) measurements. The Tx radio is mounted on a turntable in both cases. For the beam measurements a horn antenna is mounted 3 m away and connected to a power meter and for the AoD measurements the horn antenna is replaced with the Rx radio. The setup is also surrounded with absorber material to minimise reflections from the surroundings.

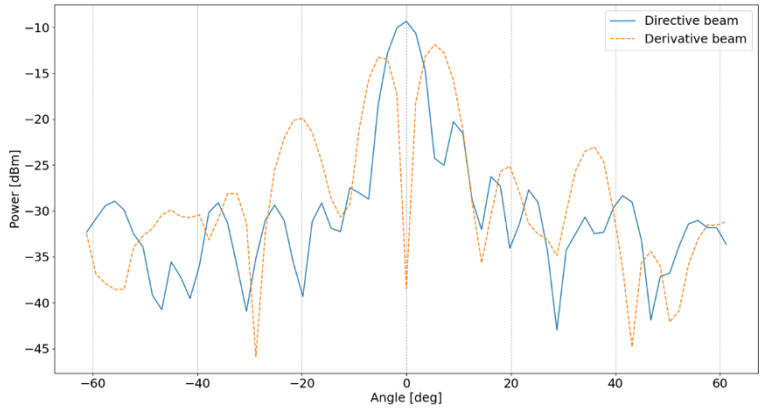

Figure 5-13 Measurement results from beam characterisation of directional beam in blue solid line and its corresponding derivative beam in dashed orange line.

For the measurements, an OFDM waveform with N = 384 subcarriers and M = 1120 symbols is transmitted. A total of 10 beams are employed (5 directional/sum and 5 derivative/diff beams), and each occupying a certain number of symbols in the time domain, as shown in Figure 5-14. Each pair of directional and derivative beams is steered towards a certain angle, leading to a total of 5 angles (beam look directions) given by [-5.8 -2.9 0 2.9 5.8] degrees, respectively.

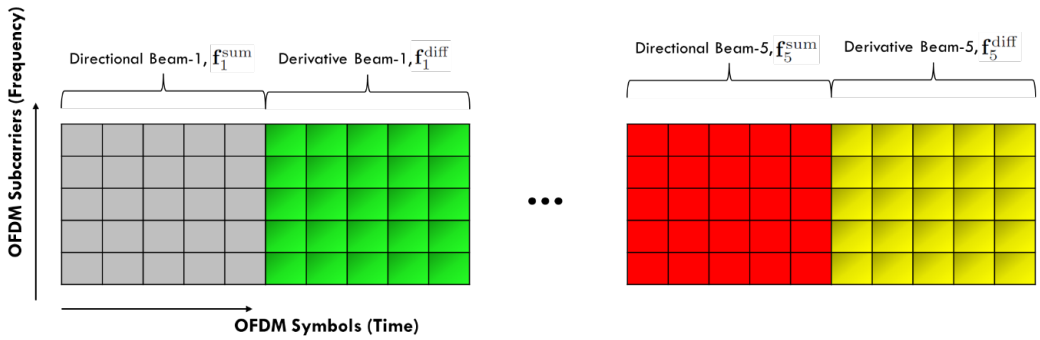

Figure 5-14 OFDM time-frequency beam assignment for AoD estimation experiments.

To achieve finer resolution in AoD estimation, measured beam responses in Figure 5-13 are interpolated to obtain 0.01 deg resolution, as shown in Figure 5-15. The interpolated responses are very close to the original measured responses, and thus used in AoD estimation.

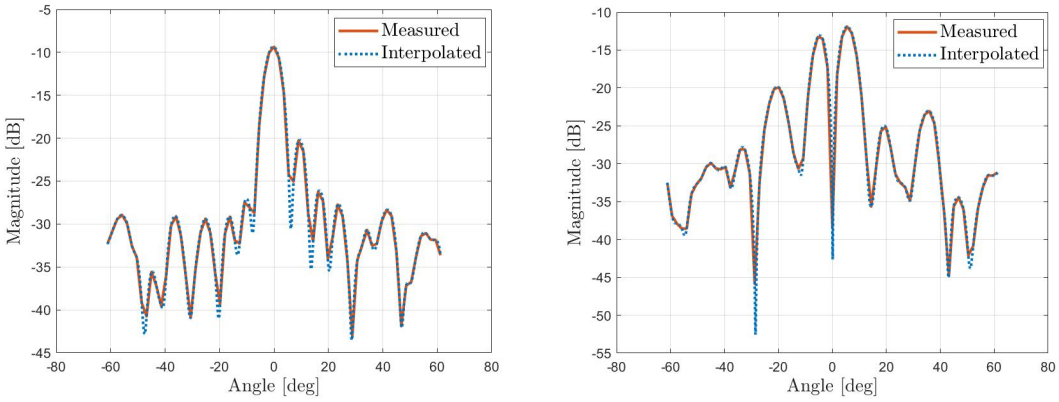

(a) (b)

Figure 5-15 Measured and interpolated beam responses to be employed in AoD estimation, corresponding to (a) directional and (b) derivative beams.

Since the beam responses are real, a non-coherent processing strategy is adopted to estimate AoDs:

1. The observed time-frequency OFDM matrix is coherently integrated over the frequency domain. Since the time delay of the LOS path is zero through synchronization procedures, no phase change occurs across subcarriers, implying that directly adding up the subcarriers for each symbol is equivalent to coherent integration.
2. Absolute squares of the resulting integrated observations are computed.
3. A least-squares (LS) problem is formulated to estimate AoDs, given the interpolated version of the beam response measurements.

In Figure 5-16, several AoD estimation results are presented for different true AoD values, corresponding to different turntable orientations in Figure 5-12. It is observed that the AoD estimates obtained via the proposed non-coherent processing algorithm are quite accurate for various values of the true AoD.

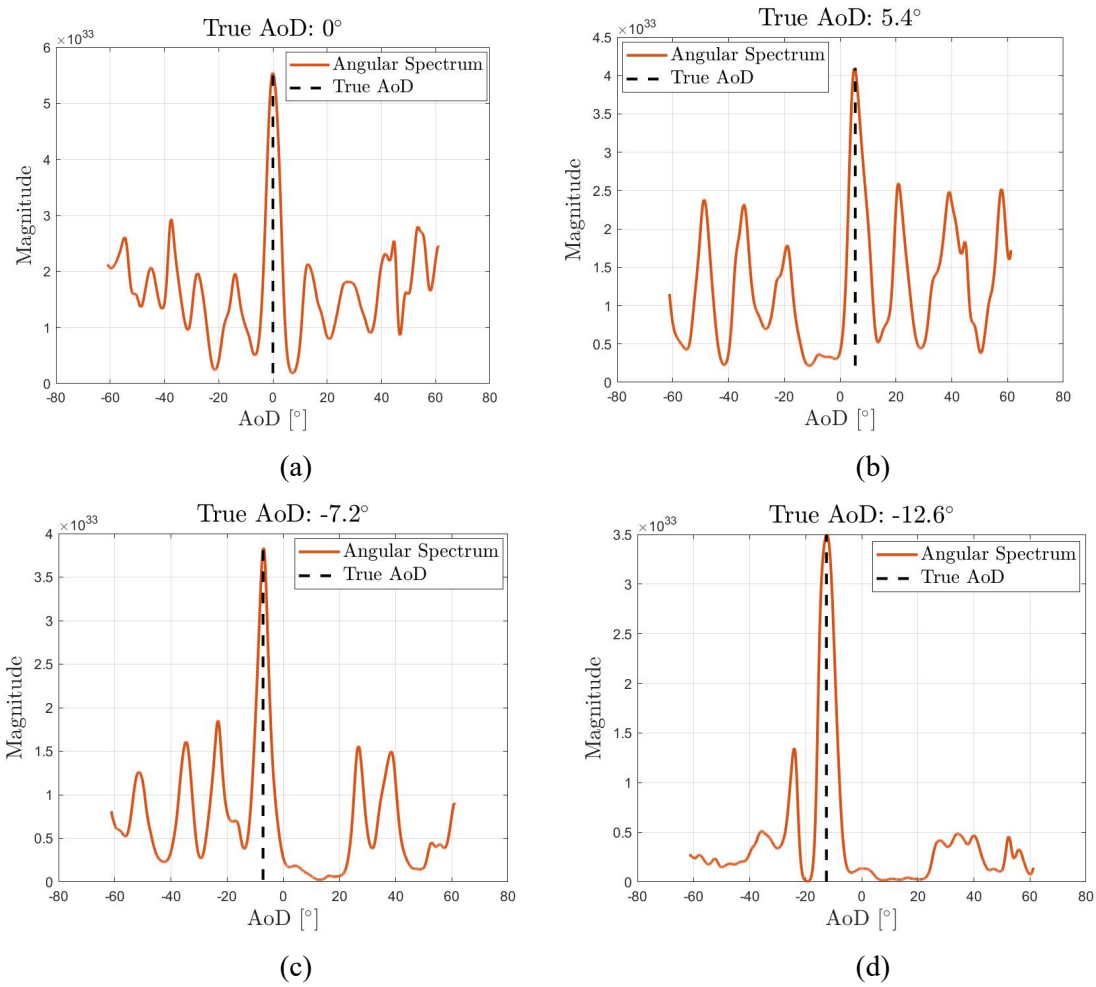

Figure 5-16 AoD estimation results for different AoD values (turntable orientations). The angular spectrum corresponds to the objective function of the LS problem as a function of AoD.

In Figure 5-17, the AoD estimation errors are reported as a function of the ratio of the number of derivative beams to the total number of beams employed while keeping this total number fixed. Note that Figure 5-14 represents a special case of this ratio (50%). The goal of this experiment is to evaluate the accuracy improvement provided using derivative beams in AoD estimation. As seen from the figure, around 80% usage of derivative beams yields the best AoD estimation performance, suggesting that the conventional directional-beam only transmission (corresponding to 0% in Figure 5-17) is not an optimal strategy for AoD estimation and positioning (though it might be optimal for communication metrics).

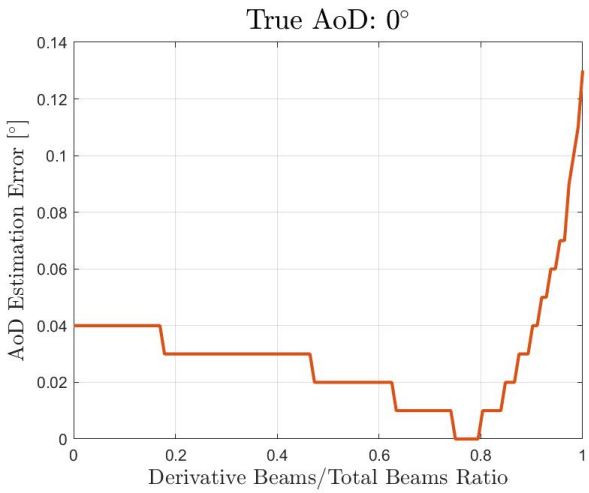

Figure 5-17 AoD estimation error with respect to the ratio of the number of derivative beams to the total number of beams employed (directional + derivative beams).

In summary, several key take-aways from OTA localisation experiments are as follows: Firstly, very accurate AoD estimation results can be achieved in the presence of a-priori information on the receiver location (11.6 degrees in our case) in a LOS-only propagation environment. In particular, with perfect Tx/Rx beam alignment, 0.01 degrees accuracy can be attained, while with 5 degrees Tx/Rx beam misalignment, 0.2 degrees accuracy can be attained (note that 16-element array implies approximately 6 degrees of resolution). Also, optimal beams for communications (i.e., SNR-maximizing directional beams) do not necessarily correspond to optimal beams for localisation. Finally, using a combination of directional and derivative beams leads to better performance in AoD estimation than using only directional beams.

The AoD estimation accuracy can be translated into localisation accuracy as follows: a UE at a known distance of R meters with an angle estimation error θ is localised with a position error of $\delta = R\theta$ [Rao17]. Hence at 10 meters, 0.2 degrees AoD errors leads to a position error of 35 cm, while 0.01 degrees AoD error leads to a position error of 0.2 cm.

5.2.2 Sensing

The sensing measurements were performed in an office area with the Tx and Rx radios placed 6.6 m apart, as shown in Figure 5-18, Figure 5-19, and Figure 5-20. Both radios have beam steering capabilities with 63 different available beams, equally distributed in the range ±45º. During the measurements 50 different Tx beams and 56 different Rx beams are used. They are swept so that all different combinations of Tx and Rx beams are measured, in total 2800 combinations. All measurements are done on 5600 symbols, i.e., 2 symbols per beam combination. With a symbol duration of about 1.1 µs, the total measurement time is 6.25 ms.

Figure 5-18 Measurement setup with Tx radio to the left and Rx radio to the right, separated by 6.6 m. Both radios are oriented facing 45º from each other out from the wall.

Figure 5-19 View from Tx radio. The Rx radio is visible in the left part of the figure at an angle of 45º.

Figure 5-20 View from Rx radio. The Tx radio is visible in the right part of the figure at an angle of 45º.

The aim of the radar functionality is to be able to detect and possibly track objects in a surrounding. In an area such as an office there are lots of different static objects which would give reflections and hence detections. To improve the capability of detecting moving objects a background measurement can be performed which then can be subtracted from subsequent measurements. In this case, 10 different background measurements were performed during night in the office when nobody was present. The results from these measurements are shown in Figure 5-21. The left plot shows the received power in arbitrary units as a function of transmitted and received beam direction. The right figure shows a range plot generated from an FFT of the channel estimation. The system is calibrated so that the LOS path corresponds to 0º angle on Tx and Rx, and 0 m distance in the range plot. These are also the most pronounced peaks in the background measurement. In addition to these a few more details can be observed. In the direction plot there are two blobs in the bottom right corner as well as two more faint

ones around [Tx angle, Rx angle] = [48,40] and [35,60]. In the range plot several peaks can be seen in addition to the LOS-peak. These are found around 1, 2 and 8 m. The 8 m peak comes from reflections in the windows visible in Figure 5-19 and Figure 5-20. The perpendicular distance from each radio to the windows is 6.6 m, which gives a pathlength of about 8.2 m longer than the LOS-path. These are also the reflections which cause the blobs in the bottom right of the angle plot. At 2 m the peak comes from reflections around the cupboards also visible in Figure 5-19 and Figure 5-20. The perpendicular distance from the radios to the cupboards is around 2.8 m which corresponds to and increased distance from the LOS-path of 2.1 m. These peaks correspond to the other two blobs in the angle plot at [Tx angle, Rx,angle] = [48,40] and [35,60]. The last peak at around 1 m has no obvious explanation, but it is always visible in all background measurements. Possibly it is reflections from the ceiling or floor, even though that should result in a shorter distance.

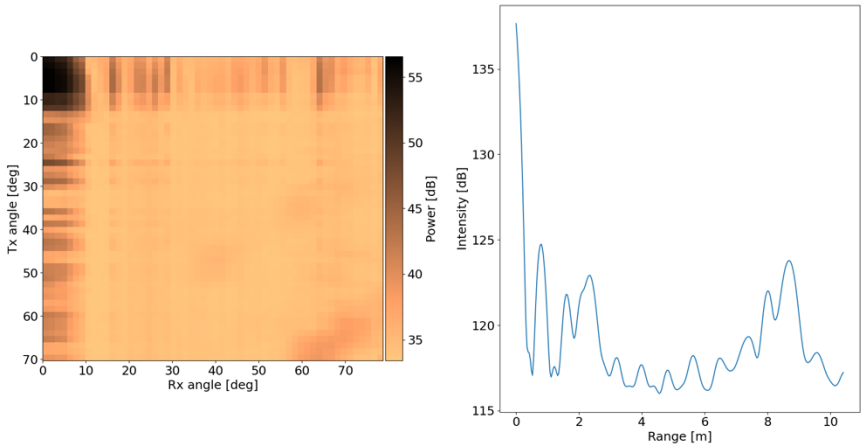

Figure 5-21 Background measurement when the office area is empty. The left figure shows the received power in arbitrary units as a function of the beam direction of the Tx and Rx radios. The right figure shows the range plot where several peaks are visible. The system is calibrated so that the LOS-path corresponds to 0 m distance and 0º angle.

Using the knowledge about the response from the background in the office, the detection and tracking capability of new obstacles can be improved. This is done by subtracting the background from subsequent measurements, in that way enhancing the difference from the empty office space [SV14]. A test was made where a person is tracked when moving parallel to the radios at a perpendicular distance of about 2 m. Starting from a position in line with the Tx radio and then taking a measurement every 0.5 m, stopping when being in line with the Rx radio. The results from some of these measurements are shown in Figure 5-22 to Figure 5-24. From the results some positions are more favourable than others as the peak heights varies. This is due to the geometry of the setup where the waves are better reflected at certain angles, so it depends both on the position and orientation of the person. What can also be noted is that the person is not only introducing a new reflection point, but at some positions the background reflections are also suppressed as they are blocked by the person. This is shown as negative peaks in the plots that always have the same Tx or Rx angle as a corresponding positive peak.

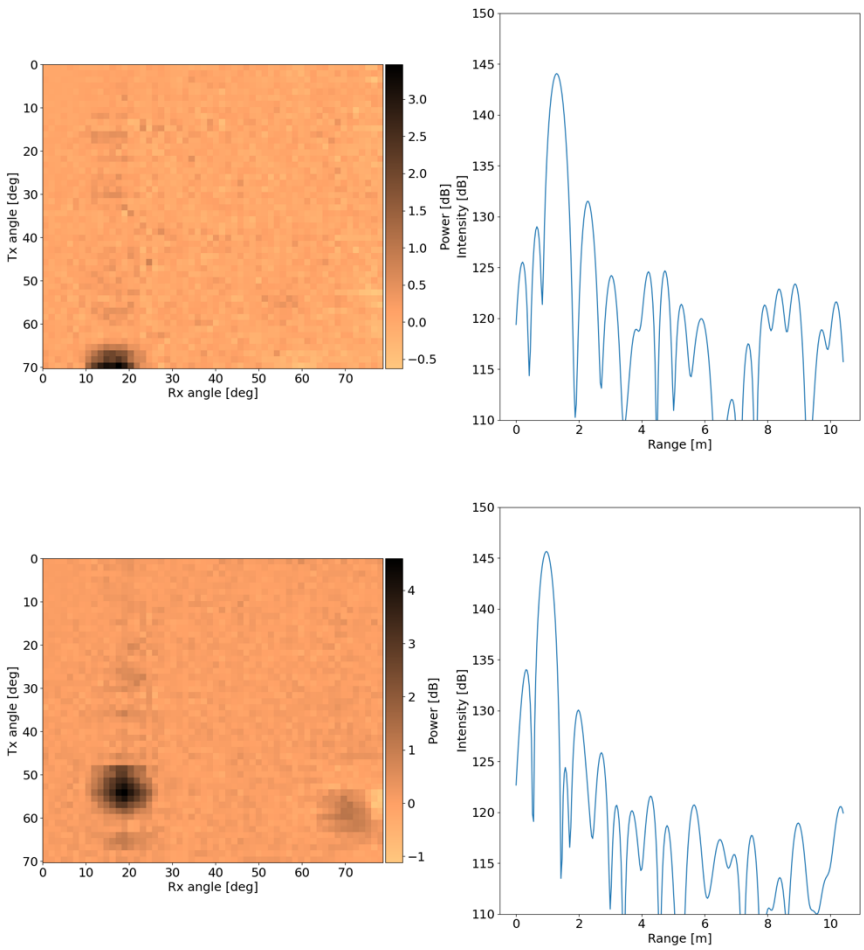

Figure 5-22 Top figure shows results when standing 0.5 m in front of Tx, and the bottom figures shows results when moving 1 m towards Rx.

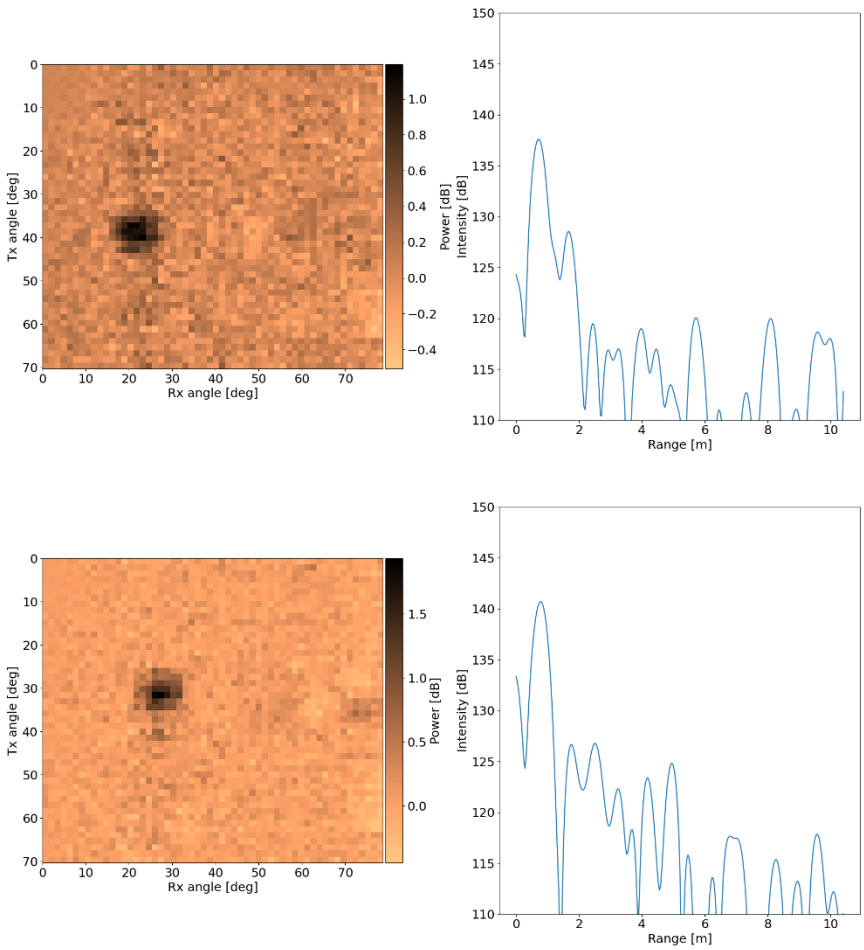

Figure 5-23 When the person continues to move along the setup, 1 m at a time, the movement can be tracked as the blob in the angle plot moves accordingly.

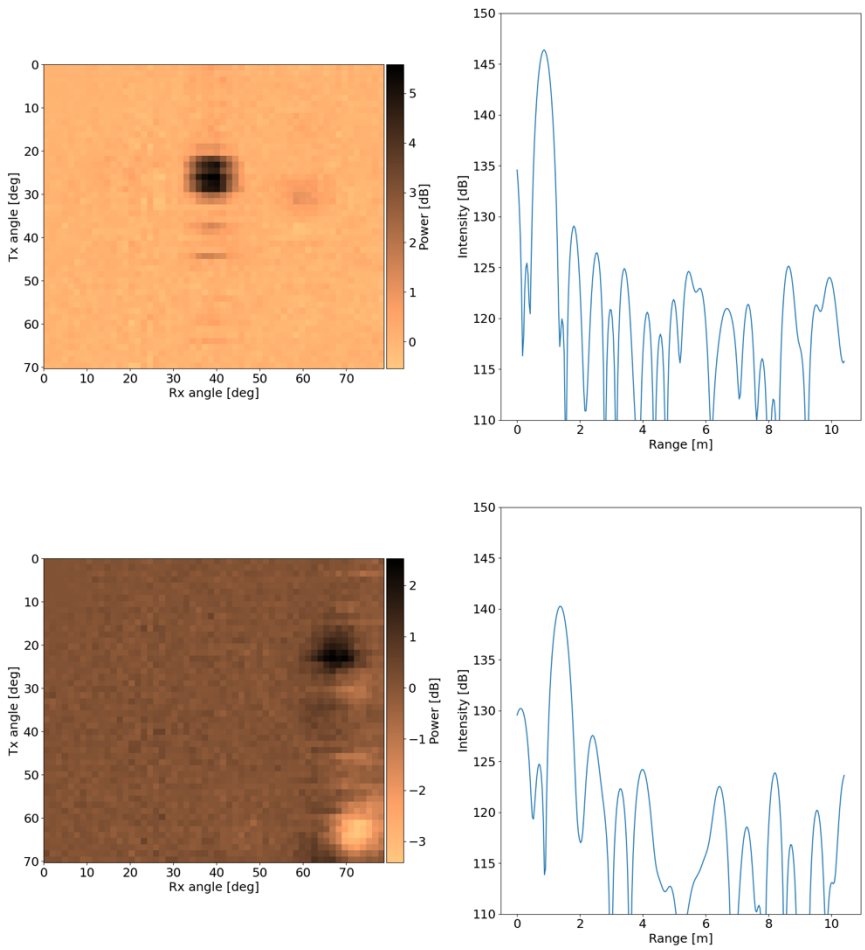

Figure 5-24 As the person continues the movement some positions generate better reflections than others. It can also be noted that some reflections visible in the background get cancelled out by the presence of the person, shown as negative values in the angle plots.

For each peak in the angle plots a two-dimensional Gaussian can be fitted to obtain the angles and a corresponding error. This can be used to calculate the intersection points for each position and track the path of the moving person. In addition, the error can also be plotted based on the width of the Gaussian fit. To improve the position estimates the range measurements can be utilised. Again, with a Gaussian fit the peak position and the width can be obtained to calculate both the range and its corresponding error. In Figure 5-25 the measurement results are shown where the blue dots are the measured positions, based on the angle information, encircled with their corresponding 1 sigma error, the red crosses the nominal positions and the green stars represents the Tx (0,0) and Rx (0,6.6) radios. The black lines show the possible positions based on the range information with the one sigma error indicated by the dashed lines for the position at y=0.5 m and the dotted lines for the position at y=3.5 m. The results from the angle and range measurements can be combined to obtain a more accurate position and decrease the total error. This is shown in Figure 5-26, where the most probable position also is indicated based on both the angle and range data. From this figure, it can be concluded that the uncertainties in the measurements are lower for positions closer to the Tx or Rx radio. This is because the angle uncertainty has a smaller effect at smaller distances, meaning that if the object is close to one radio the angle uncertainty of that radio does not add much to the total error. On the other hand, larger distance to the other radio causes an increased sensitivity to the uncertainty of that angle. That is compensated for by also taking the range information into account, but as can be seen in Figure 5-25, the range information does not help as much for the positions where the distances to Tx and Rx are similar.

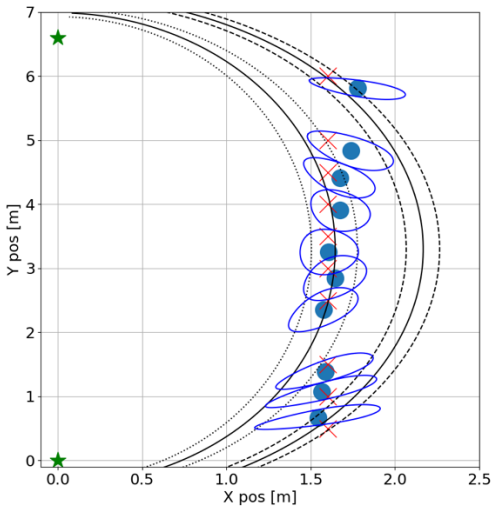

Figure 5-25 The path of the passing person. The green stars represent the Tx and Rx radios, the red crosses the expected positions and the blue dots the measured positions based on the intersection points of the angles. The blue lines show the 1 sigma error of the position estimate. The black lines show the measured range with its corresponding 1 sigma error, dashed lines for the position at y=0.5 m and dotted lines for the position at y=3.5 m.

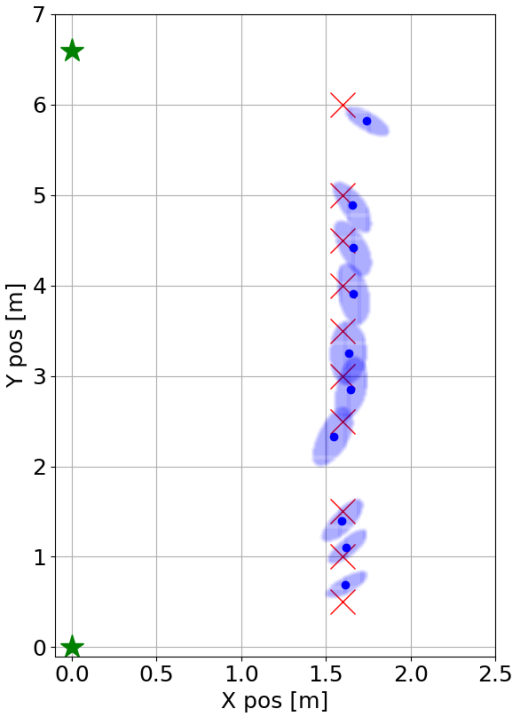

Figure 5-26 The blue dots are the measured positions calculated from a combination of the angle and range information. The shaded blue regions show the 1 sigma error bound for each position while the red crosses indicate the expected position and the green stars show the positions of the Tx (y=0 m) and Rx (y=6.6 m) radios.

In general, the measurement error is in the order of 0.1 m to 0.3 m, depending on the position relative to the radios. However, there are several ways of improving these results. One obvious thing to investigate is the AoD and AoA estimations. In this example it is the index values of the beams that have been used. With a more precise way of determining these angles, e.g., using derivative beams shown in section 5.2.1, the results could be much improved. Another way to improve the results would be to increase the number of subcarriers in the signal to increase the resolution in the range estimation. This can be achieved by either increasing the bandwidth or decreasing the subcarrier spacing.

6 Conclusions

Localisation/positioning and sensing are expected to be tightly integrated with communication in 6G systems. This integration can come in various forms (device-level, waveform-level, resource-level) and will significant implications in terms of new services and applications that can be supported, as well as in terms of the communication capabilities themselves.

For such an integration, localisation and sensing must be an inherent part of the 6G architecture, which must ensure sufficient sensing infrastructure, optimized and adaptive space-time-frequency resources, as well as computational and storage resources for signal processing methods with different interfaces (from raw data to processed object trajectories) to the external services and with support for sensor fusion. Since sensing and localisation services may in some cases reduce available resources for communication, management and orchestration should ensure that all services and application (both from within the network as well as external to it) can be fulfilled by the network. Further work on the integration of localisation and sensing in the 6G architecture is thus recommended.

Supporting the KPIs of the Hexa-X use case families places demands on the infrastructure, the hardware, as well as the bandwidth and time resources. Suitable allocation, optimization, and selection of all these resources is needed to meet the stringent localisation and sensing KPIs. It was found via real-world demonstrations that large contiguous spectrum is necessary, as well as large arrays at both the Tx and Rx sides, if both extreme location and extreme orientation accuracy is needed. Determination of infrastructure placement and space-time-frequency resources can be solved by suitable optimization problems, which can account for both the KPIs and to some extent the KVIs (e.g., energy consumption).

While 6G localisation and sensing will be able to support use cases with extreme requirements in terms of KPIs, Hexa-X has taken a broader view and considered the implications in terms of the KVIs, namely trustworthiness, sustainability, and inclusiveness. For each of these KVIs, localisation and sensing play a dual role. On the one hand, localisation and sensing can contribute to improved trustworthiness, sustainability, and inclusiveness, while on the other hand, the localisation and sensing processes themselves should be trustworthy, sustainable, and inclusive. Focusing on the latter role (the processes) and on trustworthiness, there are important issues related to security (protection against attacks of the sensing signals and processes), to dependability (ensuring integrity of the sensing information), and privacy (of both connected users and assets). All these topics require further study.

This deliverable also reported final results regarding models and methods.

- In terms of models, the use of geometric channel propagation models is recommended, with inherent consistency in time, space, and frequency bands. Moreover, since localisation, sensing and communication will all occur over the same channel, unified channel models that can support both traditional communications, but also localisation and sensing, should be further developed. Complementary to channel models, realistic hardware models are also important in the development and analysis of localisation and sensing methods and designs. Several such models have been presented.
- In terms of methods, results on both localisation and sensing have been reported, considering both model-based and machine learning-based (AI-based) approaches. In the absence of hardware impairments, high accuracy can be achieved, including centimetre-level and decimetre-level localisation accuracy under LOS and obstructed LOS conditions. AI-based methods have revealed new signal designs and signal processing methods, even in the presence of hardware impairments. Coverage analyses with 1 and 2 BSs were conducted to provide a uniform quality of service. Finally, the impact of location information for improving communication was studied, aided by the introduction of a RIS.

Finally, this deliverable bridged the gap from theory to practice, by providing both an in-depth analysis on the impact of hardware impairments and by listing the achievable performance from OTA demonstrations. Hardware impairments can be transformed to higher noise floors, leading to masking effects, which is important for safety-critical applications. It was also shown that, in most cases, hardware impairments tend to be more detrimental for localisation and sensing than for communication,

though there are certain exceptions, and in some rare cases impairments can even be harnessed to improve performance. The OTA demonstrations of new localisation beams shows that conventional communication beams, corresponding to SNR-maximizing directional beams, are sub-optimal for localisation and sensing. Specifically, combined use of standard directional beams and newly proposed derivative beams leads to optimal performance for localisation and sensing (with the percentage of derivative beams dependent on the specific scenario; see Figure 5-17), while using only directional beams is optimal for communications as they maximize SNR at the targeted angle. For sensing, results from a bistatic setup at 60 GHz showed that even with simple signal processing, localisation errors between 0.1 and 0.3 meter were achievable for passive objects. For localisation of UEs, AoD errors of around 0.01-0.2 degrees were reported, which can be related to positioning errors around 0.2-3.5 cm at a range of 10 meters under the assumption of known BS position and orientation. To further improve localisation accuracy, three interrelated aspects must be considered: better hardware impairment mitigation, better algorithms, and better system calibration.

As for communication, the future work should focus on holistic optimization of radio design considering different degrees of freedom not only in the infrastructure but also in the signal processing, to ensure meeting the sustainability goals, while fulfilling the extreme requirements of emerging use cases.

7 References

[36.901] 3GPP TS 36.901 “Study on channel model for frequencies from 0.5 to 100 GHz," version 14.3.0 Release 14, 2018.

[36.873] 3GPP TR 36.873, “Study on 3D channel model for LTE,” V12.2.0, July 2015.

[38.901] 3GPP TR 38.901, “Study on channel model for frequencies from 0.5 to 100 GHz,” version 17.0.0, Release 17, 2022

[AEL+14] Alkhateeb, A., El Ayach, O., Leus, G. and Heath, R.W., 2014. Channel estimation and hybrid precoding for millimeter wave cellular systems. *IEEE Journal of Selected Topics in Signal Processing*, *8*(5), pp.831-846.

[AH13] Adam, R. and Hoeher, P.A., 2013, March. Semi-blind channel estimation for joint communication and positioning. In *2013 10th Workshop on Positioning, Navigation and Communication (WPNC)*.

[AKG+21] Aydogdu, C., Keskin, M.F., Garcia, N., Wymeersch, H. and Bliss, D.W., 2019. RadChat: Spectrum sharing for automotive radar interference mitigation. *IEEE Transactions on Intelligent Transportation Systems*, *22*(1), pp.416-429.

[ASB+22] Albanese, A., Sciancalepore, V., Banchs, A. and Costa-Perez, X., 2022. LOKO: Localization-aware roll-out planning for future mobile networks. *IEEE Transactions on Mobile Computing*.

[ASE+19] Alnoman, A., Sharma, S.K., Ejaz, W. and Anpalagan, A., 2019. Emerging edge computing technologies for distributed IoT systems. *IEEE Network*, *33*(6), pp.140-147.

[BBP+22] Behravan, A., Baldemair, R., Parkvall, S., Dahlman, E., Yajnanarayana, V., Björkegren, H. and Shrestha, D., 2022, March. Introducing sensing into future wireless communication systems. In *2022 2nd IEEE International Symposium on Joint Communications & Sensing (JC&S)*.

[BJJ+18] van den Biggelaar, A.J., Johannsen, U., Mattheijssen, P. and Smolders, A.B., 2018. Improved statistical model on the effect of random errors in the phase and amplitude of element excitations on the array radiation pattern. *IEEE Transactions on Antennas and Propagation*, *66*(5), pp.2309-2317.

[BK19] Bică, M. and Koivunen, V., 2019, May. Multicarrier radar-communications waveform design for RF convergence and coexistence. In *ICASSP 2019-2019 IEEE International Conference on Acoustics, Speech and Signal Processing (ICASSP)* (pp. 7780-7784).

[BLH+21] Barneto, C.B., Liyanaarachchi, S.D., Heino, M., Riihonen, T. and Valkama, M., 2021. Full duplex radio/radar technology: The enabler for advanced joint communication and sensing. *IEEE Wireless Communications*, *28*(1), pp.82-88.

[BMM+20] Bariah, L., Mohjazi, L., Muhaidat, S., Sofotasios, P.C., Kurt, G.K., Yanikomeroglu, H. and Dobre, O.A., 2020. A prospective look: Key enabling technologies, applications and open research topics in 6G networks. *IEEE Access*, *8*, pp.174792-174820.

[BPA19] Boulogeorgos, A.A.A., Papasotiriou, E.N. and Alexiou, A., 2019. Analytical performance assessment of THz wireless systems. *IEEE Access*, *7*, pp.11436-11453.

[BTL+19] Carlos Baquero Barneto, Matias Turunen, Sahan Damith Liyanaarachchi, Lauri Anttila, Alberto Brihuega, Taneli Riihonen, and Mikko Valkama. High-accuracy radio sensing in 5g new radio networks: Prospects and self-interference challenge. Conference Record - Asilomar Conference on Signals, Systems and Computers, 2019-Novem:1159–1163, 2019.

[BYK+22] Behravan, A., Yajnanarayana, V., Keskin, M.F., Chen, H., Shrestha, D., Abrudan, T.E., Svensson, T., Schindhelm, K., Wolfgang, A., Lindberg, S. and Wymeersch, H., 2022. Positioning and sensing in 6G: Gaps, challenges, and opportunities. *IEEE Vehicular Technology Magazine*.

[BUS52] Bussgang, J.J., "Crosscorrelation functions of amplitude-distorted Gaussian signals," Research Lab. Electronics, Massachusetts Inst. Technology, Cambridge, MA, Tech. Rep. 216, 1952. [Online]. Available: http://hdl.handle.net/1721.1/4847

[CB06] Chorti, A. and Brookes, M., 2006. A spectral model for RF oscillators with power-law phase noise. *IEEE Transactions on Circuits and Systems I: Regular Papers*, *53*(9), pp.1989-1999.

[CBK+22] Chorti, A., Barreto, A.N., Köpsell, S., Zoli, M., Chafii, M., Sehier, P., Fettweis, G. and Poor, H.V., 2022. Context-aware security for 6G wireless: The role of physical layer security. *IEEE Communications Standards Magazine*, *6*(1), pp.102-108.

[CKA+23a] Chen, H., Kim, H., Ammous, M., Seco-Granados, G., Alexandropoulos, G.C., Valaee, S. and Wymeersch, H., 2023. RISs and Sidelink Communications in Smart Cities: The Key to Seamless Localization and Sensing. *arXiv preprint arXiv:2301.03535*.

[CKA+23b] Chen, H., Keskin, M.F., Aghdam, S.R., Kim, H., Lindberg, S., Wolfgang, A., Abrudan, T.E., Eriksson, T. and Wymeersch, H., 2023. Modeling and Analysis of 6G Joint Localization and Communication under Hardware Impairments. *arXiv preprint arXiv:2301.01042*.

[CLE22] Chung, M., Liu, L. and Edfors, O., 2021. Phase-noise compensation for OFDM systems exploiting coherence bandwidth: Modeling, algorithms, and analysis. *IEEE Transactions on Wireless Communications*, *21*(5), pp.3040-3056.

[CSB+22] Chen, Hui, Hadi Sarieddeen, Tarig Ballal, Henk Wymeersch, Mohamed-Slim Alouini, and Tareq Y. Al-Naffouri. "A tutorial on terahertz-band localization for 6G communication systems." *IEEE Communications Surveys & Tutorials* (2022), 24(3), pp.1780-1815.

[DBB+21] De Lima, C., Belot, D., Berkvens, R., Bourdoux, A., Dardari, D., Guillaud, M., Isomursu, M., Lohan, E.S., Miao, Y., Barreto, A.N. and Aziz, M.R.K., 2021. Convergent communication, sensing and localization in 6G systems: An overview of technologies, opportunities and challenges. *IEEE Access*, *9*, pp.26902-26925.

[Dem06] Demir, A., 2006. Computing timing jitter from phase noise spectra for oscillators and phase-locked loops with white and 1/f noise. *IEEE Transactions on Circuits and Systems I: Regular Papers*, *53*(9), pp.1869-1884.

[DSM+21] Dwivedi, S., Shreevastav, R., Munier, F., Nygren, J., Siomina, I., Lyazidi, Y., Shrestha, D., Lindmark, G., Ernström, P., Stare, E. and Razavi, S.M., 2021. Positioning in 5G networks. *IEEE Communications Magazine*, *59*(11), pp.38-44.

[FGG+17] Fortunati, S., Gini, F., Greco, M.S. and Richmond, C.D., 2017. Performance bounds for parameter estimation under misspecified models: Fundamental findings and applications. *IEEE Signal Processing Magazine*, *34*(6), pp.142-157.

[GAI+20] Ghaseminajm, F., Abu-Shaban, Z., Ikki, S.S., Wymeersch, H. and Benson, C.R., 2020. Localization error bounds for 5G mmWave systems under I/Q imbalance. *IEEE Transactions on Vehicular Technology*, *69*(7), pp.7971-7975.

[GCH20] Guruacharya, S., Chalise, B.K. and Himed, B., 2020. MAP ratio test detector for radar system. *IEEE Transactions on Signal Processing*, *69*, pp.573-588.

[GLV+18] Grossi, E., Lops, M., Venturino, L. and Zappone, A., 2018. Opportunistic radar in IEEE 802.11 ad networks. *IEEE Transactions on Signal Processing*, *66*(9), pp.2441-2454.

[GLV20] Grossi, E., Lops, M. and Venturino, L., 2020. Adaptive detection and localization exploiting the IEEE 802.11 ad standard. *IEEE Transactions on Wireless Communications*, *19*(7), pp.4394-4407.

[GMA+22] Guo, H., Makki, B., Alouini, M.S. and Svensson, T., 2022. High-Rate Uninterrupted Internet of Vehicle Communications in Highways: Dynamic Blockage Avoidance and CSIT Acquisition. *IEEE Communications Magazine*, *60*(7), pp.44-50.

[GMA+22b] Guo, H., Makki, B., Åström, M., Alouini, M.S. and Svensson, T., 2022. Dynamic blockage pre-avoidance using reconfigurable intelligent surfaces. *arXiv preprint arXiv:2201.06659*.

[GMP+21] Guo, H., Makki, B., Phan-Huy, D.T., Dahlman, E., Alouini, M.S. and Svensson, T., 2021. Predictor antenna: A technique to boost the performance of moving relays. *IEEE Communications Magazine*, *59*(7), pp.80-86.

[GSY+22] Geng, Y., Shrestha, D., Yajnanarayana, V., Dahlman, E. and Behravan, A., 2022. Joint scatterer localization and material identification using radio access technology. *EURASIP Journal on Wireless Communications and Networking*, *2022*(1), p.87.

[Han86] Hanle, E., 1986, December. Survey of bistatic and multistatic radar. In *IEE Proceedings F (Communications, Radar and Signal Processing)* (Vol. 133, No. 7, pp. 587-595). IET Digital Library.

[HAE20] Hajiabdolrahim, N., Aghdam, S.R. and Eriksson, T., 2020, August. An extended Kalman filter framework for joint phase noise, CFO and sampling time error estimation. In *2020 IEEE 31st Annual International Symposium on Personal, Indoor and Mobile Radio Communications*.

[HEX20-D11] Hexa-X Deliverable D1.1, "6G Vision, use cases and key societal values", 2020.

[HEX21-D12] Hexa-X, "Deliverable D1.2: Expanded 6G vision, use cases and societal values – including aspects of sustainability, security and spectrum (D1.2 is an extension of D1.1)", Apr. 2021.

[HEX23-D23] Hexa-X Deliverable D2.3, "Radio models and enabling techniques towards ultra-high data rate links and capacity in 6G", Mar. 2023.

[HEX21-D31] Hexa-X, "Deliverable D3.1: Localisation and sensing use cases and gap analysis," Dec. 2021.

[HEX22-D13] Hexa-X, "Deliverable D1.3: Targets and requirements for 6G - initial E2E architecture
", Mar. 2022.

[HEX22-D32] Hexa-X, "Deliverable D3.2: Initial models and measurements for localisation and sensing," Oct. 2022.

[HEX22-D62] Hexa-X, "Deliverable D6.2: Design of service management and orchestration functionalities," May 2022.

[HEX22-D72] Hexa-X, "Deliverable 7.2: Special-purpose functionalities: intermediate solutions", May, 2022.

[HJT+16] Haneda, K., Zhang, J., Tan, L., Liu, G., Zheng, Y., Asplund, H., Li, J., Wang, Y., Steer, D., Li, C. and Balercia, T., 2016, May. 5G 3GPP-like channel models for outdoor urban microcellular and macrocellular environments. In *2016 IEEE 83rd vehicular technology conference (VTC spring)* (pp. 1-7). IEEE.

[HJW+19] He, H., Jin, S., Wen, C.K., Gao, F., Li, G.Y. and Xu, Z., 2019. Model-driven deep learning for physical layer communications. *IEEE Wireless Communications*, *26*(5), pp.77-83.

[Hol11] Hol, J.D., 2011. *Sensor fusion and calibration of inertial sensors, vision, ultra-wideband and GPS* (Doctoral dissertation, Linköping University Electronic Press).

[HRY+22] Hong, J., Rodríguez-Piñeiro, J., Yin, X. and Yu, Z., 2022. Joint Channel Parameter Estimation and Scatterers Localization. *IEEE Transactions on Wireless Communications*.

[HST19] He, S., Shin, H.S. and Tsourdos, A., 2019. Trajectory optimization for target localization with bearing-only measurement. *IEEE Transactions on Robotics*, *35*(3), pp.653-668.

[JRT+19] Jaeckel, S., Raschkowski, L., Thiele, L., et al., "QuaDRiGa−Quasi deterministic radio channel generator, user manual and documentation," Tech. Rep., v2.2.0, Fraunhofer Heinrich Hertz Institute, 2019.

[JVG+22] Jeremy Johnston, Luca Venturino, Emanuele Grossi, Marco Lops, and Xiaodong Wang. MIMO OFDM Dual-Function Radar-Communication Under Error Rate and Beampattern Constraints. IEEE Journal on Selected Areas in Communications, 40(6):1951–1964, 2022.

[KCO19] Kuschel, H., Cristallini, D. and Olsen, K.E., 2019. Tutorial: Passive radar tutorial. *IEEE Aerospace and Electronic Systems Magazine*, *34*(2), pp.2-19.

[KG21] Kota, S. and Giambene, G., 2021, June. 6G integrated non-terrestrial networks: Emerging technologies and challenges. In *2021 IEEE International Conference on Communications Workshops (ICC Workshops)* (pp. 1-6). IEEE.

[KKW21] Keskin, M.F., Koivunen, V. and Wymeersch, H., 2021. Limited feedforward waveform design for OFDM dual-functional radar-communications. *IEEE Transactions on Signal Processing*, *69*, pp.2955-2970.

[KME+22] Keskin, M.F., Marcus, C., Eriksson, O., Wymeersch, H. and Koivunen, V., 2022. On the Impact of Phase Noise on Monostatic Sensing in OFDM ISAC Systems. *arXiv preprint arXiv:2211.13600*.

[KMH+07] P. Kyösti , J. Meinilä, L. Hentila, X. Zhao, T. Jämsä, et al., IST-4-027756 WINNER II D1.1.2 v1.2 WINNER II channel models. Inf. Soc. Technol. 11, 2007.

[KWK21] Keskin, M.F., Wymeersch, H. and Koivunen, V., 2021. MIMO-OFDM joint radar-communications: Is ICI friend or foe?. *IEEE Journal of Selected Topics in Signal Processing*, *15*(6), pp.1393-1408.

[KWK22] Keskin, M.F., Wymeersch, H. and Koivunen, V., 2022. OFDM Joint Radar-Communications under Phase Noise: From Mitigation to Exploitation. *arXiv preprint arXiv:2205.08376*.

[LAH+19] Li, J., Ai, B., He, R., Yang, M., Zhong, Z. and Hao, Y., 2019. A cluster-based channel model for massive MIMO communications in indoor hotspot scenarios. *IEEE Transactions on Wireless Communications*, *18*(8), pp.3856-3870.

[LCM+22] Liu, F., Cui, Y., Masouros, C., Xu, J., Han, T.X., Eldar, Y.C. and Buzzi, S., 2022. Integrated sensing and communications: Towards dual-functional wireless networks for 6G and beyond. *IEEE journal on selected areas in communications*.

[LHS+20] Xiang Liu, Tianyao Huang, Nir Shlezinger, Yimin Liu, Jie Zhou, and Yonina C. Eldar. Joint Transmit Beamforming for Multiuser MIMO Communications and MIMO Radar. IEEE Transactions on Signal Processing, 68:3929–3944, 2020

[LJW+22] Li, Z., Jiang, F., Wymeersch, H. and Wen, F., 2022. An Iterative 5G Positioning and Synchronization Algorithm in NLOS Environments with Multi-Bounce Paths. *arXiv preprint arXiv:2209.01562*.

[LLL+22] Fan Liu, Ya-Feng Liu, Ang Li, Christos Masouros, and Yonina C. Eldar. Cram´er-Rao Bound Optimization for Joint Radar-Communication Beamforming. IEEE Transactions on Signal Processing, 70:240–253, 2022

[LML+18] Fan Liu, Christos Masouros, Ang Li, Huafei Sun, and Lajos Hanzo. MU-MIMO Communications With MIMO Radar: From Co-Existence to Joint Transmission. IEEE Transactions on Wireless Communications, 17(4):2755–2770, 2018.

[LXW+19] Li, Z., Xu, K., Wang, H., Zhao, Y., Wang, X. and Shen, M., 2019. Machine-learning-based positioning: A survey and future directions. *IEEE Network*, *33*(3), pp.96-101.

[LY17] Leshem, A. and Yemini, M., 2017. Phase noise compensation for OFDM systems. *IEEE Transactions on Signal Processing*, *65*(21), pp.5675-5686.

[LZC+22] Liu, F., Zheng, L., Cui, Y., Masouros, C., Petropulu, A.P., Griffiths, H. and Eldar, Y.C., 2022. Seventy years of radar and communications: The road from separation to integration. *arXiv preprint arXiv:2210.00446*.

[LZM+18] Liu, F., Zhou, L., Masouros, C., Li, A., Luo, W. and Petropulu, A., 2018. Toward dual-functional radar-communication systems: Optimal waveform design. *IEEE Transactions on Signal Processing*, *66*(16), pp.4264-4279.

[Magic22] mmMagic, [online] "https://5g-ppp.eu/mmmagic/."

[MHK+22] Mateos-Ramos, J.M., Häger, C., Keskin, M.F., Magoarou, L.L. and Wymeersch, H., 2022. Model-Driven End-to-End Learning for Integrated Sensing and Communication. *arXiv preprint arXiv:2212.10211*.

[Mie19] J. Mietzner, 2019. DFT-Spread OFDM MIMO-Radar – An Alternative for Reduced Crest Factors. *20th International Radar Symposium (IRS), Ulm, Germany, 2019*, pp. 1-10.

[MLH21] Mozaffari, M., Lin, X. and Hayes, S., 2021. Toward 6G with connected sky: UAVs and beyond. *IEEE Communications Magazine*, *59*(12), pp.74-80.

[MRS+15] Maccartney, G.R., Rappaport, T.S., Sun, S. and Deng, S., 2015. Indoor office wideband millimeter-wave propagation measurements and channel models at 28 and 73 GHz for ultra-dense 5G wireless networks. *IEEE access*, *3*, pp.2388-2424.

[MRW+11] Mathecken, P., Riihonen, T., Werner, S. and Wichman, R., 2011. Performance analysis of OFDM with Wiener phase noise and frequency selective fading channel. *IEEE Transactions on Communications*, *59*(5), pp.1321-1331.

[MSW+22] Mateos-Ramos, J.M., Song, J., Wu, Y., Häger, C., Keskin, M.F., Yajnanarayana, V. and Wymeersch, H., 2022, May. End-to-end learning for integrated sensing and communication. In *ICC 2022-IEEE International Conference on Communications* (pp. 1942-1947).

[MT21] Mohammadian, A. and Tellambura, C., 2021. RF impairments in wireless transceivers: Phase noise, CFO, and IQ imbalance–A survey. *IEEE Access*, *9*, pp.111718-111791.

[MZW20] Ma, Y., Zhou, G. and Wang, S., 2019. WiFi sensing with channel state information: A survey. *ACM Computing Surveys (CSUR)*, *52*(3), pp.1-36.

[Nist22] NIST, [online] https://www.nist.gov/ctl/wireless-networks-division

[NSJ+23] Nazari, M.A., Seco-Granados, G., Johannisson, P. and Wymeersch, H., "MmWave 6D Radio Localisation with a Snapshot Observation from a Single BS," in IEEE Transactions on Vehicular Technology, 2023.

[ONA+22] de Oliveira, L.G., Nuss, B., Alabd, M.B., Diewald, A., Pauli, M. and Zwick, T., 2021. Joint radar-communication systems: Modulation schemes and system design. *IEEE Transactions on Microwave Theory and Techniques*, *70*(3), pp.1521-1551.

[PBA21] Papasotiriou, E.N., Boulogeorgos, A.A.A. and Alexiou, A., 2021, September. Fading modeling in indoor THz wireless systems. In *2021 International Balkan Conference on Communications and Networking (BalkanCom)* (pp. 161-165).

[PFS+22] Prol, Fabricio S., R. Morales Ferre, Zainab Saleem, Petri Välisuo, Cristina Pinell, Elena-Simona Lohan, Mahmoud Elsanhoury et al. "Position, navigation, and timing (PNT) through low earth orbit (LEO) satellites: A survey on current status, challenges, and opportunities." *IEEE Access* (2022), pp. 83971-84002).

[PHC+21] Kyösti, P., Haneda, K., Conrat, J.M. and Pärssinen, A., 2021, June. Above-100 GHz wave propagation studies in the european project Hexa-X for 6G channel modelling. In *2021 Joint European Conference on Networks and Communications & 6G Summit (EuCNC/6G Summit)* (pp. 538-543).

[PPG22] Pucci, L., Paolini, E. and Giorgetti, A., 2022. System-level analysis of joint sensing and communication based on 5G new radio. *IEEE Journal on Selected Areas in Communications*, *40*(7), pp.2043-2055.

[PRF07] Petrovic, D., Rave, W. and Fettweis, G., 2007. Effects of phase noise on OFDM systems with and without PLL: Characterization and compensation. *IEEE Transactions on communications*, *55*(8), pp.1607-1616.

[Rao17] Rao, S., 2017. Introduction to mmWave sensing: FMCW radars. Texas Instruments (TI) mmWave Training Series, pp.1-11.

[RHC+19] Reid, T.G., Houts, S.E., Cammarata, R., Mills, G., Agarwal, S., Vora, A. and Pandey, G., 2019. Localization requirements for autonomous vehicles. *arXiv preprint arXiv:1906.01061*.

[RK89] R. Roy and T. Kailath, 1989. ESPRIT-estimation of signal parameters via rotational invariance techniques. *IEEE Transactions on Acoustics, Speech, and Signal Processing*, 37(7), pp. 984-995.

[Rob21] Roberts, I.P., 2021. MIMO for MATLAB: A toolbox for simulating MIMO communication systems. *arXiv preprint arXiv:2111.05273*." http://mimoformatlab.com.

[RSM+13] Rappaport, T.S., Sun, S., Mayzus, R., Zhao, H., Azar, Y., Wang, K., Wong, G.N., Schulz, J.K., Samimi, M. and Gutierrez, F., 2013. Millimeter wave mobile communications for 5G cellular: It will work!. *IEEE access*, *1*, pp.335-349.

[RMS+15] Rappaport, T.S., MacCartney, G.R., Samimi, M.K. and Sun, S., 2015. Wideband millimeter-wave propagation measurements and channel models for future wireless communication system design. *IEEE transactions on Communications*, *63*(9), pp.3029-3056.

[SD03] Scott, L. and Denning, D.E., 2003. Geo-encryption: using GPS to enhance data security.(Innovation). *GPS world*, *14*(4), pp.40-46.

[Sch08] Schenk, T., 2008. *RF imperfections in high-rate wireless systems: impact and digital compensation*. Springer Science & Business Media.

[SFE+21] Shlezinger, N., Farsad, N., Eldar, Y.C. and Goldsmith, A., 2021. 6 Model-Based Machine Learning for Communications.

[SFY+22] Shao, S., Fan, M., Yu, C., Li, Y., Xu, X. and Wang, H., 2022. Machine Learning-Assisted Sensing Techniques for Integrated Communications and Sensing in WLANs: Current Status and Future Directions. *Progress In Electromagnetics Research*, *175*.

[Sko80] Skolnik, M.I., 1980. Introduction to radar systems. *New York*.

[SNA+20] Sarieddeen, H., Saeed, N., Al-Naffouri, T.Y. and Alouini, M.S., 2020. Next generation terahertz communications: A rendezvous of sensing, imaging, and localization. *IEEE Communications Magazine*, *58*(5), pp.69-75.

[SNM+14] Salim, O.H., Nasir, A.A., Mehrpouyan, H., Xiang, W., Durrani, S. and Kennedy, R.A., 2014. Channel, phase noise, and frequency offset in OFDM systems: Joint estimation, data detection, and hybrid Cramer-Rao lower bound. *IEEE Transactions on Communications*, *62*(9), pp.3311-3325.

[Sou99] Soumekh, M., 1999. *Synthetic aperture radar signal processing* (Vol. 7, pp. 25-130). New York: Wiley.

[SRR+22] Singh, M., Roeschlin, M., Ranganathan, A. and Capkun, S., 2022. V-Range: Enabling Secure Ranging in 5G Wireless Networks. In *NDSS*.

[SV87] Saleh, A.A. and Valenzuela, R., 1987. A statistical model for indoor multipath propagation. *IEEE Journal on selected areas in communications*, *5*(2), pp.128-137.

[SV14] Sobral, A. and Vacavant, A., 2014. A comprehensive review of background subtraction algorithms evaluated with synthetic and real videos. *Computer Vision and Image Understanding*, *122*, pp.4-21.

[SVB+22] Shastri, A., Valecha, N., Bashirov, E., Tataria, H., Lentmaier, M., Tufvesson, F., Rossi, M. and Casari, P., 2022. A review of millimeter wave device-based localization and device-free sensing technologies and applications. *IEEE Communications Surveys & Tutorials*.

[SW11] Sturm, C. and Wiesbeck, W., 2011. Waveform design and signal processing aspects for fusion of wireless communications and radar sensing. *Proceedings of the IEEE*, *99*(7), pp.1236-1259.

[SWE+20] Shlezinger, N., Whang, J., Eldar, Y.C. and Dimakis, A.G., 2020. Model-based deep learning. *arXiv preprint arXiv:2012.08405*.

[SWS+18] Shi, C., Wang, F., Sellathurai, M., Zhou, J. and Salous, S., 2017. Power minimization-based robust OFDM radar waveform design for radar and communication systems in coexistence. *IEEE Transactions on Signal Processing*, *66*(5), pp.1316-1330.

[Tay79] Taylor, J., 1979. The Cramér-Rao estimation error lower bound computation for deterministic nonlinear systems. *IEEE Transactions on Automatic Control*, *24*(2), pp.343-344.

[TSB16] Tan, P.S., Stiles, J.M. and Blunt, S.D., 2016, May. Optimizing sparse allocation for radar spectrum sharing. In *2016 IEEE Radar Conference (RadarConf)*.

[TSC+21] Tarboush, S., Sarieddeen, H., Chen, H., Loukil, M.H., Jemaa, H., Alouini, M.S. and Al-Naffouri, T.Y., 2021. TeraMIMO: A channel simulator for wideband ultra-massive MIMO terahertz communications. *IEEE Transactions on Vehicular Technology*, *70*(12), pp.12325-12341.

[TSF+17] Tranter, J., Sidiropoulos, N.D., Fu, X. and Swami, A., 2017. Fast unit-modulus least squares with applications in beamforming. *IEEE Transactions on Signal Processing*, *65*(11), pp.2875-2887.

[URB+21] Uusitalo, M.A., Rugeland, P., Boldi, M.R., Strinati, E.C., Demestichas, P., Ericson, M., Fettweis, G.P., Filippou, M.C., Gati, A., Hamon, M.H. and Hoffmann, M., 2021. 6G vision, value, use cases and technologies from european 6G flagship project Hexa-X. *IEEE Access*, *9*, pp.160004-160020.

[VMJ+22] Vargas, E., Mishra, K.V., Jacome, R., Sadler, B.M. and Arguello, H., 2022. Dual-blind deconvolution for overlaid radar-communications systems. *arXiv preprint arXiv:2208.04381*.

[WGP+18] Wang, J., Gao, Q., Pan, M. and Fang, Y., 2018. Device-free wireless sensing: Challenges, opportunities, and applications. *IEEE network*, *32*(2), pp.132-137.

[WLH+22] Wu, Y., Lemic, F., Han, C. and Chen, Z., 2022. Sensing integrated DFT-spread OFDM waveform and deep learning-powered receiver design for terahertz integrated sensing and communication systems. *IEEE Transactions on Communications*.

[WPA+22] Wymeersch, H., Pärssinen, A., Abrudan, T.E., Wolfgang, A., Haneda, K., Sarajlic, M., Leinonen, M.E., Keskin, M.F., Chen, H., Lindberg, S. and Kyösti, P., 2022, June. 6G radio requirements to support integrated communication, localization, and sensing. In *2022 Joint European Conference on Networks and Communications & 6G Summit (EuCNC/6G Summit)* (pp. 463-469).

[WS22] Wymeersch, H. and Seco-Granados, G., 2022. Radio localization and sensing—Part I: Fundamentals. *IEEE Communications Letters*, *26*(12), pp.2816-2820.

[WSC+21] Wymeersch, H., Shrestha, D., De Lima, C.M., Yajnanarayana, V., Richerzhagen, B., Keskin, M.F., Schindhelm, K., Ramirez, A., Wolfgang, A., De Guzman, M.F. and Haneda, K., 2021, September. Integration of communication and sensing in 6G: A joint industrial and academic perspective. In *2021 IEEE 32nd Annual International Symposium on Personal, Indoor and Mobile Radio Communications (PIMRC)* (pp. 1-7). IEEE.

[WWM+22] Wei, Z., Wang, Y., Ma, L., Yang, S., Feng, Z., Pan, C., Zhang, Q., Wang, Y., Wu, H. and Zhang, P., 2022. 5G PRS-based sensing: A sensing reference signal approach for joint sensing and communication system. *IEEE Transactions on Vehicular Technology*.

[XWW+21] Xing, Z., Wang, R., Wu, J. and Liu, E., 2021. Achievable rate analysis and phase shift optimization on intelligent reflecting surface with hardware impairments. *IEEE Transactions on Wireless Communications*, *20*(9), pp.5514-5530.

[YDX+09] Ye, Z., Dai, J., Xu, X. and Wu, X., 2009. DOA estimation for uniform linear array with mutual coupling. *IEEE Transactions on Aerospace and Electronic Systems*, *45*(1), pp.280-288.

[YH22] Yajnanarayana, V. and Wymeersch, H., 2022. Multistatic Sensing of Passive Targets Using 6G Cellular Infrastructure. *arXiv preprint arXiv:2211.05340*.

[YL08] Ye, Z. and Liu, C., 2008. 2-D DOA estimation in the presence of mutual coupling. *IEEE Transactions on Antennas and Propagation*, *56*(10), pp.3150-3158.

[YL22] Yassine, T. and Le Magoarou, L., 2022. mpNet: variable depth unfolded neural network for massive MIMO channel estimation. *IEEE Transactions on Wireless Communications*, *21*(7), pp.5703-5714.

[YND+17] Yousefi, S., Narui, H., Dayal, S., Ermon, S. and Valaee, S., 2017. A survey on behavior recognition using WiFi channel state information. *IEEE Communications Magazine*, *55*(10), pp.98-104.

[YXX+19] Yang, P., Xiao, Y., Xiao, M. and Li, S., 2019. 6G wireless communications: Vision and potential techniques. *IEEE network*, *33*(4), pp.70-75.